

The Metabook of Aircraft Design

Compiled on Sunday 17th October, 2021 at 06:26

Joaquim R. R. A. Martins

Contents

1	Introduction	4
1.1	Aircraft Design Process	4
2	First Estimate of Takeoff Weight	6
2.1	Introduction	6
2.2	Empty Weight	7
2.3	Fuel Weight	9
2.3.1	Mission Segments	9
2.3.2	Cruise Segment	10
Specific Fuel Consumption	10	
Preliminary Estimate for L/D	11	
2.3.3	Final Fuel Fraction	14
2.4	Battery Weight for Electric Aircraft	15
2.5	Determining Takeoff Weight	16
2.5.1	Debugging Tips	16
3	Cost Analysis	19
3.1	Introduction	19
3.2	Adjusting for Inflation	19
3.3	Aircraft Price	21
3.4	Operations and Maintenance Costs	22
3.4.1	Cash Operating Cost	22
3.4.2	Fixed Operating Cost	25
3.4.3	Indirect Operating Cost	26
4	Preliminary Sizing	30
4.1	Wing Loading	31
4.2	Thrust-to-Weight Ratio	32
4.3	Drag Polar Estimate	34
4.4	Stall Speeds	36
4.5	Takeoff Field Length	37
4.5.1	Sizing to FAR 25 requirements for jet transport aircraft	37
4.5.2	Sizing to FAR 23 requirements for propeller aircraft	37
4.6	Landing Field Length	38
4.7	Climb	38
4.7.1	Climb requirements for jet-powered aircraft	38
4.7.2	Climb requirements for propeller aircraft	41
4.8	Ceiling	42
4.9	Maneuver	42

4.10	Cruise	43
4.10.1	For Jet-powered aircraft	43
4.10.2	For propeller-powered aircraft	43
4.11	Putting it All Together	44
4.12	<i>T</i> – <i>S</i> Plot and Objective Function Contours	47
4.12.1	Updating the weight estimation	47
4.12.2	Solving for the constraint lines	50
5	Fuselage Sizing and Design	52
5.1	Cross-Section Design	52
5.2	Cabin Planform Layout	54
5.3	Nose and Tail Cone	55
5.4	Cockpit	57
5.5	Relevant Federal Aviation Regulations	57
6	Wing Design	58
6.1	Wing Design Parameters	58
6.1.1	Span	59
6.1.2	Area	60
6.1.3	Sweep	61
6.1.4	Thickness	61
6.1.5	Taper	61
6.1.6	Twist	62
6.2	Lift Distributions	62
6.2.1	Lift and C_l Distributions	62
6.2.2	Wing Geometry and Lift Distributions	63
6.2.3	Lift Distributions and Performance	64
6.3	Winglets and Other Nonplanar Wings	65
6.4	Transonic Wave Drag	67
6.5	Airfoil Design	67
6.5.1	Airfoil Geometry	67
6.5.2	Airfoil Pressure Distributions	68
6.5.3	Airfoil Pressures and Performance	70
Relating Airfoil Geometry and Pressures	70	
6.5.4	Airfoil Design Methods	70
Direct Methods for Airfoil Design	73	
Inverse Design	73	
7	Weights	75
7.1	Introduction	75
7.2	Preliminary Empty Weight and Center of Gravity Calculation	75
7.3	Detailed Component Weights Method	78
7.3.1	Load Factor	78
7.3.2	Wing	78
7.3.3	Engine/Motor	79
Jet engines	79	
Turboprop engines	79	
Electric motors	80	

7.3.4 Fudge factors	80
7.3.5 Other Components	80
7.3.6 A More Sophisticated Weight Estimate	80
8 Stability and Control	83
8.1 Preliminary Empennage Sizing	83
8.2 Longitudinal Static Stability	84
8.2.1 Center of Pressure of an Airfoil	84
8.2.2 Aerodynamic Center	85
8.2.3 Mean Aerodynamic Chord	85
8.2.4 Equations for Trim Static Stability	86
8.3 Dynamic Stability	90
8.3.1 Introduction	90
8.3.2 Longitudinal Dynamic Modes	91
Short-Period	91
Phugoid	91
8.3.3 Lateral Dynamic Modes	92
9 Landing Gear	93
9.1 Preliminary Landing Gear Positioning	93
9.2 Landing Gear Sizing	94
10 Propulsion	98
10.1 Introduction	98
10.2 The Tradeoff Between Thrust and Efficiency	98
10.3 The Turbojet Engine	100
10.4 The Turbofan Engine	102
11 Structures and Loads	105
11.1 Introduction	105
11.2 Preliminary Structural Arrangement	105
11.3 Aircraft Structural Loads	106
11.3.1 Operating and Design Flight Envelopes	108
11.3.2 Design Airspeeds	108
11.3.3 Limit and Ultimate Load Factors	109
11.3.4 $V-n$ Diagram	109
Basic Flight Envelope	109
Gust Envelope	109
12 Sensitivity Studies	119
12.1 Introduction	119
12.2 Methods for Computing Sensitivities	119
12.2.1 Finite Differences	119
12.2.2 Complex-Step Method	121
12.2.3 Basic Theory	121
12.2.4 Other Methods	123

Chapter 1

Introduction

1.1 Aircraft Design Process

1. Requirements: Study the requirements and classify objective and constraints, comparison with existent aircraft
2. First weights estimate — takeoff gross, empty and fuel (Ch. 2)
3. Direct operating cost and acquisition cost
4. Perform preliminary sizing: decide on wing area and installed thrust
 - 4.1 Program first drag polar (Assume an aspect ratio. Span efficiency and parasitic drag coefficient from historical data)
 - 4.2 Compute stall speed, takeoff field length, landing field length, climb and cruise constraints as a function of wing area and thrust (assume maximum lift coefficient, follow federal aviation regulations)
 - 4.3 Make a plot showing the constraints and objective function with respect to wing area and thrust
 - 4.4 Choose the best wing area and thrust (keep the shortcomings of the estimates in mind)
5. Configuration layout (based on rough calculations, intuitive knowledge and historical configurations)
 - 5.1 Configuration type
 - 5.2 Fuselage sizing and layout (including cockpit, passenger cabin, cargo arrangement and fuel tanks) — Ch. 5
 - 5.3 Propulsion system selection and integration
 - 5.4 Wing planform design (span, sweep, taper) — Sec. 6.1
 - 5.5 Control surfaces and high-lift system layout
 - 5.6 Empennage layout and initial sizing (area, span, sweep, taper) — Sec. 8.1
 - 5.7 Better weight estimate and CG position using the preliminary buildup method — Sec. 7.2
 - 5.8 Neutral point and static margin — Sec. 8.2.4
 - 5.9 Landing gear disposition considering takeoff rotation and tip-over

- 5.10 Structural arrangement for major load paths — Sec. 11.2
- 5.11 Draw complete configuration — “Dash-1” drawing
- 5.12 Evaluate feasibility and iterate design and drawing
- 6. Preliminary design report (PDR) and presentation, downselect configuration
- 7. Sizing refinement
 - 7.1 Replace approximate buildup weight estimate with detailed component buildup method
 - 7.2 Replace first drag polar with one that takes actual geometry into account
 - 7.3 Program multidisciplinary analysis (given the design variables, this analysis outputs the objective and constraints)
 - 7.4 Program the computation of sensitivities
 - 7.5 Optimize the design
- 8. Finalize the design and make the final drawings

Chapter 2

First Estimate of Takeoff Weight

2.1 Introduction

In this chapter, we provide a rough initial method for estimating the weight¹ of your aircraft. The weight is a major design parameter, since it determines the size of the aircraft. This method relies on regressions of historical data, and does not depend on design parameters (such as wing planform, cabin arrangement, etc.). In Chapter 7 we will provide a more detailed approach, which considers design parameters, to estimate the aircraft weight and replace this early estimate.

The *takeoff weight*, W_0 , is the total weight of the aircraft as it begins the mission for which it was designed. Note that this is not necessarily the *maximum* takeoff weight (MTOW), but these are commonly used interchangeably. The takeoff weight—sometimes referred to as *takeoff gross weight* (TOGW)—correlates well with aircraft manufacturing and operating costs. Hence we usually want to minimize it while satisfying the design requirements.

The takeoff weight can be broken down into crew weight, payload weight (including passengers), fuel weight, and empty weight, i.e.,

$$W_0 = W_{\text{crew}} + W_{\text{payload}} + W_f + W_e \quad (2.1)$$

The crew and payload weights can be estimated from the requirements, but the fuel weight and empty weight depend on the takeoff weight. For example, fuel burn depends on the drag, which in turn depends on the weight; and the empty weight depends on the weight of the structure, which must be designed to sustain loads that depend on the total weight.

At first, the designer knows very little about the aircraft except for the requirements. The designer might not even know what kind of configuration, shape of wing, or engines will be used. Thus, the difficulty in starting the design process is that most of the other design parameters depend on W_0 , and W_0 in turn is affected by those same parameters. However, one must start somewhere, so a preliminary sizing of that aircraft in the form of an estimate of W_0 is needed.

The solution to this conundrum is to guess a reasonable value for W_0 based on historical data or other available knowledge, and then improve this estimate as more details are determined. For the preliminary estimate, we will improve the first W_0 guess by using estimates for the fuel fraction (W_f/W_0) and the empty weight fraction (W_e/W_0). The empty weight fraction can be found from historical data for the same type of aircraft, and an estimate for the fuel fraction can be computed as explained in Sec. 2.3. Since we want to work with these fractions, we divide Eqn. (2.1) by W_0

¹We all know from basic physics that mass and weight are not the same thing. However, in aircraft design, we use these terms interchangeably.

and rearrange it to get

$$W_0 = \frac{W_{\text{crew}} + W_{\text{payload}}}{1 - \frac{W_f}{W_0} - \frac{W_e}{W_0}}. \quad (2.2)$$

Again, note that these two fractions both depend on W_0 itself, so we need to iterate the above equation in order to get a converged result, as explained in Sec. 2.5. For preliminary sizing, both passengers and crew (including carry-on bags) can be assumed to weigh an average of 180 lb (82 kg), and to check about 60lb (27kg) of luggage.

2.2 Empty Weight

The aircraft *empty weight*, W_e , includes structure, engines, systems, avionics, and instruments. The preliminary estimate of the aircraft empty weight is the weakest part of the conceptual design stage because it is almost impossible to accurately determine the empty weight of such a complex system that has not been built. The accuracy suffers even more if a new technology is being used. However, we must proceed with the best estimates we can get.

There are various methods for estimating (W_e/W_0) from historical data. Most of these methods are based on a regression of the data for the particular type of aircraft in question. Raymer (2006, Sec. 3) provides the following regression,

$$\frac{W_e}{W_0} = A W_0^C \quad (2.3)$$

where A and C are the regression constants that vary according to aircraft type. For example, for a jet transport, $A = 1.02$ and $C = -0.06$, assuming W_0 is in pounds. The constants for other types of aircraft are given in Raymer (2006, Table 3.1) and shown in Table 2.1. Raymer assumes a conventional metallic structure. For composite aircraft, he suggests multiplying the result by 0.95.

Other methods for the preliminary estimation of W_e can be found in Nicolai and Carichner (2010, Appendix I) and in Roskam (1989, Vol. I, Ch. 2). Roskam's method does not provide the weight fraction explicitly, but it can be manipulated into doing so.

$$\log_{10}(W_0) = A + B \log_{10}(W_e) \quad (2.4)$$

In fact if we can manipulate Roskam's method into looking the same as Raymer's method

$$\frac{W_e}{W_0} = 10^{-A/B} W_0^{1/B-1} \quad (2.5)$$

These other methods are equivalent to Raymer's, but result in different estimates. Jenkinson et al. (1999, Figs. 11.6–11.7) shows plots of empty weight ratios for various airliners as a function of maximum range. The variability in these estimates and the actual data points in the plots shown in those books will give you an idea of the accuracy of your estimates.

Note that each data point used in these regressions corresponds to an aircraft that was designed, built and flown, and thus it is not subject to uncertainty. However, your aircraft requirements probably does not match any given real airplane exactly. It is generally difficult to achieve a much lower (W_e/W_0) than what is shown in that data, but new technologies can probably reduce it somewhat. This is shown in Raymer (2006, Figure 3.1), which is Figure 2.1, when comparing aircraft of the same type with different technologies such as "Homebuilt-metal/wood" and "Homebuilt-composite".

$W_e/W_0 = AW_0^C K_{vs}$	A	{A-metric}	C
Sailplane—unpowered	0.86	{0.83}	-0.05
Sailplane—powered	0.91	{0.88}	-0.05
Homebuilt—metal/wood	1.19	{1.11}	-0.09
Homebuilt—composite	1.15	{1.07}	-0.09
General aviation—single engine	2.36	{2.05}	-0.18
General aviation—twin engine	1.51	{1.4}	-0.10
Agricultural aircraft	0.74	{0.72}	-0.03
Twin turboprop	0.96	{0.92}	-0.05
Flying boat	1.09	{1.05}	-0.05
Jet trainer	1.59	{1.47}	-0.10
Jet fighter	2.34	{2.11}	-0.13
Military cargo/bomber	0.93	{0.88}	-0.07
Jet transport	1.02	{0.97}	-0.06
UAV—Tac Recce & UCAV	1.67	{1.53}	-0.16
UAV—high altitude	2.75	{2.48}	-0.18
UAV—small	0.97	{0.86}	-0.06

K_{vs} = variable sweep constant = 1.04 if variable sweep = 1.00 if fixed sweep

Table 2.1: Empty weight correlation constants from [Raymer \(2006, Table 3.1\)](#)

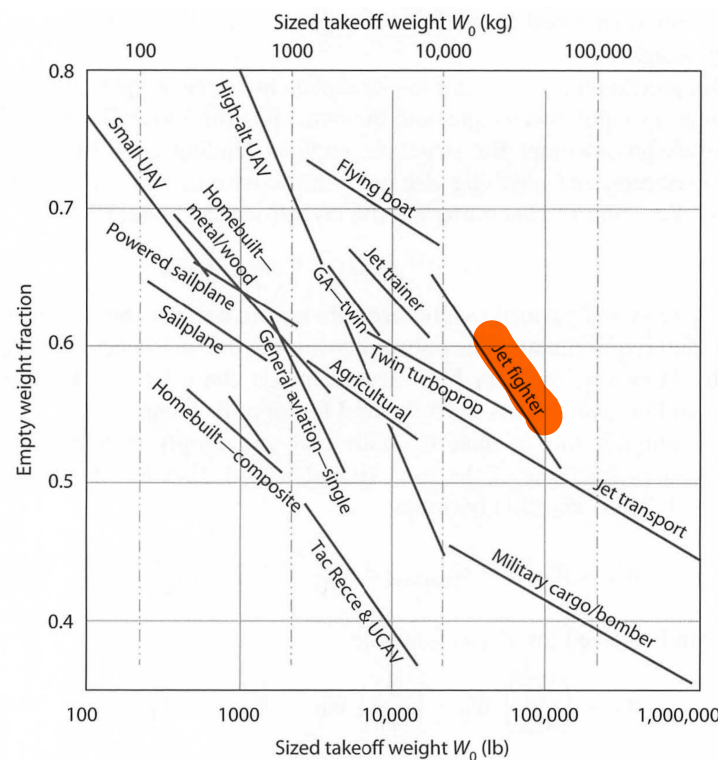


Figure 2.1: Empty weight fractions trends for each aircraft type [Raymer \(2006, Figure 3.1\)](#)

To improve the preliminary estimate of the empty weight, you should do a regression of your own using the data from aircraft that most resemble the one you are trying to design. For example, if you are designing a long haul airliner, instead of relying on the regression constants provided for a general jet transport category, you can use only data for other existing long haul airliners with similar capabilities and levels of technology.

For electric aircraft, for example, it is particularly important that you use your own regression, because the usual regressions assume gas powered airplanes whose fuel has a much higher energy density and whose weight decreases during the mission.

After the aircraft has been drawn, a better estimate of W_e will be computed by adding the weights for all the major components based on their geometry, as detailed in Chapter 7.

Fig. 2.2 shows the historical data for operating empty weight ($W_e + W_{\text{crew}} + \text{trapped fuel}$).

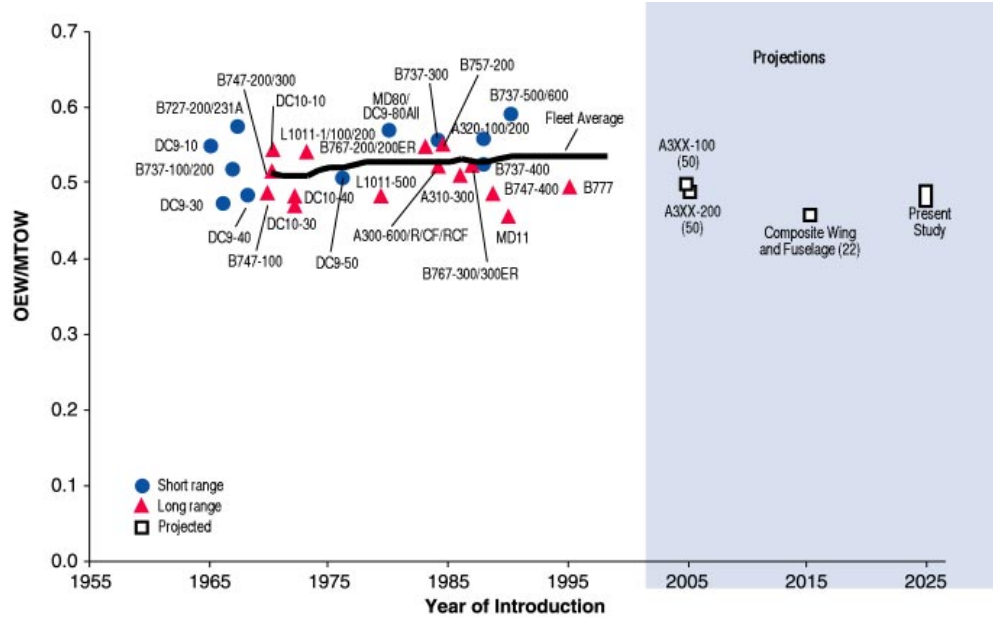


Figure 2.2: Operating empty weight historical trend for airliners (Lee et al., 2001)

2.3 Fuel Weight

Unlike the fuel weight, the fraction (W_f/W_0) is largely independent of the takeoff weight, so it is useful to work with this fraction. Usually, only part of the fuel — the *mission fuel* — is available; the rest — the *reserve fuel* — is required by regulations (e.g. diversion to an alternate airport).

2.3.1 Mission Segments

To estimate (W_f/W_0), we divide the mission into its various segments, estimate the fuel fraction for each segment, and then multiply them all to obtain the final fuel fraction. The sequence of mission segments depends on the requirements and type of aircraft. The typical mission segments are:

1. Engine start and takeoff
2. Climb and acceleration to cruise conditions

Mission segment	Fuel fraction
Engine start and takeoff	W_1/W_0
Climb	W_2/W_1
Descent	W_4/W_3
Landing	W_5/W_4

Table 2.2: Typical fuel fractions

3. Cruise

4. Loiter

5. Landing

Military aircraft will include additional segments, such as combat and cruise back.

The fuel fractions for takeoff, climb, and landing vary according to aircraft type, but at this preliminary stage it is sufficient to use historical data averaged over a wide variety of aircraft. Table 2.2 show values given by Raymer (2006, Sec. 3.4). Other fuel fractions can be found in Nicolai and Carichner (2010, Sec. 5.4).

2.3.2 Cruise Segment

For the cruise segment fuel fraction, we will need an estimate for the cruise speed and altitude, the wing aspect ratio and sweep, and the engine fuel consumption. We can then use the Breguet range equation,

$$R = \frac{V L}{c D} \ln \frac{W_2}{W_3} \quad (2.6)$$

where R is the range, c is the specific fuel consumption (SFC), V is the speed, and L/D is the lift-to-drag ratio.

Since we actually want the weight fraction we rearrange to get

$$\frac{W_3}{W_2} = \exp \left(\frac{-Rc}{V(L/D)} \right). \quad (2.7)$$

The loiter weight fraction can be estimated from the endurance equation,

$$E = \frac{(L/D)}{c} \ln \frac{W_4}{W_3} \Rightarrow \frac{W_4}{W_3} = \exp \left(\frac{-Ec}{(L/D)} \right). \quad (2.8)$$

Beware of the units: Always check that you are using consistent units. One of the checks is to make sure that the resulting fuel fraction is dimensionless. It helps to convert all values to English units (feet-lb-s) or metric (m-k-s).

Specific Fuel Consumption

The specific fuel consumption (SFC), c —also referred to as thrust-specific fuel consumption (TSFC)—is the amount of fuel ² consumed per unit time for each unit of thrust. In English units, SFC is usually quoted in pounds of fuel per hour, per pound of thrust—lb/lbf· h or 1/h if you take the liberty of using weight for the fuel and canceling with the thrust force. In metric units, SFC is

²Strictly speaking this should be quantified in units of mass, but it is common to use units of weight.

sometimes give in grams per kilonewton per second— $\text{g}/(\text{kN}\cdot\text{s})$. If, again, you take the liberty of expressing the amount of fuel as a weight, you can convert this to $1/\text{s}$. SFC varies with Mach number, throttle setting, and altitude. Fig. 2.3 show the typical variation of SFC with Mach number for various types of engines.

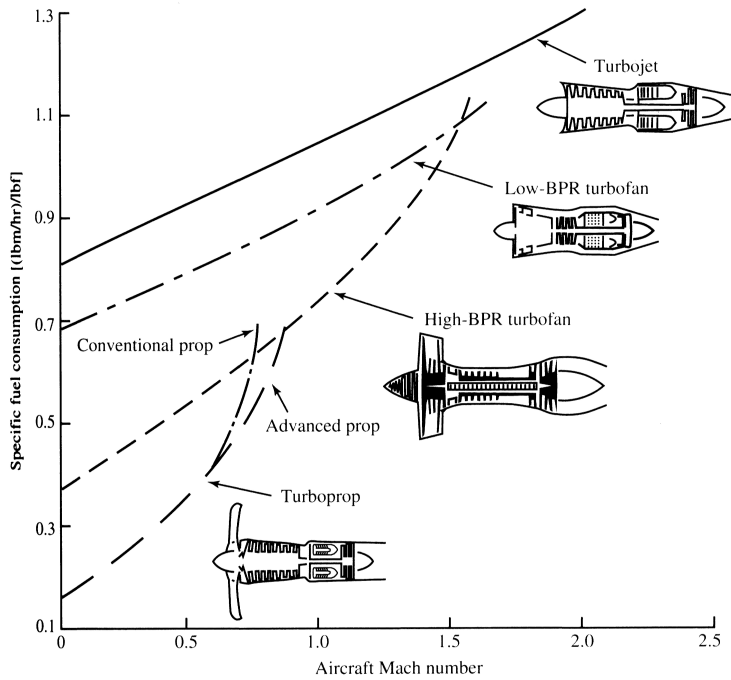


Figure 2.3: SFC vs. Mach number for various engines Mattingly (1996, Fig. 1.17b)

Typical values for a high-bypass turbofan are 0.5 lb/hr/lb for cruise and 0.4 for loiter (Raymer, 2006, Sec. 3.4).

Preliminary Estimate for L/D

The other unknown in the range and loiter equations is lift-to-drag ratio, L/D , which is a measure of aerodynamic efficiency. It is highly dependent on the aircraft configuration. For subsonic aircraft, the major design parameters that determine L/D are the wing span, b , and the wetted area, S_{wet} .

For cruise, we have level flight and therefore, the lift equals the weight, and thus we concern ourselves only with the drag. The subsonic drag is composed of lift induced drag and parasite drag (drag for zero lift). The induced drag is primarily a function of the wing span. The parasite drag is mostly due to skin friction drag, which is directly proportional to the total surface area exposed to the air (the *wetted area*, S_{wet}).

As we will see later, the maximum L/D correlates well with the *wetted aspect ratio*, which is defined as

$$\frac{b^2}{S_{\text{wet}}} = \frac{AR}{S_{\text{wet}}/S_{\text{ref}}}. \quad (2.9)$$

The wetted aspect ratio is significant because it takes into account the two design parameters that are the major drivers for induced and parasitic drag. Figure 2.4 (Raymer (2006, Fig 3.5)) shows typical values for $(L/D)_{\max}$ as a function of the wetted aspect ratio.

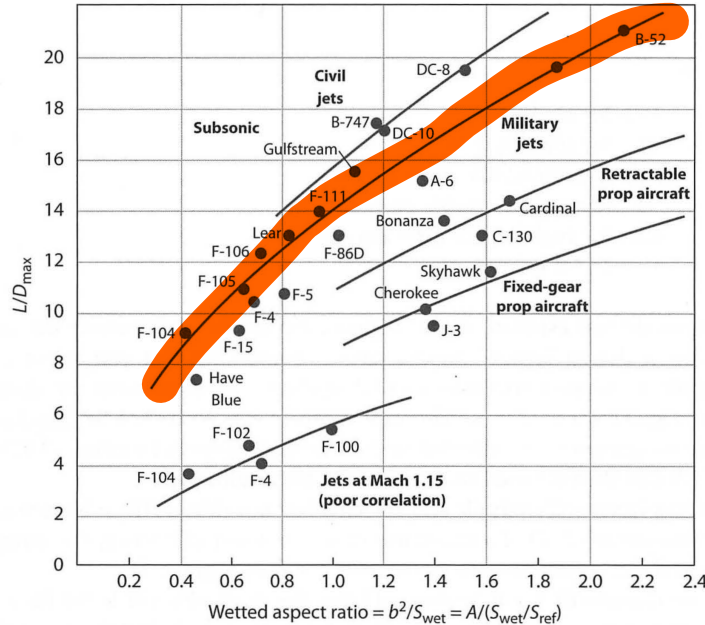


Figure 2.4: $(L/D)_{\max}$ as a function of the wetted aspect ratio as shown in Raymer (2006, Figure 3.5)

Note that wetted area ratio, $S_{\text{wet}}/S_{\text{ref}}$, depends on the type of configuration and for now you will need to estimate it based on historical data. Figure 2.5Raymer (2006, Fig 3.6) shows typical values for this ratio, which ranges from about 2 for flying wings to almost 8 for the particular case of the B-47. The Boeing 747 has a wetted area ratio of about 6.3. Two engined jet transports should have slightly lower values than this.

As the formulation of wetted aspect ratio suggests there are two basic ways to increase wetted aspect ratio, decrease the wetted area or increase the span. Either of these changes will lead to an increase in the $(L/D)_{\max}$ since wetted aspect ratio is roughly linearly correlated with $(L/D)_{\max}$. When selecting a configuration for the aircraft one should keep this in mind, since often the wetted area cannot be decreased while simultaneously increasing the span.

In Raymer (at least in the earlier versions) this fact was illustrated with a comparison of the Boeing B-47 and Avro Vulcan B-1. The B-47, built by the USA, and the Vulcan B-1, built by the UK, were designed for strategic nuclear missions deep in the heart of USSR. Both aircraft were designed for a long range missions and thus for a high cruise L/D , yet they look substantially different. The B-47 is a traditional configuration with a large aspect ratio but a large ratio of wetted area to surface area as well. The B-1 on the other hand has a low aspect ratio but also has a low ratio of wetted area to surface area because of its blended wing-body and tailless design. As a result of the trade-off between span and wetted area in the configuration selection both designs had roughly the same wetted aspect ratio and thus $(L/D)_{\max}$.

If we look at the drag polar for each of these aircraft in Figure 2.7 we can see how the concept of wetted aspect ratio is connected to C_{D0} and k and ultimately $(L/D)_{\max}$.

From the drag polars one can see visually that $(L/D)_{\max}$ is a function of the x-intercept, C_{D0} , and the curvature, k , of the parabola. Indeed we can prove this point by deriving $(L/D)_{\max}$ for a quadratic drag polar.

$$C_D = C_{D0} + kC_L^2 \quad (2.10)$$

We can find the L/D ratio by dividing C_L by the equation for C_D given by the quadratic drag

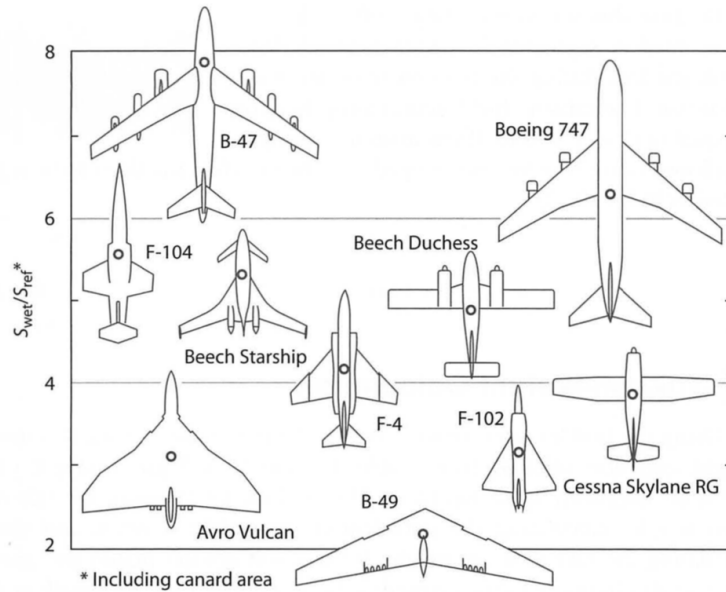


Figure 2.5: Wetted aspect ratio for various planes as shown in Raymer (2006, Figure 3.6)

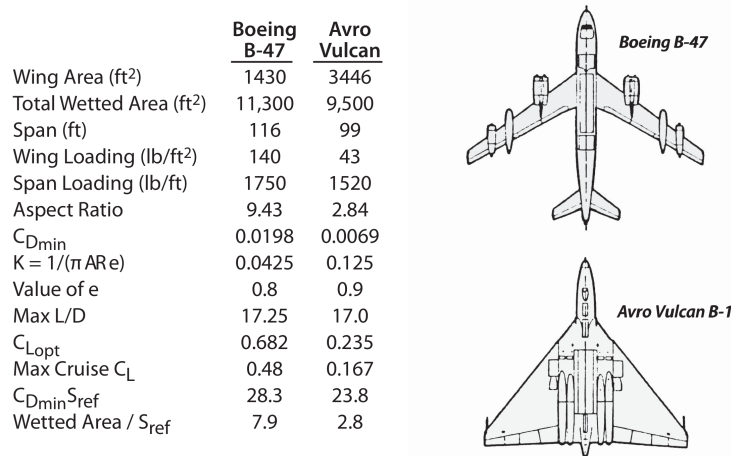


Figure 2.6: Wetted aspect ratio for various planes as shown in Raymer (2006, Figure 3.7)

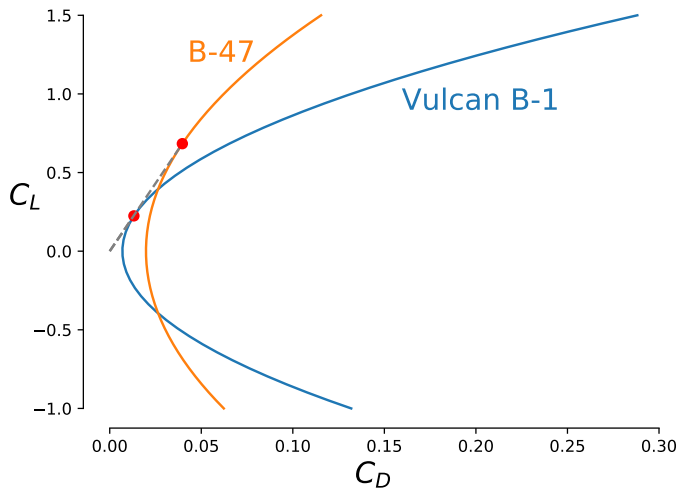


Figure 2.7: The drag polars for the B-47 and B-1 show that they have the same $(L/D)_{\max}$

polar.

$$L/D = \frac{C_L}{C_{D0} + kC_L^2} \quad (2.11)$$

From here the procedure is simple, we will take the derivative of (L/D) and set it equal to 0 to find the critical point and then $(L/D)_{\max}$

$$\frac{dL/D}{dC_L} = \frac{C_{D0} - kC_L^2}{(C_{D0} + kC_L^2)^2} \quad (2.12)$$

$$\frac{C_{D0} - kC_L^2}{(C_{D0} + kC_L^2)^2} = 0 \quad (2.13)$$

$$C_L = \sqrt{\frac{C_{D0}}{k}} \quad (2.14)$$

$$(L/D)_{\max} = \frac{1}{2} \sqrt{\frac{1}{C_{D0}k}} = \frac{1}{2} \sqrt{\frac{\pi e A R}{C_{D0}}} \quad (2.15)$$

From the equation for $(L/D)_{\max}$, Equation 2.15, it is clear that $(L/D)_{\max}$ is a function of C_{D0} and k .

As we will see later, if we want to maximize endurance of a jet, the most efficient point on the drag polar is that corresponding to $(L/D)_{\max}$. However, when maximizing range (or minimizing fuel burn per unit distance) for a given throttle level, the most efficient point is at a lower L/D , more exactly at $0.943(L/D)_{\max}$ (Nicolai and Carichner, 2010, Eq.(3.29)). Thus you may use this result to estimate the cruise L/D at this stage.

2.3.3 Final Fuel Fraction

The ratio of final to initial weight can be computed using

$$\frac{W_5}{W_0} = \frac{W_5}{W_4} \frac{W_4}{W_3} \frac{W_3}{W_2} \frac{W_2}{W_1} \frac{W_1}{W_0} \quad (2.16)$$

Then, assuming all of the weight decrease was due to fuel burn (no cargo or weapons were dropped, for example), the final fuel fraction is

$$\frac{W_f}{W_0} = \frac{W_0 - W_5}{W_0} = 1 - \frac{W_5}{W_0} \quad (2.17)$$

We usually assume that there is some *trapped fuel*, which is fuel that cannot be pumped from the tanks. To account for this, as well as the reserve fuel, we multiply the fuel fraction by 1.06 (Raymer, 2006, Sec. 3.4).

2.4 Battery Weight for Electric Aircraft

The above method for estimating the fuel weight obviously does not work for a battery powered aircraft. A new derivation of the Breguet range equation is required in this case. The range of the cruise segment can be written as:

$$R = Vt \quad (2.18)$$

where t is the duration of the cruise segment.

We need to introduce two basic metrics for battery performance: specific energy (energy per unit mass) e^* , and electric power P . When designing batteries, there is generally a trade-off between these two metrics. Given these two metrics, we can calculate the battery discharge time:

$$t = \frac{m_{\text{battery}} e^*}{P_{\text{battery}}} \quad (2.19)$$

where any units can be used, as long as they are consistent (e.g, kg for m_{battery} , Wh/kg for e^* , W for P_{battery} , yielding the time in hours).

The required power in level flight is

$$P_{\text{aircraft}} = VT = VD = V \frac{W_0}{L/D}. \quad (2.20)$$

The actual power provided by the battery will be higher, according to the overall efficiency, η :

$$P_{\text{battery}} = \frac{P_{\text{aircraft}}}{\eta} \quad (2.21)$$

Substituting this in to Eq.(2.19) and then into Eq.(2.18), we get,

$$R = \eta e^* \frac{L}{D} \frac{m_{\text{battery}}}{W_0}. \quad (2.22)$$

With this equation, you can also compute the required battery mass to obtain a desired range as

$$m_{\text{battery}} = \frac{RW_0}{\eta e^*(L/D)}. \quad (2.23)$$

If we ignore the energy requirements for taxi, takeoff, climb, descent, and landing, the following modification to Eqn. (2.2) can be used:

$$W_0 = \frac{W_{\text{crew}} + W_{\text{payload}}}{1 - \frac{W_e^*}{W_0} - \frac{m_{\text{battery}} g}{W_0}} = \frac{W_{\text{crew}} + W_{\text{payload}}}{1 - \frac{W_e^*}{W_0} - \frac{Rg}{\eta e^*(L/D)}} \quad (2.24)$$

where W_e^* does not include the weight of the battery.

However, we still want to consider other segments such as taxi and takeoff, climb, and landing. One way to do this is to use the fuel fractions described earlier (e.g., Table 2.2) to compute ratios of the energy used in each of these segments to the energy used during cruise. For example, we could first carry out the weights estimation process for an aircraft that uses hydrocarbon fuel (HCFA) and then use the fuel fractions and obtained fuel weights to compute the required energy ratios. For the engine start and takeoff segment we would compute the energy ratio as

$$\frac{E_{0 \text{ to } 1}}{E_{\text{cruise}}} = \left(1 - \left(\frac{W_1}{W_0}\right)_{\text{HCFA}}\right) \left(\frac{W_0}{W_{\text{cruise fuel}}}\right)_{\text{HCFA}}. \quad (2.25)$$

For the climb segment we would compute the ratio as

$$\frac{E_{1 \text{ to } 2}}{E_{\text{cruise}}} = \left(1 - \left(\frac{W_2}{W_1}\right)_{\text{HCFA}}\right) \left(\frac{W_1}{W_{\text{cruise fuel}}}\right)_{\text{HCFA}}. \quad (2.26)$$

Similarly, we can compute the ratios for the other segments.

Next, for example if we assume that we only have the segments in Table 2.2 along with cruise, we can modify Eq. (2.24) to

$$W_0 = \frac{W_{\text{crew}} + W_{\text{payload}}}{1 - \frac{W_e^*}{W_0} - \frac{m_{\text{battery,cruise}}g}{W_0} \left(1 + \frac{E_{0 \text{ to } 1}}{E_{\text{cruise}}} + \frac{E_{1 \text{ to } 2}}{E_{\text{cruise}}} + \frac{E_{3 \text{ to } 4}}{E_{\text{cruise}}} + \frac{E_{4 \text{ to } 5}}{E_{\text{cruise}}}\right)} \quad (2.27)$$

Further modifications would have to be made to consider other segments such as loiter.

2.5 Determining Takeoff Weight

Now we have weight fractions, W_e/W_0 and W_f/W_0 that are required to compute the takeoff weight using (2.2). We can now use this new value for W_0 to estimate a new value of W_e/W_0 using the regression (2.3), and iterate it until convergence. The pseudocode describing the procedure for the the weight iteration is shown in Algorithm 0.

Algorithm 1 Iteration for estimating TOGW

```

 $W_0 = W_{\text{guess}}$                                  $\triangleright$  Initial guess
 $\varepsilon = 10^{-6}$                                  $\triangleright$  Set the relative convergence tolerance
 $\Delta = 2\varepsilon$                                  $\triangleright$  Any value greater than the tolerance
while  $\Delta > \varepsilon$  do
     $\frac{W_e}{W_0} = A \frac{W_0^C}{W_0}$                  $\triangleright$  Compute empty weight
    Compute  $\frac{W_f}{W_0}$                              $\triangleright$  Compute fuel fraction
     $W_{0\text{new}} = \frac{W_{\text{crew}} + W_{\text{payload}}}{1 - \frac{W_f}{W_0} - \frac{W_e}{W_0}}$            $\triangleright$  Compute the new TOGW
     $\Delta = |W_{0\text{new}} - W_0| / |W_{0\text{new}}|$ 
     $W_0 = W_{0\text{new}}$                                  $\triangleright$  Update TOGW value
end while

```

2.5.1 Debugging Tips

There are generally two places where students go wrong, the calculate of $\frac{W_f}{W_0}$ and the calculate of $\frac{W_e}{W_0}$ based on the regression. Check that both of these values close to what you would expect for the

type of aircraft. Furthermore, try plotting your weight regression against those given by Raymer and/or Roskam. If there is a substantial difference that should be cause for alarm.

Example 2.1: Preliminary weight estimation based on the 777

We use the 777-200LR as an example for estimating the TOGW and comparing the results with the actual weight of the aircraft. First, we compute the crew weight and payload weight. The 777-200LR has 2 pilots and 12 flight attendants. We also assume a three-class cabin configuration that has 314 passengers. From this we get:

$$W_{\text{crew}} = 14 \times 109 = 1,526 \text{ kg} \quad (2.28)$$

$$W_{\text{payload}} = 314 \times 109 = 34,226 \text{ kg} \quad (2.29)$$

Next, we need an estimate for L/D in order to compute the fuel fraction. We can estimate $(L/D)_{\max}$ using [Raymer \(2006, Fig 3.6\)](#). Based on this, an estimate of $(L/D)_{\max} = 18$ seems appropriate. Now we can compute the fuel fractions for cruise and loiter, and also obtain the total fuel fraction. Using $R = 9150 \text{ nmi}$, $E = 30 \text{ min}$, $c = 0.52 \text{ lb/(lbf hr)}$ for the GE-90, and $V = 251 \text{ m/s}$, $L/D = 0.94(L/D)_{\max}$, we get the following.

$$\frac{W_3}{W_2} = \exp\left(\frac{-Rc}{V(L/D)}\right) = 0.562 \quad (2.30)$$

$$\frac{W_4}{W_3} = \exp\left(\frac{-Ec}{(L/D)}\right) = 0.986 \quad (2.31)$$

$$\frac{W_5}{W_0} = \frac{W_5}{W_4} \frac{W_4}{W_3} \frac{W_3}{W_2} \frac{W_2}{W_1} \frac{W_1}{W_0} = 0.527 \quad (2.32)$$

The combined fuel fraction with 6% for reserves and trapped fuel is

$$\frac{W_f}{W_0} = \left(1 - \frac{W_5}{W_0}\right) \times 1.06 = 0.502 \quad (2.33)$$

We can see that this aircraft has a very large fuel fraction due to its long range capability. For a long range flight, roughly half of the takeoff weight will be the weight of the fuel. Specifications show that the 700-200LR has a maximum fuel fraction of about 0.50. This fortuitously happens to be exactly what we estimated.

With the fuel fraction computed, we can use the weight iteration code from the previous section to compute the TOGW. In the iteration loop, the empty weight fraction is estimated using $\frac{W_e}{W_0} = 0.97W_0^{-0.06}$, which corresponds to jet transport in Table 2.1. This results in an empty weight of 255,377 kg and an TOGW of 583,973 kg (empty weight fraction of 0.437). Both of which are significantly higher than the 777-200LR's actual empty weight of about 145,000 kg and actual MTOW of about 347,800 kg. The empty weight fraction estimated using the regression happens to be a little higher than the actual empty weight fraction (about 0.41) for the 777-200LR. This has a major impact on the weight estimates. The constants in Table 2.1 for jet transport are not very specific to a particular sub-category of jet transport and this contributes to the error in the predictions. Using a custom regression based on aircraft belonging to the same category may lead to more accurate estimates.

Bibliography

- Lloyd R. Jenkinson, Paul Simpkin, and Darren Rhodes. *Civil Jet Aircraft Design*. Arnold, 1999.
- Joosung J. Lee, Stephen P. Lukachko, A. Waitz, and Andreas Schafer. Historical and future trends in aircraft performance, cost, and emissions. *Annual Review of Energy and the Environment*, 26: 167–200, 2001.
- Jack D. Mattingly. *Elements of Gas Turbine Propulsion*. McGraw–Hill, 1996.
- Leland M. Nicolai and Grant E. Carichner. *Fundamentals of Aircraft and Airship Design, Vol I — Aircraft Design*. AIAA, Reston, VA, 2010.
- Daniel P. Raymer. *Aircraft Design: A Conceptual Approach*. AIAA, 4th edition, 2006.
- J. Roskam. *Airplane Design, Volumes 1-8*. Roskam Aviation and Engineering Corporation, 1989.

Chapter 3

Cost Analysis

3.1 Introduction

Aircraft cost estimation is probably the estimate with most uncertainty (even more than the preliminary weight estimation!). Like weight estimation, the cost is estimated using historical data that have been correlated to certain design parameters.

The *life cycle cost* of an aircraft is the total cost of the aircraft “from cradle to grave”. It includes the following:

- Research, development, testing and evaluation (RDT&E)
- Production (airframe, engine and avionics)
- Operations and maintenance
- Disposal

The two first categories must be offset by selling aircraft. The typical curves for the cash flow of new project and a derivative project are shown in Fig. 3.1.

An inherent trade-off exists between the production cost and the cost of operating the aircraft. Manufacturers have the choice to design aircraft that have low acquisition cost, but are costly to operate, or vice-versa. It is difficult to predict where to position a new aircraft within this trade space because manufacturers must anticipate the preferences of multiple airlines. The airline preference depends on several factors including the future price of fuel (which contributes to operating cost), the routes they will operate, and the cost of financing. The trend of over the last few decades has been an increase of the acquisition cost, as shown in Fig.3.2, indicating that airlines have been willing to pay more for aircraft with more capability and lower fuel burn.

3.2 Adjusting for Inflation

When comparing costs, it is essential that they be adjusted for inflation whenever amounts from different years are used. This conversion can be done using,

$$\text{Cost}_{\text{then year}} = \text{Cost}_{\text{base year}} (1 + r)^n \quad (3.1)$$

where r is the rate of inflation over the n is the number of years between the “base year” and the “then year”. This is the same formula that governs compound interest. A quick useful rule based

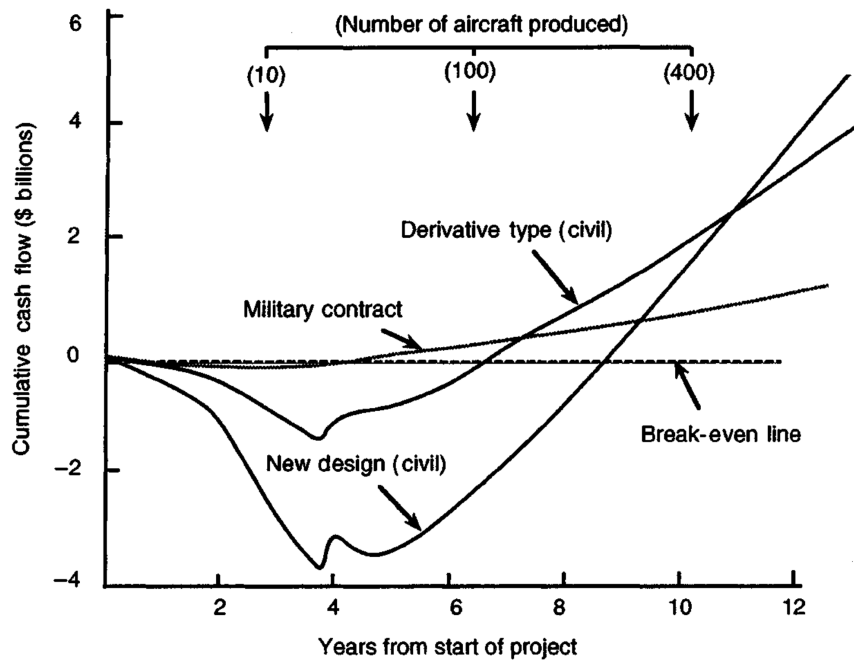


Figure 3.1: Typical project cash flow (Jenkinson et al., 1999, Fig. 12.1).

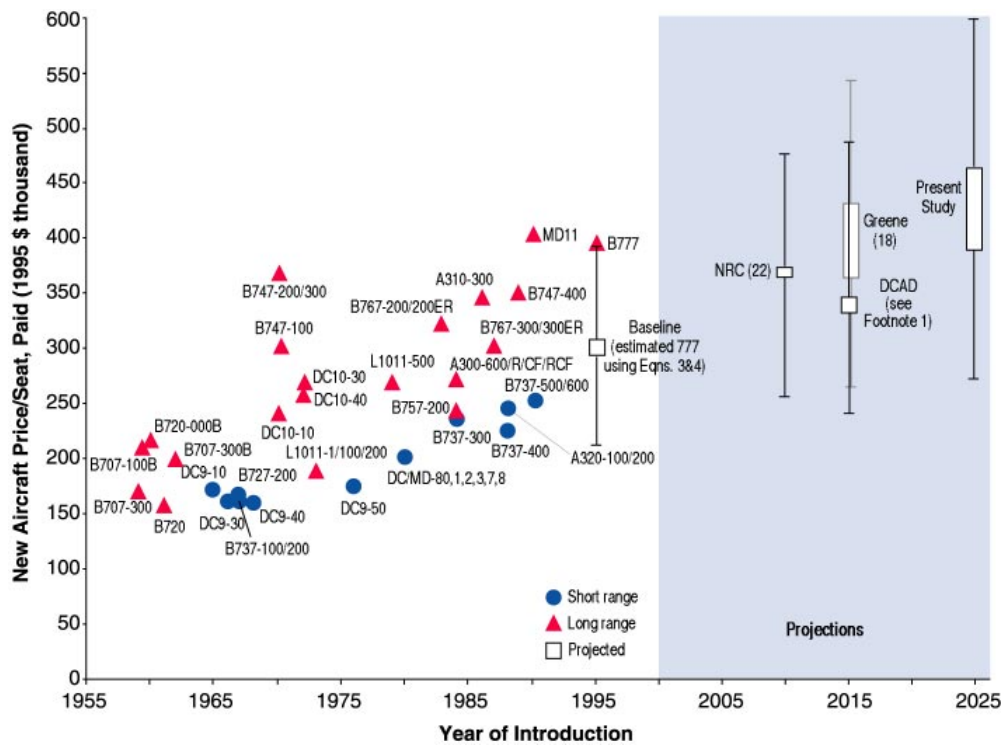


Figure 3.2: Historical trend for aircraft price per seat in 1995 USD (Lee et al., 2001).

on this formula is the “rule of 72”, derived from the fact that if $r = 1$, it takes 72 years for the future cost to double relative to the reference year. Hence dividing 72 by r gives the number of years needed to double the number.

Since the rate of inflation varies continuously, Eq. (3.1) should be integrated over the years with a varying r . Instead of doing this, we use the cost escalation factor (CEF) to convert the costs between different years. For 2006, the “base CEF” and the “then CEF” are given by

$$b_{\text{CEF}} = 5.17053 + 0.104981 (b_{\text{year}} - 2006) \quad (3.2)$$

$$t_{\text{CEF}} = 5.17053 + 0.104981 (t_{\text{year}} - 2006) \quad (3.3)$$

where b_{year} and t_{year} are the base and then years. Then year is the year representing the technology level of the aircraft in consideration. For example, when estimating the aircraft price for 2025 using Eq. (3.6) in Section 3.4.1, b_{year} should be 1989 and t_{year} should be 2025.

The effective CEF is,

$$\text{CEF} = \frac{t_{\text{CEF}}}{b_{\text{CEF}}} \quad (3.4)$$

This CEF estimate is similar to the Air Transportation Association of America (ATA) method similar to the one described by [Liebeck et al. \(1995\)](#).

3.3 Aircraft Price

The first two items in the above list (RDT&E and production) directly affect the purchase price for civil aircraft, which is set to recoup those costs. There are various methods to compute these costs—see [Raymer \(2006, Ch. 18\)](#) and [Nicolai and Carichner \(2010, Ch. 24\)](#).

The production costs consists on the materials and labor costs required to manufacture the aircraft, and it includes tooling costs. The production cost per aircraft decreases with the cumulative number of aircraft produced due to the learning curve effect.

Once RDT&E and production costs are estimated, the aircraft manufacturer can find the *break even point* for a given aircraft price. At the break even point, the manufacturer has recouped its investment and starts making a profit. This price is then decided based on estimates for total number of aircraft that are expected to sell, and when the manufacturer wants to break even.

Total aircraft and engine prices are calculated using CEF values with a base year of 1989, using the following relations ([Roskam, 1989, Part VIII, Appendix A](#)).

For a turboprop commuter aircraft (valid between 6,000 and 50,000 lbs):

$$C_{\text{aircraft}} = 10^{(1.1846 + 1.2625 \log_{10} \text{MTOW})} \text{ (CEF)} \quad (3.5)$$

For a commerical jet transport aircraft (valid between 60,000 and 1,000,000 lbs):

$$C_{\text{aircraft}} = 10^{(3.3191 + 0.8043 \log_{10} \text{MTOW})} \text{ (CEF)} \quad (3.6)$$

For a business jet (valid between 10,000 and 60,000 lbs):

$$C_{\text{aircraft}} = 10^{(0.6570 + 1.4133 \log_{10} \text{MTOW})} \text{ (CEF)} \quad (3.7)$$

Refer to [Roskam \(1989, Part VIII, Appendix A\)](#) for other types of aircraft.

For turboprop engines (valid for 400 to 5,000 shaft hp):

$$C_{\text{engines}} = 10^{(2.5262 + 0.9465 \log_{10} \text{SHP}_{\text{TO}})} \text{ (CEF)} \quad (3.8)$$

where SHP_{TO} is the takeoff shaft horsepower.

For jet engines (valid for 1,000 to 50,000 lbs):

$$C_{\text{engines}} = 10^{(2.3044 + 0.8858 \log_{10} \text{MTOW})} \text{ (CEF)} \quad (3.9)$$

where MTOW is in pounds.

Refer to [Roskam \(1989, Part VIII, Appendix A\)](#) for other engines.

Then, the airframe price is:

$$C_{\text{airframe}} = C_{\text{aircraft}} - C_{\text{engines}} \quad (3.10)$$

3.4 Operations and Maintenance Costs

Airlines divide the total operating cost (TOC) into *direct operating cost* (DOC) and *indirect operating cost* (IOC). DOC is the cost directly associated with aircraft operation, and is divided into flight operations, aircraft maintenance, crew and fuel, and navigation and airport fees. IOC involves the costs that are independent of the aircraft design, and is divided into marketing, ground handling, sales and administrative costs. DOC and IOC are each roughly 50% of the TOC ([Roskam, 1989, Part VIII, Sec. 5.5](#)). The DOC can be further divided into fixed operating cost (FOC) and cash operating cost (COC), where the COC consists of the costs strictly related to the flights. Summarizing:

IOC: Indirect operating cost are the costs not directly related to the flights

COC: Cash operating cost are the costs directly related to the flights

FOC: Fixed operating cost are the costs incurred when not flying (e.g. financing and depreciation)

DOC: Direct operating cost = COC + FOC

TOC: Total operating cost = IOC + DOC

3.4.1 Cash Operating Cost

The DOC is often expressed in USD/passenger-nmi. The major parameters governing the estimation of DOC are the maximum takeoff weight, MTOW (in lbs), mission block time, t_b (in hours), and CEF.

Block time t_b is the overall time for which the aircraft is in use for a given mission, measured from the time the wheel blocks are removed before departure, to the time they are placed after arrival at the destination. The block time is obtained by adding the times taken for each mission segment. The mission segment time for cruise is computed using the cruise speed and range, and the time for all other segments can be estimated from historical data if no computations are available.

We now explain how to estimate the twelve components of DOC (in USD). Many of these estimates are based on [Liebeck et al. \(1995\)](#), who uses a 1993 base year, and [Roskam \(1989, Part VIII\)](#), who uses 1989 as the base year.

1. **Crew:** This is the cost incurred through flight crew wages and other expenses. [Harris \(2005\)](#) provides an equation for crew cost with 1999 as the base year:

$$C_{\text{crew}} = AF \left[K (\text{MTOW})^{0.40} t_b \right] \text{ (CEF)} \quad (3.11)$$

where AF is the airline factor found using regression analysis. For example, $AF = 0.608$ was found for Southwest and a value of $AF = 1.063$ was found for American Airlines. AF ranges from values of 0.34 to 1.6, with an average value of 0.8.

- $AF = \text{Very, Very Low} = 0.34$
- $AF = \text{Very Low} = 0.44$
- $AF = \text{Low} = 0.63$
- $AF = \text{Average} = 0.80$
- $AF = \text{High} = 1.00$
- $AF = \text{Very High} = 1.30$
- $AF = \text{Very, Very High} = 1.60$

K is the route factor, where $K = 2.75$ for regional routes, $K = 5.25$ for domestic routes with 2 crew, and $K = 6.50$ for transpacific or transatlantic with 3 crew. MTOW is the maximum takeoff weight in pounds and t_b is the block time in hours.

Some alternative formulas are provided by [Liebeck et al. \(1995\)](#). The curve-fit expression for domestic flights is

$$C_{\text{crew}} = \left[440 + 0.532 \left(\frac{\text{MTOW}}{1000} \right) \right] (\text{CEF}) (t_b), \quad (3.12)$$

and for international flights as

$$C_{\text{crew}} = \left[482 + 0.590 \left(\frac{\text{MTOW}}{1000} \right) \right] (\text{CEF}) (t_b) \quad (3.13)$$

where MTOW is the maximum takeoff weight in pounds and t_b is the flight block time. [Liebeck et al. \(1995\)](#) uses 1993 as the base year.

2. Attendants: This is the cost associated with the flight attendant wages and is given by the formulation of [Liebeck et al. \(1995\)](#). For domestic flights,

$$C_{\text{attd}} = 60 n_{\text{attd}} (\text{CEF}) (t_b), \quad (3.14)$$

and for international flights,

$$C_{\text{attd}} = 78 n_{\text{attd}} (\text{CEF}) (t_b). \quad (3.15)$$

3. Fuel: This is a function of the fuel weight, W_f , the fuel density, ρ_f , and the price per gallon of Jet-A fuel, P_f :

$$C_{\text{fuel}} = 1.02 W_f \frac{P_f}{\rho_f} \quad (3.16)$$

The factor 1.02 indicates 2% of non-revenue flying ([Kroo](#)). Use consistent units (e.g., the weight in lbs, the density in lbs/gal, and the cost in USD/gal). The fuel used by jet aircraft is Jet-A, which is a form of high grade kerosene.

If electric propulsion is used, we also need to estimate the cost of electricity per mission based on the weight of the battery:

$$C_{\text{elec}} = 1.05 W_b P_{\text{elec}} e_{\text{elec}}^* \quad (3.17)$$

Make sure you use consistent units for this. For example, W_b is the weight of the battery in kg, P_{elec} is the price of electricity in \$/kWh, and e_{elec}^* is the specific energy of the battery in Wh/kg. 1.05 corresponds to the charging efficiency.

4. **Oil:** This is the cost of the oil and lubricants, given as a function of oil weight, W_{oil} , density ρ_{oil} , and cost per gallon of oil, P_{oil} :

$$C_{\text{oil}} = 1.02 W_{\text{oil}} \frac{P_{\text{oil}}}{\rho_{\text{oil}}} \quad (3.18)$$

The weight of oil can be estimated based on fuel weight. Assuming 100 block hour per oil change, the weight of oil is:

$$W_{\text{oil}} = 0.0125 W_f \frac{t_b}{100} \quad (3.19)$$

5. **Landing fees:** These are computed as described by Liebeck et al. (1995). For domestic flights,

$$C_{\text{airport}} = 1.5 \left(\frac{\text{MTOW}}{1000} \right) (\text{CEF}), \quad (3.20)$$

and for international flights,

$$C_{\text{airport}} = 4.25 \left(\frac{\text{MTOW}}{1000} \right) (\text{CEF}). \quad (3.21)$$

6. **Navigation fees:** The following describes a formula for international-flight navigation fees, which includes the cost for the use of air traffic control systems:

$$C_{\text{navigation}} = 0.5 (\text{CEF}) \left(\frac{1.852 R}{t_b} \right) \sqrt{\frac{0.00045359237 \text{ MTOW}}{50}} \quad (3.22)$$

The CEF in this formula has a base year of 1989. R is the range in nmi and MTOW is in lbs.

7. **Airframe maintenance:** This term includes costs for maintenance of the airframe, based on maintenance labor hours, labor cost, material cost. The maintenance cost is a function of the airframe price, which can be estimated by following the procedure detailed in Sec. 3.3. Once the airframe price is known, the maintenance cost for aircraft with turbine engines can be found as a function of the block time, the labor cost, C_{ML} , the material cost, C_{MM} (Roskam, 1989, Part VIII, Chapter 5):

$$C_{ML} = 1.03 \left(3 + \frac{0.067 W_A}{1000} \right) R_L \quad (3.23)$$

$$C_{MM} = 1.03 (30 \text{ CEF}) + 0.79 \times 10^{-5} C_{\text{airframe}} \quad (3.24)$$

$$(3.25)$$

where W_A is the airframe weight. This value is the empty weight minus the engine weight. R_L is the maintenance labor rate in USD/hr for the year of interest. The total airframe maintenance cost is (Schaufele, 2007):

$$C_{\text{airframe maintenance}} = (C_{ML} + C_{MM}) t_b \quad (3.26)$$

8. **Engine maintenance:** The engine maintenance cost for turbine engines is calculated in much the same way as the airframe maintenance cost (Liebeck et al., 1995). It uses correlations in terms of the engine maximum thrust.

$$C_{ML} = (0.645 + (0.05T_0/10^4)) (0.566 + 0.434/t_b) R_L \quad (3.27)$$

$$C_{MM} = ((25 + (18T_0/10^4)) (0.62 + 0.38/t_b) (\text{CEF})) \quad (3.28)$$

$$(3.29)$$

Where the base year is 1993. T_0 is the engine maximum thrust in lbs. R_L is the maintenance labor rate in USD/hr.

For turboprop engines, we can use [Roskam \(1989, Part VIII, Chapter 5\)](#):

$$C_{ML} = 1.03 \cdot 1.3 \left(0.4956 + 0.0532 \frac{(SHP_{TO}/n_{engines})}{1000} \frac{1100}{H_{em}} + 0.1 \right) R_L \quad (3.30)$$

where SHP_{TO} is the takeoff shaft horsepower and H_{em} is the number of hours between engine overhauls (usually between 3,000 to 5,000).

The total engine maintenance cost is multiplied by the number of engines n_{eng} :

$$C_{\text{engine maintenance}} = n_{engines} (C_{ML} + C_{MM}) t_b \quad (3.31)$$

For electric motors and batteries, we will assume that the maintenance costs are negligible. However, replacement will be necessary so they will contribute to depreciation costs. The cost of an electric motor can be roughly estimated using the following specific cost (base year 2018)

$$c_{\text{motors}} = 150/\text{hp}, \quad (3.32)$$

and the cost of batteries can be estimated using (base year 2018)

$$c_{\text{batteries}} = 520/\text{kWh}. \quad (3.33)$$

These numbers are from on ‘A study in reducing the cost of vertical flight with electric propulsion’ by Michael J. Duffy et al (2017). Also, we can roughly estimate the price of an electric aircraft as

$$C_{\text{electric aircraft}} = C_{\text{aircraft}} - C_{\text{engines}} + C_{\text{motors}} + C_{\text{batteries}} \quad (3.34)$$

where C_{aircraft} and C_{engines} are computed using the formulas for non-electric aircraft given in the previous pages.

3.4.2 Fixed Operating Cost

- Insurance:** The insurance cost is an annual cost and is expressed in terms of the aircraft initial cost. It requires the calculation of a term called *annual utilization*, U_{annual} , which represents how much the aircraft is used annually, expressed in hours. If the annual utilization is unknown, it maybe be estimated as ([Roskam, 1989, Part VIII](#)):

$$U_{\text{annual}} = 1.5 \times 10^3 \left[3.4546 t_b + 2.994 - (12.289 t_b^2 - 5.6626 t_b + 8.964)^{0.5} \right] \quad (3.35)$$

The insurance cost is then calculated using the ATA method ([Kroo, Ch. 13](#)):

$$C_{\text{insurance}} = \left(\frac{\text{IR}_a C_{\text{aircraft}}}{U_{\text{annual}}} \right) t_b \quad (3.36)$$

where IR_a is the hull insurance rate, usually assumed to be 2% ([Kroo, Ch. 13](#)).

- Financing:** This is the interest applied on the initial loan used to buy the aircraft. This can be computed using the aircraft price, interest rates, estimates for spares, etc. According to [Roskam \(1989, Part VIII, Chapter 5\)](#), this can be very roughly estimated as 7% of the DOC.

- 11. Depreciation:** This is the allocation of the purchase price over the life of the aircraft, explained by [Raymer \(2006, p. 592\)](#) and similarly in [Harris \(2005\)](#):

$$C_{\text{depreciation}} = \frac{C_{\text{unit}} (1 - K_{\text{depreciation}}) t_b}{n (U_{\text{annual}})} \quad (3.37)$$

where $K_{\text{depreciation}}$ is the aircraft residual value factor (usually something small around 0.1), which estimates the depreciated value over the lifetime, and n is the number of years the aircraft is used.

For electric aircraft we assumed that maintenance costs for motors and batteries were negligible. However, we have to consider their replacement costs which we will include in the depreciation cost. For this, use the costs for the batteries and motors, and estimates for how often they need to be replaced (which is not the same as the life of the aircraft). We can assume that the batteries need to be replaced roughly every 7,500 cycles and the motors every 6,000 hours (from ‘A study in reducing the cost of vertical flight with electric propulsion’ by Michael J. Duffy et al (2017)). Make sure not to double count depreciation costs for the electric motors and batteries in the aircraft depreciation cost.

- 12. Registration taxes:** This is the tax paid by the customer to register the aircraft, and is expressed as a fixed percentage of the maximum takeoff weight, as well as a fraction of all prior costs.

$$C_{\text{registration}} = (0.001 + 10^{-8} \text{ MTOW}) \text{ DOC} \quad (3.38)$$

where DOC refers to the sum of all previous costs.

The total DOC is the sum of all twelve costs shown above. The historical trend for DOC is shown in Fig. 3.3; you can see that DOC has reduced by about 70% since the early 60s.

3.4.3 Indirect Operating Cost

The indirect operating cost (IOC) depends very little on the aircraft design, and any computation of IOC is at best a rough estimate. The methods below are based on approximate correlations and curve-fit equations. Note that the following costs are expressed in USD/hr. IOC is divided into the following components:

- 1. Servicing:** This is composed of all costs related to servicing the aircraft. It is indirectly related to the mission, and is dependent on the number of passengers n_{pax} and block time t_b .

$$C_{\text{serv}} = (0.285 + 0.0025) \left(\frac{n_{\text{pax}}}{t_b} \right) \text{ (CEF)} \quad (3.39)$$

where the base year for the CEF is 1976.

- 2. Food:** This is the cost for mission food supplies, that can involve a number of externalities.

$$C_{\text{food}} = 1.05 \left[2.42 \left(\frac{n_{\text{pax}}}{1 + R_p} \right) + \frac{n_{\text{pax}} R_p}{1 + R_p} \right] \text{ (CEF)} \quad (3.40)$$

where R_p is the passenger distribution ratio

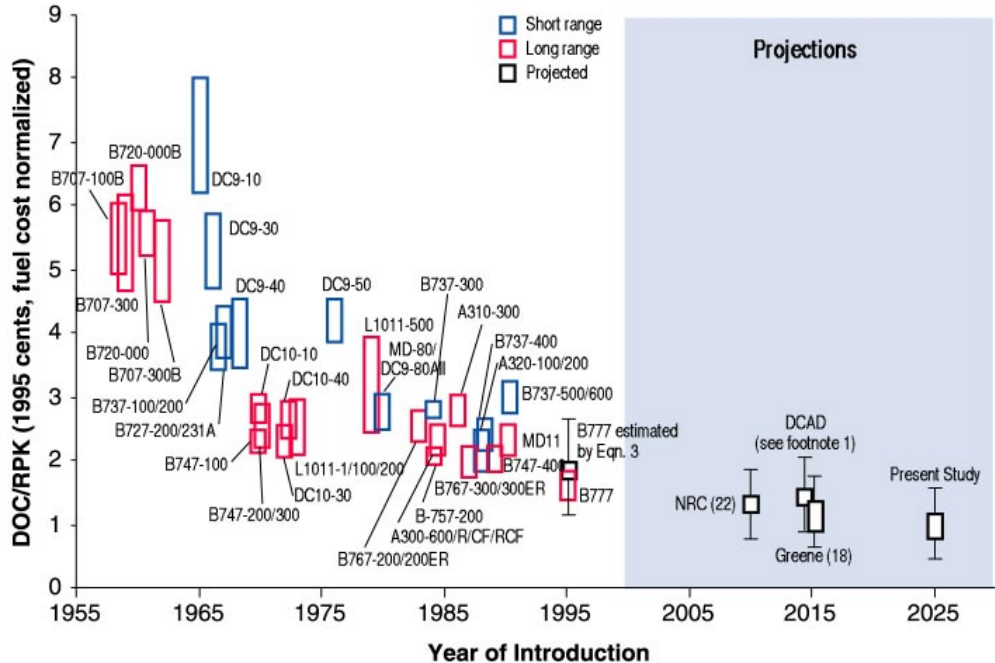


Figure 3.3: Historical trends of DOC per revenue passenger-kilometer (RPK) for short- and long-range aircraft [Lee et al. \(2001\)](#)

3. **Entertainment:** This involves the cost in procuring media and related material for in-flight entertainment. It is expressed in terms of block time:

$$C_{\text{ent}} = \frac{196}{t_b} \text{ (CEF)} \quad (3.41)$$

4. **Liability insurance:** This is an additional insurance cost incurred by the airline that covers passenger liability. It is proportional to number of passengers and the aircraft range.

$$C_{\text{pax ins}} = 0.52 \left(\frac{n_{\text{pax}} \text{ PLF } R}{1000 t_b} \right) \text{ (CEF)} \quad (3.42)$$

where PLF is the passenger load factor, which is a measure of how much of the aircraft's carrying capacity is used during a mission. R is the range of the aircraft.

5. **Payload handling:** This includes the passenger, baggage and cargo handling costs. It involves the passenger load factor, PLF, block time, and the cargo weight.

$$C_{\text{paxh}} = 2.87 \left(\frac{n_{\text{pax}} \text{ PLF}}{t_b} \right) \text{ (CEF)} \quad (3.43)$$

$$C_{\text{bagh}} = 1.31 \left(\frac{n_{\text{pax}} \text{ PLF}}{t_b} \right) \text{ (CEF)} \quad (3.44)$$

$$C_{\text{cargh}} = 131.08 \left(\frac{W_{\text{cargo}}}{2000 t_b} \right) \text{ (CEF)} \quad (3.45)$$

where C_{paxh} , C_{bagh} , C_{cargh} are the passenger, baggage and cargo handling costs respectively. The total handling cost is the sum of these costs.

$$C_{\text{payload handling}} = C_{\text{paxh}} + C_{\text{bagh}} + C_{\text{cargh}} \quad (3.46)$$

6. Marketing: This is amount spent on airline marketing of the aircraft to prospective passengers through publicity and advertising. It includes the reservation and sales cost, and the publicity cost.

$$C_{\text{res}} = 4.4 \left(\frac{n_{\text{pax}} \text{PLF}}{t_b} \right) (\text{CEF}) \quad (3.47)$$

$$C_{\text{pub}} = 0.023 \left(\frac{R C_f n_{\text{pax}} \text{PLF}}{t_b} \right) (\text{CEF}) \quad (3.48)$$

where R is the aircraft range, and C_f is the ticket fare price factor (in USD/pax-nmi). The total marketing cost is:

$$C_{\text{marketing}} = C_{\text{res}} + C_{\text{pub}} \quad (3.49)$$

7. Administrative: This is the final component of IOC, which includes all general costs and commissions involved in the continued operation of the aircraft for a particular mission.

$$C_{\text{comm}} = 2.35 \left(\frac{n_{\text{pax}} \text{PLF} R}{1000 t_b} \right) (\text{CEF}) \quad (3.50)$$

$$C_{\text{gen}} = \left(\frac{0.18 n_{\text{pax}}}{t_b} \right) (\text{CEF}) \quad (3.51)$$

The total administrative cost is thus:

$$C_{\text{admin}} = C_{\text{comm}} + C_{\text{gen}} \quad (3.52)$$

The total IOC is the sum of the seven components described above. It involves a high degree of uncertainty due to the empirical nature of the relations and the variability of aircraft types and customer intent. For most purposes, at the initial design stage, a rough estimate of this cost is sufficient.

Bibliography

Franklin D. Harris. An economic model of U.S. airline operating expenses. Technical Report CR-2005-213476, NASA Ames Research Center, Moffett Field, CA 94035, Dec 2005.

Lloyd R. Jenkinson, Paul Simpkin, and Darren Rhodes. *Civil Jet Aircraft Design*. Arnold, 1999.

Ilan M. Kroo. Aircraft design: Synthesis and analysis. URL <http://adg.stanford.edu/aa241/AircraftDesign.html>.

Joosung J. Lee, Stephen P. Lukachko, A. Waitz, and Andreas Schafer. Historical and future trends in aircraft performance, cost, and emissions. *Annual Review of Energy and the Environment*, 26: 167–200, 2001.

R. H. Liebeck, D. A. Andrastek, J. Chau, R. Girvin, R. Lyon, B. K. Rawdon, P. W. Scott, and R. A. Wright. Advanced subsonic airplane design and economic studies. Technical Report CR-195443, NASA, April 1995.

Leland M. Nicolai and Grant E. Carichner. *Fundamentals of Aircraft and Airship Design, Vol I — Aircraft Design*. AIAA, Reston, VA, 2010.

Daniel P. Raymer. *Aircraft Design: A Conceptual Approach*. AIAA, 4th edition, 2006.

J. Roskam. *Airplane Design, Volumes 1-8*. Roskam Aviation and Engineering Corporation, 1989.

R. D. Schaufele. *The Elements of Aircraft Preliminary Design*. Aries Publications, 2007.

Chapter 4

Preliminary Sizing

The preliminary sizing is performed by making sure that the critical requirements that drive the design **are** satisfied. These requirements are:

- Minimum stall speed
- Maximum take-off and landing distance
- Minimum rate of climb
- Ability to maneuver
- Ability to reach cruise speed

There are a number of design parameters that could be considered that affect the metrics involved in these requirement, but because we are doing a preliminary sizing, we want to restrict the parameters to the most significant ones.

The wing loading (W/S) and thrust-to-weight ratio (T/W) are two such parameters. They size the wing planform area, and the engine, respectively.

Note that for propeller aircraft, we would consider the power-to-weight ratio, P/W . Here we assume a gas turbine engine, for which T/W is preferred, without loss of generality.

To meet the above requirements, we will express all of them in terms of W/S and T/W . Since each of the requirements corresponds to an inequality constraint in $W/S - T/W$ space, satisfying all the requirements will restrict the combinations of these two parameters to a region in that space. The result will be a plot that clearly shows what combinations of W/S and T/W that make the aircraft feasible. You will then try to choose the best point in that feasible space. It will be a preliminary optimization.

The $W/S - T/W$ plot showing the feasible space is convenient because no iterative process is required. However, choosing a point in this plot only gives you these ratios but not the actual aircraft weight, thrust, and wing area. Therefore, we will also learn how to make a $S - T$ (or $S - P$) plot (see Chapter ??). In this plot, in addition to the wing area and thrust, each point will correspond to an aircraft with a converged weight. We then have enough information to compute other performance metrics that can be overlaid as contours.

The other major design parameters that come into play at this preliminary stage are the aircraft $C_{L_{\max}}$ and the aspect ratio, AR , which are estimated based on historical data and assumptions on your configuration.

4.1 Wing Loading

The wing loading, W/S , is an important parameter for anything that has wings and represents the average lift per unit planform area. Since weight W usually changes during flight due to fuel burn, we use the takeoff weight, W_0 , in the wing loading calculation. Thus, this is actually the *takeoff wing loading*, but we will simply refer to it as wing loading. Therefore, you will need to convert all wing loading values to takeoff conditions. For example, suppose that you are in the landing phase, and $W = W_5$, then

$$\left(\frac{W}{S}\right)_0 = \left(\frac{W_5}{S}\right) \left(\frac{W_0}{W_5}\right). \quad (4.1)$$

The wing area S is defined to be the reference wing area, S_{ref} , which represents the area of the simplest trapezoid that approximates the shape of the actual wing extended to the aircraft centerline, as shown in Fig. 4.1. For more complex unconventional planform shapes, this definition might become somewhat arbitrary, so be careful when comparing the wing loading of these planforms against conventional ones.

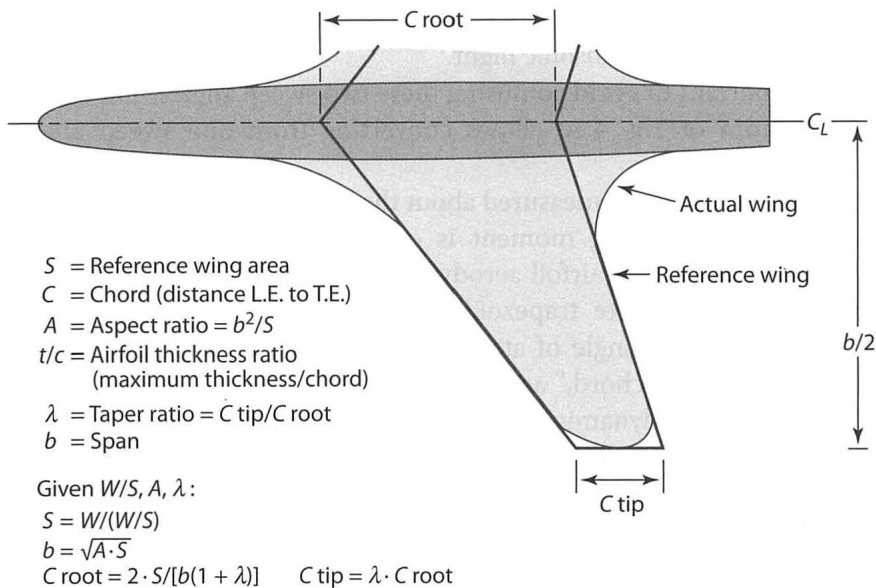


Figure 4.1: Definition of reference wing area (Raymer, 2012, Fig. 4.15)

The wing loading can be expressed as a function of lift coefficient, air density and speed:

$$W = L = \frac{1}{2} \rho V^2 S C_L \Rightarrow \boxed{\frac{W}{S} = \frac{1}{2} \rho V^2 C_L}. \quad (4.2)$$

Higher wing loading (smaller wing) generally means:

- Higher stall speed
- Longer takeoff and landing distances
- Poorer maneuvering performance
- Lower drag, weight, and cost

Type	W/S [lbs/ft ²]	Example
Competition sailplanes	6–12	Schleicher ASW 17
Light aircraft with short range and field length	1–30	Cessna 172
Air-to-air fighters	50–80	F-22
Long-range transports	110–150	Boeing 777
Interceptor fighters	120–150	F-104
Low-altitude subsonic cruise missiles	200–240	Konsberg NSM

Table 4.1: Typical wing loading values for various aircraft types

The first three items are undesirable, but the last one is a combination of desirable attributes. Thus W/S must be picked carefully to offer the right tradeoff between all these attributes, depending on what the objective and requirements are for the aircraft being designed. [Raymer \(2012, Table 5.5\)](#) and [Nicolai and Carichner \(2010, Table 6.1\)](#) list typical wing loading values for various types of aircraft.

It is useful to think about how wing loading varies with the linear dimension of an aircraft (or bird). The linear dimension that is significant when it comes to lift is the span, b . Assuming the volume (and therefore the weight) increases cubically with the linear dimension, we have $W \propto b^3$. The wing area increases quadratically with span, so $S \propto b^2$. This means that $W/S \propto b$. Since $b \propto W^{1/3}$, we have that

$$\frac{W}{S} \propto W^{1/3}. \quad (4.3)$$

Therefore, heavier vehicles tend to have higher wing loadings. They also tend to fly at higher speeds, since Eq. (4.2) yields,

$$V = \sqrt{\frac{2}{\rho C_L}} \left(\frac{W}{S} \right)^{1/2} \quad (4.4)$$

Fig. 4.2 shows a log-log plot of the weight versus wing loading for various insects, birds and airplanes.

Another interesting thing to observe is the required power to fly as a function of wing loading:

$$P = TV = DV = \frac{1}{2} \rho C_D S V^3 = \frac{1}{2} \rho C_D S \left(\frac{2W}{\rho C_L S} \right)^{3/2} \Rightarrow P \propto W \sqrt{\frac{W}{S}} \quad (4.5)$$

This explains why the lowest wing loading airplanes in Fig. 4.2 are the human and solar powered ones. There is, however, a lower limit to this trend: the weight of the wing as well as the increased drag coefficient due to low Reynolds number eventually catches up.

4.2 Thrust-to-Weight Ratio

The thrust-to-weight ratio, T/W is another important measure of aircraft performance. An aircraft with higher T/W accelerates more quickly, climbs faster, and has a higher maximum speed. On the other hand, higher thrust engines are heavier and burn more fuel, affecting the takeoff weight adversely.

Both the thrust and the weight vary during flight. As we will see later, the thrust varies with altitude and speed. Unless otherwise stated, the thrust value corresponds to the maximum value at

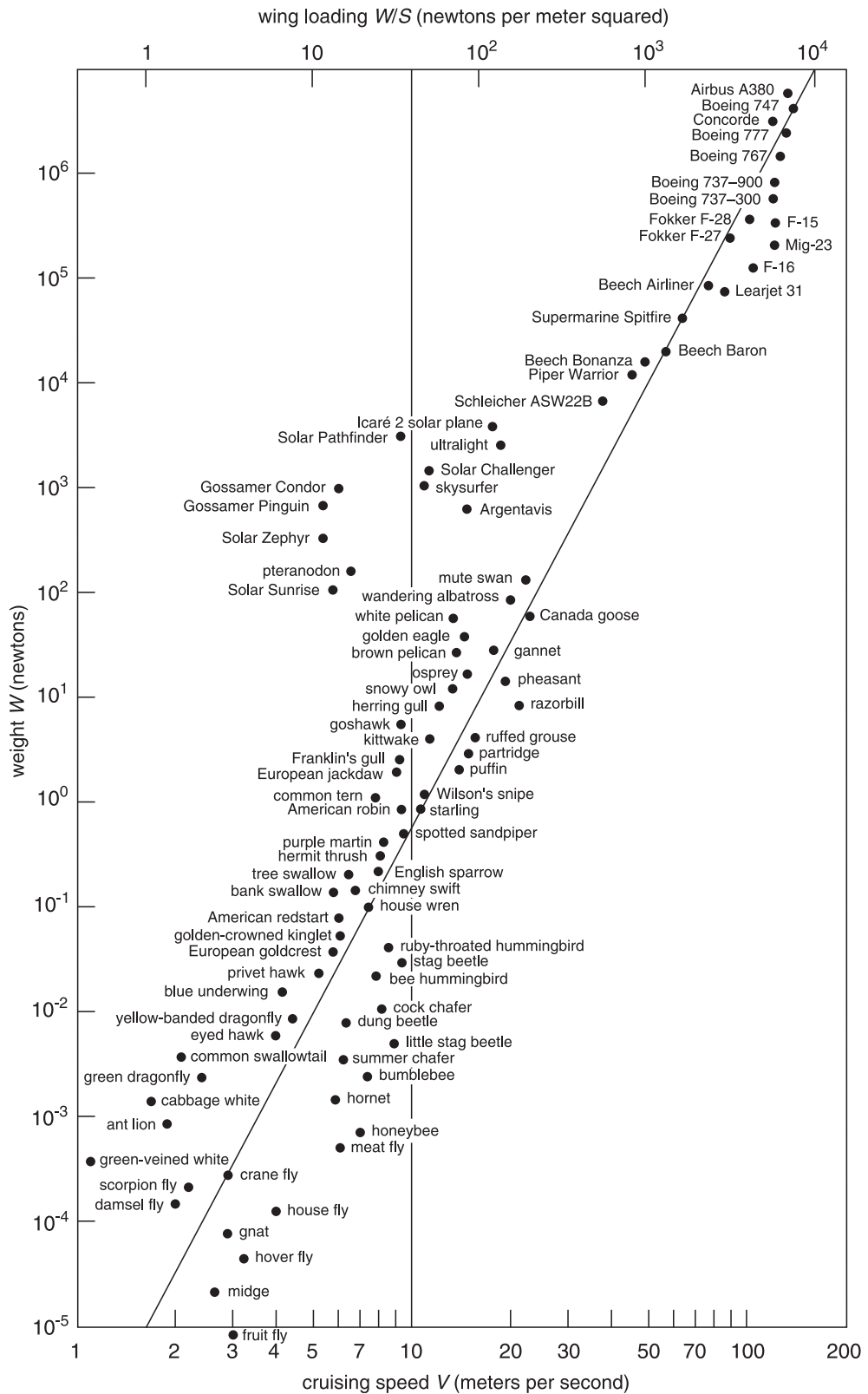


Figure 4.2: Weight vs. wing loading for various animals and aircraft (Tennekes, 2009, Fig. 2).

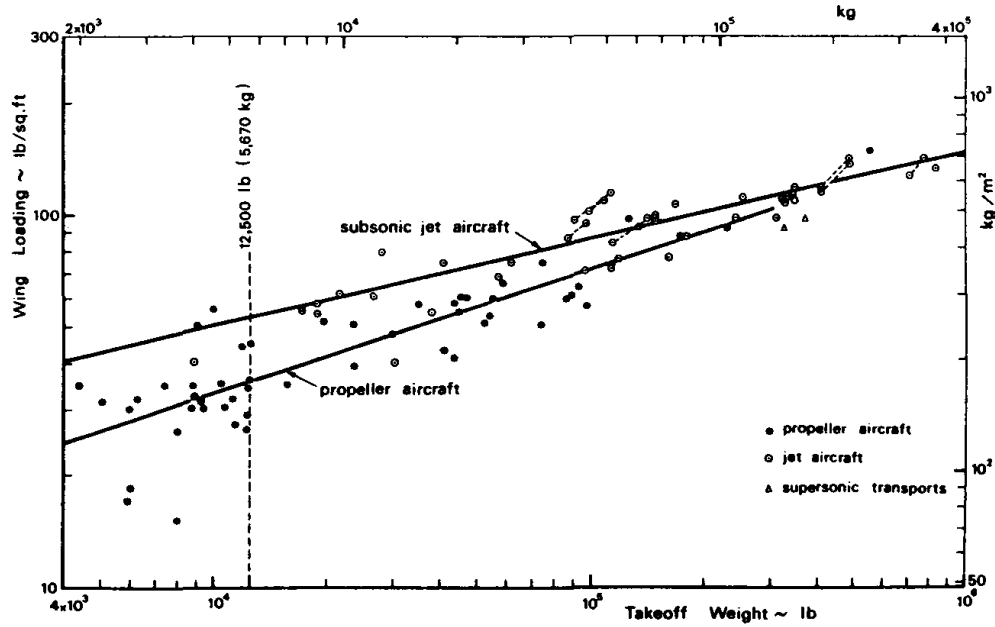


Figure 4.3: Wing loading trend with takeoff weight ([Torenbeek, 1990](#), Fig. 7.4).

sea-level-static (SLS) conditions. As in the case of wing loading, it is important to convert T/W to a standard condition (takeoff SLS in this case). As an example, to convert from cruise conditions,

$$\left(\frac{T}{W}\right)_0 = \left(\frac{T_3}{W_3}\right) \left(\frac{W_3}{W_0}\right) \left(\frac{T_0}{T_3}\right). \quad (4.6)$$

[Raymer \(2006, Table 5.1\)](#) lists typical T/W values for different types of aircraft.

Note that for propeller aircraft, we usually use *power loading*, P/W , instead. However, this can be converted to an equivalent T/W (see [Raymer \(2006, Sec. 5.2\)](#)).

4.3 Drag Polar Estimate

Drag polars — functions that give the drag coefficient as a function of the lift coefficient — are required for several of the sizing procedures. In this section we explain how to obtain a simple drag polar based on the limited information we have so far and historical data. Later on, when more details are known, we will have a better method to produce the drag polar based on the drawing and drag buildup calculations.

You should be aware that the drag polar changes with Reynolds number, Mach number, and geometry. Therefore, there will be different drag polars for the various flight stages. Between takeoff, cruise and landing, not only do the Reynolds number and Mach number change, but more significantly, the geometry changes considerably when using high-lift systems and retractable landing gear.

Assuming a parabolic drag polar, we have

$$C_D = C_{D_0} + \frac{C_L^2}{\pi A Re} \quad (4.7)$$

where C_{D_0} is the parasite drag coefficient, and e is the span efficiency factor (also known as the Oswald efficiency factor). The parasite drag coefficient can be written as,

$$C_{D_0} = C_f \frac{S_{\text{wet}}}{S} \quad (4.8)$$

Where the ratio of wetted area to wing reference area can be found using Figure 2.5 (Raymer (2006, Figure 3.6))

The first step in estimating the parasite drag coefficient is to get an approximate value for the wetted area. Since we still do not have a drawing of the aircraft configuration, and might not even have its overall dimensions, we resort to historical data. Roskam (1989, Eqn.(3.22), Vol. 1) provides an approximate relationship between the wetted area and the takeoff weight,

$$S_{\text{wet}} = 10^c W_0^d, \quad (4.9)$$

where c and d are configuration dependent regression constants. A list for the values of these constants is given in Roskam (1989, Table 3.5, Vol. 1). For transport jets, $c = 0.0199$ and $d = 0.7531$. This regression is shown to result in a wetted area within a $\pm 10\%$ band of actual aircraft.

The next step is to get an estimate for the wing reference area, S . Fig. 4.3 can be used for this. Now we need the equivalent parasite area, f . This can be estimated using Eq. (??) and the equivalent skin friction estimates for a range of aircraft types listed in Fig. 4.4.

$C_{D_0} = C_{f_e} (S_{\text{wet}}/S_{\text{ref}})$	C_{f_e}
Bomber	0.0030
Civil transport	0.0026
Military cargo (high upsweep fuselage)	0.0035
Air Force fighter	0.0035
Navy fighter	0.0040
Clean supersonic cruise aircraft	0.0025
Light aircraft—single engine	0.0055
Light aircraft—twin engine	0.0045
Prop seaplane	0.0065
Jet seaplane	0.0040

Figure 4.4: Equivalent skin friction coefficients (Raymer, 2012, Table 12.3).

To construct the drag polar, we also need to know how C_{D_0} and span efficiency change with the takeoff and landing high-lift system settings. Table 4.2 lists approximate values for these parameters.

Example 4.1: Drag Polar for a business jet Find the clean, takeoff, and landing drag polars for a business jet airplane with a gross take-off weight of 10,000 lbs and a takeoff wing loading of 75 psf.

Using the business jet coefficients in the wetted area regression Eq. (4.9), we estimate the wetted area to be

$$S_{\text{wet}} = 10^{0.2263} \times 10000^{0.6977} = 1040 \text{ ft}^2. \quad (4.10)$$

We then assume $C_f = 0.0030$ (somewhere between the civil aircraft and twin engine light aircraft C_f estimates from Fig. 4.4) to get the equivalent parasite area,

$$f = 0.003 \times 1040 = 3.12 \text{ ft}^2. \quad (4.11)$$

Configuration	ΔC_{D_0}	e
Clean	0	0.80–0.85
Takeoff flaps	0.010–0.020	0.75–0.80
Landing flaps	0.055–0.075	0.70–0.75
Landing gear	0.015–0.025	no effect

Table 4.2: Approximate values for drag coefficient increase and span efficiency for different flight configurations (Roskam, 1989, Part I, Table 3.6)

Based on this, C_{D_0} for a clean configuration can be calculated to be

$$C_{D_0} = \frac{3.12}{10000/75} = 0.0234 . \quad (4.12)$$

Assuming a typical aspect ratio ($AR = 10$) and using values from Table 4.2, we can get the following five drag polars for different configurations:

Clean	$C_D = 0.0234 + 0.0374 C_L^2$
Takeoff flaps, gear up	$C_D = 0.0334 + 0.0398 C_L^2$
Takeoff flaps, gear down	$C_D = 0.0484 + 0.0398 C_L^2$
Landing flaps, gear up	$C_D = 0.0784 + 0.0424 C_L^2$
Landing flaps, gear down	$C_D = 0.0934 + 0.0424 C_L^2$

4.4 Stall Speeds

The stall speeds are an important factor in flying safety. One of the reasons for this is that they determine the takeoff, approach, and landing speeds. The higher the approach and landing speeds, the more challenging it is to land the aircraft, and the higher the kinetic energy after touchdown. These speeds are specified by requirements or rules, and are required to be a certain fraction above the stall speeds. For civil aircraft, the takeoff speed is about 1.1 times the stall speed with takeoff flap settings, the approach speed is usually 1.3 times the stall speed with approach flap settings, and the landing speed is about 1.15 times the stall speed with landing flap settings (Raymer, 2012, Sec. 5.3.3 and Sec. 5.3.5).

Recall that we aim to write all the requirements related metrics as functions of W/S and T/W so that we can determine what combinations of those values are feasible. To achieve this for the stall speed, we write

$$W = L = \frac{1}{2} \rho V_{\text{stall}}^2 S C_{L_{\max}} \Rightarrow \boxed{\frac{W}{S} = \frac{1}{2} \rho V_{\text{stall}}^2 C_{L_{\max}}} \quad (4.13)$$

were the $C_{L_{\max}}$ is the maximum lift coefficient of the aircraft (changes with flap settings). This coefficient is challenging to compute accurately due to the nonlinear behavior of stall. A rough estimate can be obtained from Raymer (2006, Fig. 5.3). For a double-slotted flap and slat configuration and a 30 deg sweep, for example, $C_{L_{\max}} \approx 2$. The calculation of a more precise value that takes into account the size of the flaps and slats will be explained latter on.

Note that Eqn. (4.13) defines a line of constant wing loading, to the right of which it is not possible to obtain the required stall speed for the given $C_{L_{\max}}$.

4.5 Takeoff Field Length

There are various distances related to takeoff. The *ground roll* is the distance traveled from brake release to when the wheels leave the ground. The *obstacle clearance distance* is the distance required to takeoff and clear an obstacle of specified height. For the case of commercial aircraft, this distance is 35 ft.

The *balanced field length* (BFL) is the total field length required for safety in the event of a one engine failure at the worst possible time during takeoff. As the speed increases during takeoff, the distance required for braking to a complete stop increases, and the distance left to takeoff decreases. At the *decision speed*, the distance required to takeoff with one engine out is equal to the distance required to brake to a stop. Thus, when an engine fails below the decision speed, the pilot should abort the landing, and if it fails above the decision speed, the pilot should proceed with the takeoff and turn around to land. This is because above the decision speed, the distance required to brake would be greater than to proceed with the takeoff, even with one engine out. The BFL is the total distance required to takeoff and clear the obstacle when one engine fails at the decision speed. This length must not exceed the available field length of the airfield, where the aircraft is required to operate, that provides the most limiting combination of air density and available field length.

4.5.1 Sizing to FAR 25 requirements for jet transport aircraft

Both W/S and T/W contribute to the BFL. A lower W/S means a lower stall speed and thus a shorter BFL. A higher T/W results in greater acceleration and thus a shorter BFL. In order to compute the BFL accurately, we must perform a time integration with time-varying lift, drag and rolling resistance. The FAR requires that the worst of either BFL or a value 15 % greater than the all-engines-operating takeoff distance be met (Raymer, 2012, Sec. 5.3.3). For now, however, we will use a quicker estimate based on the *takeoff parameter* (TOP), defined as

$$\text{TOP}_{25} = \frac{W/S}{(\rho/\rho_{\text{SL}})C_{L_{\max}}T/W}, \quad (4.14)$$

where ρ is the air density expected at the field, and ρ_{SL} is the sea level standard value (Roskam, 1989, Eqn.(3.7)). Roskam (1989, Eqn.(3.8)) gives the following linear relationship for the TOP for FAR 25 aircraft,

$$\text{TOP}_{25} = \text{BFL}/37.5 \quad (4.15)$$

Rearranging Eq. (4.14) to write T/W as a function of W/S we get,

$$\frac{T}{W} = \frac{W/S}{(\rho/\rho_{\text{SL}})C_{L_{\max}}\text{TOP}_{25}}. \quad (4.16)$$

Given a BFL requirement, we can compute TOP_{25} from Eq. (4.15) and use it in Eq. (4.16) to relate T/W and W/S . This defines a sloped straight line in T/W - W/S space below which the takeoff field length requirement is not met. For a more detailed method for estimating takeoff distance, see Jenkinson et al. (1999, Eqs. (10.12, 10.13)) or Anderson Jr. (1999, Sec. 6.7).

4.5.2 Sizing to FAR 23 requirements for propeller aircraft

FAR 23 aircraft are usually propeller driven and are not required to meet a BFL requirement by the FAR. Their takeoff distance is proportional to the takeoff wing loading, W/S , the takeoff power

loading, W/P , and the maximum takeoff coefficient of lift, $C_{L_{\max}}$. The takeoff parameter can be defined as

$$\text{TOP}_{23} = \frac{W/S}{(P/W)(\rho/\rho_{SL})C_{L_{\max}}}. \quad (4.17)$$

Using data from existing single and twin engine FAR 23 aircraft, Roskam (1989, Part I, Chapter 3) provides the following relation that can be used to approximate the takeoff distance.

$$s_{TO} = 8.134\text{TOP}_{23} + 0.0149\text{TOP}_{23}^2 \quad (4.18)$$

where s_{TO} is the takeoff distance in ft and TOP_{23} is in $\text{lbs}^2/(\text{ft}^2\text{hp})$. This quadratic equation can be used to solve for the required P/W given a takeoff distance. For jet-powered FAR 23 aircraft, see Roskam (1989, Part I, Chapter 3).

4.6 Landing Field Length

The landing distance depends on landing weight, approach speed and deceleration method, which could include brakes, thrust reversers, parachutes, arresting systems and crash barriers. The approach speed for civil aircraft must be 1.3 times the stall speed.

The *total landing distance* is defined as the distance required to clear a 50 ft obstacle clearance at approach speed prior to touchdown, and then come to a complete stop. The FAR 25 *landing field length* is the total landing distance plus a 2/3 safety margin.

Raymer (2006, Eqn. (5.11)) gives the following approximation for the landing distance (in ft),

$$s_{\text{land}} = 80 \frac{W}{S} \left(\frac{1}{(\rho/\rho_{SL})C_{L_{\max}}} \right) + s_a \quad (4.19)$$

where the first term represents the ground roll, and the second one is the obstacle-clearance distance. For airliner-type aircraft $s_a = 1000$ ft, and for general aviation type aircraft $s_a = 600$ ft. This landing distance must be multiplied by 1.67 to obtain the FAR 25 landing field length. Note that only the brakes are allowed in the estimate above (no thrust reversers), according to FAR 25. The extra factor is not required for FAR 23 aircraft.

Eq. 4.19 can be rearranged to obtain an equation for the wing loading (W/S). As in the case of the stall requirement, the landing distance is independent of T/W or P/W and therefore this requirement corresponds to a line of constant W/S to the right of which it is not possible to meet the requirement. The line can be moved to the right by increasing $C_{L_{\max}}$.

4.7 Climb

Takeoff climb starts at lift-off and finishes 1,500 ft above the runway. When the aircraft climbs after takeoff, it goes through three different configurations: flaps down and gear down, flaps down and gear up, and flaps up and gear up.

4.7.1 Climb requirements for jet-powered aircraft

The climb gradient, G is the ratio between vertical and horizontal distance traveled. For small angles, from equilibrium in the direction of the aircraft velocity we have

$$T = D + GW \Rightarrow \frac{T}{W} = \frac{D}{W} + G \quad (4.20)$$

If we assume $L = W$, which is approximately the case for small climb gradients, then (Roskam, 1989)

$$\frac{T}{W} = \frac{1}{L/D} + G \quad (4.21)$$

where L/D can be obtained from the drag polar. This gives an estimate for the T/W required for climb that does not depend on W/S . Using the parabolic drag polar from Sec. 4.3 we can rewrite this as,

$$\frac{T}{W} = \frac{C_{D_0} + \frac{C_L^2}{\pi A Re}}{C_L} + G \quad (4.22)$$

Also, for the different climb segments, we can write the coefficient of lift as,

$$C_L = \frac{C_{L_{max}}}{k_s^2} \quad (4.23)$$

where $C_{L_{max}}$ is the maximum coefficient of lift for the climb configuration and k_s is that ratio of the flight speed in the climb segment to the stall speed. By substituting Eqn. (4.23) in Eqn. (4.22) we get,

$$\frac{T}{W} = \frac{k_s^2}{C_{L_{max}}} C_{D_0} + \frac{C_{L_{max}}}{k_s^2 \pi A Re} + G \quad (4.24)$$

The thrust to weight ratio obtained from this equation needs to be further corrected as follows,

$$\left(\frac{T}{W} \right)_{takeoff} = \left(\frac{1}{0.8} \right) \left(\frac{1}{0.94} \right) \left(\frac{N_{engines}}{N_{engines}-1} \right) \left(\frac{W}{W_{takeoff}} \right) \left(\frac{T}{W} \right) \quad (4.25)$$

The first correction factor, $(\frac{1}{0.8})$, corresponds to the loss of thrust due to a 50 F increase over the standard temperature. The second correction factor, $(\frac{1}{0.94})$, is the ratio between maximum thrust and maximum continuous thrust (use this ratio only if the climb phase requires maximum continuous thrust). The third correction factor, $(\frac{N_{engines}}{N_{engines}-1})$, is used for the one engine inoperative (OEI) conditions. The fourth correction factor, $(\frac{W}{W_{takeoff}})$, accounts for changes in weight. This is important for the balked landing climbs, when the maximum landing weight is used instead of the takeoff weight.

The following lists the FAR 25 climb requirements (Roskam, 1989). See ecfr.gov for more details and up-to-date requirements.

1. FAR 25.111 (takeoff climb)

- OEI. Remaining engines at takeoff thrust or power.
- $G \geq 1.2\%$ (two-engine airplanes)
- $G \geq 1.5\%$ (three-engine airplanes)
- $G \geq 1.7\%$ (four-engine airplanes)
- Takeoff flaps, landing gear deployed.
- $k_s = 1.2$
- Maximum takeoff weight

2. FAR 25.121 (transition segment climb)

- OEI. Remaining engines at takeoff thrust or power.
- $G \geq 0.0\%$ (two-engine airplanes)
- $G \geq 0.3\%$ (three-engine airplanes)
- $G \geq 0.5\%$ (four-engine airplanes)
- Takeoff flaps, landing gear deployed.
- $1.1 < k_s < 1.2$
- Maximum takeoff weight

3. FAR 25.121 (second segment climb)

- OEI. Remaining engines at takeoff thrust or power.
- $G \geq 2.4\%$ (two-engine airplanes)
- $G \geq 2.7\%$ (three-engine airplanes)
- $G \geq 3.0\%$ (four-engine airplanes)
- Takeoff flaps, retracted landing gear.
- $k_s = 1.2$
- Maximum takeoff weight

4. FAR 25.121 (enroute climb)

- OEI. Remaining engines at maximum continuous thrust or power.
- $G \geq 1.2\%$ (two-engine airplanes)
- $G \geq 1.5\%$ (three-engine airplanes)
- $G \geq 1.7\%$ (four-engine airplanes)
- Retracted flaps, retracted landing gear.
- $k_s = 1.25$
- Maximum takeoff weight

5. FAR 25.119 (balked landing climb)

- AEO (all engines operative).
- $G \geq 3.2\%$
- Landing flaps, landing gear deployed.
- $k_s = 1.3$
- Maximum landing weight

6. FAR 25.121 (balked landing climb)

- OEI. Remaining engines at takeoff thrust or power.
- $G \geq 2.1\%$ (two-engine airplanes)
- $G \geq 2.4\%$ (three-engine airplanes)
- $G \geq 2.7\%$ (four-engine airplanes)
- Approach flaps, landing gear deployed. Approximate the approach C_{D_0} as the mean of the landing and takeoff values. Approximate the approach $C_{L_{max}}$ as $0.85C_{L_{max,landing}}$.
- $k_s = 1.5$
- Maximum landing weight

4.7.2 Climb requirements for propeller aircraft

The climb gradient parameter (CGRP) ([Roskam, 1989](#), Part I, Chapter 3), defined as

$$\text{CGRP} = \frac{G + (L/D)^{-1}}{C_L^{1/2}} = \frac{18.97\eta_p(\rho/\rho_{SL})(P/W)}{(W/S)^{1/2}}, \quad (4.26)$$

can be used for sizing propeller aircraft. Here η_p is the propeller efficiency, P is in hp, and rest of the variables are in FPS units. Given a required climb gradient, G , this equation can be rearranged to write P/W as a function of W/S . This equation requires the C_L and L/D for the different climb configurations. [Roskam \(1989\)](#) recommends using a margin of 0.2 to the $C_{L_{\max}}$ corresponding to the climb configuration. The power-to-weight ratio obtained from this equation needs to be further corrected as follows:

$$\left(\frac{P}{W}\right)_{\text{takeoff}} = \left(\frac{N_{\text{engines}}}{N_{\text{engines}} - 1}\right) \left(\frac{W}{W_{\text{takeoff}}}\right)^{3/2} \left(\frac{P}{W}\right). \quad (4.27)$$

The first correction factor, $\left(\frac{N_{\text{engines}}}{N_{\text{engines}} - 1}\right)$, is used for the one engine inoperative (OEI) conditions. The second correction factor, $\left(\frac{W}{W_{\text{takeoff}}}\right)$, accounts for changes in weight. This is important for the balked landing climbs, when the maximum landing weight is used instead of the takeoff weight.

The following lists the FAR 23.2120 climb requirements for a Level 3 (maximum seating configuration of 7 to 9 passengers) low-speed (for airplanes with a V_{NO} and $V_{MO} \leq 250$ Knots Calibrated Airspeed (KCAS) and a $M_{MO} \leq 0.6$) airplane.

1. FAR 23.2120a (initial climb)

- AEO (all engines operative)
- $G \geq 4\%$
- Takeoff flaps, landing gear deployed.
- Maximum takeoff weight

2. FAR 23.2120b (one engine inoperative)

- OEI (one engine inoperative)
- $G \geq 1\%$
- Takeoff flaps, retracted landing gear.
- Maximum takeoff weight
- 400 ft above the takeoff surface

3. FAR 23.2120c (balked landing)

- AEO (all engines operative)
- $G \geq 3\%$
- Landing flaps, landing gear deployed.
- Maximum landing weight

See the FAR 23 requirements on [ecfr.gov](#) for other aircraft levels and up-to-date requirements. Note that the FAR 23 requirements changed after the Small Airplane Revitalization Act of 2013, which is why some requirements summarized in older books (e.g., [Roskam \(1989\)](#)) will be a little different.

4.8 Ceiling

Ceiling can be considered a special case of of the climb requirement. For the absolute ceiling, you would just need to set $G = 0$ in Eqn. (4.21). However, it is more realistic to require a nonzero climb gradient at the ceiling altitude otherwise it might prove challenging to climb up to the ceiling altitude in the first place. Eqn. (4.21) can also be written as,

$$\frac{T}{W} = \frac{qC_{D_0}}{W/S} + \frac{W}{S} \left(\frac{1}{q\pi A Re} \right) + G. \quad (4.28)$$

If a ceiling altitude and speed requirement is given, then we can compute the corresponding dynamic pressure, q , and use it in the above equation to obtain the required T/W as a function of W/S .

If we do not have specifications for ceiling altitude and speed, we obtain the minimum required T/W as follows. Differentiating Eq. (4.28) with respect to the dynamic pressure, q , and equating it to 0 gives the following:

$$q = \frac{W}{S} \sqrt{\frac{1}{C_{D_0} \pi A Re}}. \quad (4.29)$$

If we substitute Eqn. (4.29) in Eqn. (4.28), we get

$$\frac{T}{W} = 2 \sqrt{\frac{C_{D_0}}{\pi A Re}} + G. \quad (4.30)$$

Note that this gives the minimum T/W , so the corresponding dynamic pressure (Eq. (4.29)), depending on the wing loading, may be very low (i.e., corresponding to a very high altitude at cruise speeds).

4.9 Maneuver

There are various maneuver requirements, depending on the type of aircraft being designed and the requirements. For transports, this is usually not a requirement that results in an active constraint.

One common requirement is the *sustained turn*. This assumes a turn that the aircraft can perform indefinitely, without loosing speed or altitude. The sustained turn capability is usually expressed in terms of the load factor n (or “g’s”). In a sustained turn, speed is maintained, so $T = D$ and $L = nW$, so we can write,

$$n = \left(\frac{L}{W} \right) \left(\frac{T}{D} \right) \Rightarrow n = \left(\frac{T}{W} \right) \left(\frac{L}{D} \right) \quad (4.31)$$

To sustain the turn we need,

$$T = D = qSC_{D_0} + qS \frac{C_L^2}{\pi A Re} = qSC_{D_0} + \frac{n^2 W^2}{qS \pi A Re} \quad (4.32)$$

Dividing by W we get,

$$\frac{T}{W} = \frac{qC_{D_0}}{W/S} + \frac{W}{S} \left(\frac{n^2}{q\pi A Re} \right) \quad (4.33)$$

4.10 Cruise

4.10.1 For Jet-powered aircraft

The equations for the cruise requirement can be obtained by setting $n = 1$ in the maneuver equations. In this case, Eqn. (4.33) becomes,

$$\frac{T}{W} \equiv \frac{qC_{D_0}}{W/S} + \frac{W}{S} \left(\frac{1}{q\pi A Re} \right) \quad (4.34)$$

This gives the required thrust-to-weight ratio for the desired wing loading. As we will see later, each aircraft has an optimal wing loading depending on what we are trying to achieve. To obtain the best range performance for a jet, the wing loading is

$$\frac{W}{S} = q \sqrt{\frac{\pi A Re C_{D_0}}{3}} \quad (4.35)$$

Later we will derive similar expressions for best loiter performance and for propeller aircraft.

4.10.2 For propeller-powered aircraft

The power required to fly at some speed and altitude is given by

$$P = TV = 0.5\rho V^2 S C_D V. \quad (4.36)$$

For propeller aircraft, assuming that we are using FPS units, this can be written as

$$550 P \eta_p = 0.5\rho V^3 S C_D, \quad (4.37)$$

where P is the power in hp and 550 is the conversion factor from lb ft/s to hp. Assuming a quadratic drag polar we can write this as

$$P = \frac{qV S C_D}{550 \eta_p} = \frac{qV S (C_{D_0} + \frac{C_L^2}{\pi A Re})}{550 \eta_p}. \quad (4.38)$$

With the weight of the aircraft, W , we can replace C_L and further write this as

$$P = \frac{qV S (C_{D_0} + \frac{W^2}{q^2 S^2 \pi A Re})}{550 \eta_p}. \quad (4.39)$$

Dividing both sides by W gives

$$\frac{P}{W} = \frac{qV (C_{D_0} + \frac{(W/S)^2}{q^2 \pi A Re})}{550 \eta_p (W/S)}. \quad (4.40)$$

This can be used to relate the power-to-weight ratio to wing loading for a given cruise speed and altitude. To relate this back to the required power-to-weight ratio and wing loading at takeoff, we have to include the following corrections:

$$\frac{P}{W} = \left(\frac{qV (C_{D_0} + \frac{(W/S)^2 (W_{cruise}/W_{takeoff})^2}{q^2 \pi A Re})}{550 \eta_p (W/S)} \right) \left(\frac{P_{takeoff}}{P_{cruise}} \right). \quad (4.41)$$

P_{cruise} is usually around 75% to 80% of rated power.

4.11 Putting it All Together

For a given set of requirements (field lengths, climb, ceiling, cruise, etc.), we can express the thrust-to-weight ratio or power-to-weight ratio as a function of the wing loading. Now we can visualize these all the performance requirements in a single plot and establish what combinations of T/W and W/S satisfy all constraints. Each of the requirements will appear as a line in the $T/W-W/S$ or $P/W-W/S$ two-dimensional space, where any choice of these parameters must be on the correct side of these lines. We now illustrate this with the example below.

Example 4.2: Preliminary sizing of a 777-size long-range airliner

This example shows the preliminary sizing for a long-range aircraft based on the Boeing 777-200LR with GE90-110B engines. The results will be compared to the actual parameters for the 777-200LR listed in Table 4.3.

AR	9.8
Span	64.80 m (212 ft)
Wing area	427.8 m ² (4,605 ft ²)
MTOW	347,815 kg (766,800 lbs)
TO W/S	695.5 kg/m ² (142.45 lbs/ft)

Table 4.3: Parameters for the 777-200LR

Drag Polars

The first step is to estimate the aerodynamic properties of the aircraft, in particular, the drag polar. Using the transport jet coefficients in the wetted area regression Eq. (4.9), we estimate the wetted area to be

$$S_{\text{wet}} = 10^{0.0199} \times 766,800^{0.7531} = 28,291 \text{ ft}^2. \quad (4.42)$$

We then assume $C_f = 0.0026$ in Eq. (??) to get the equivalent parasite area,

$$f = 0.0026 \times 28,291 = 73.56 \text{ ft}^2. \quad (4.43)$$

Then, we can obtain the parasite drag coefficient.

$$C_{D_0} = \frac{f}{S} = 0.01597 \quad (4.44)$$

Given the aspect ratio ($AR = 9.8$), and span efficiency and ΔC_{D_0} values from Table 4.2, we can get all five drag polars and plot them as shown in Fig. 4.5 (note that the curves end at their assumed $C_{L_{\max}}$ values):

Clean	$C_D = 0.01597 + 0.03815C_L^2$
Takeoff flaps, gear up	$C_D = 0.03597 + 0.04054C_L^2$
Takeoff flaps, gear down	$C_D = 0.06097 + 0.04054C_L^2$
Landing flaps, gear up	$C_D = 0.09097 + 0.04324C_L^2$
Landing flaps, gear down	$C_D = 0.11597 + 0.04324C_L^2$

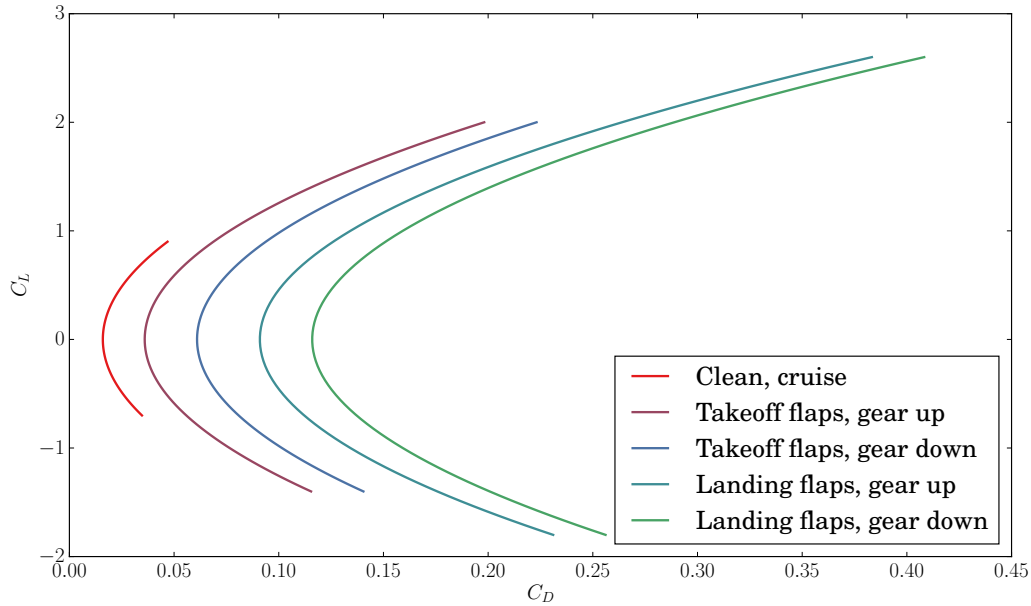


Figure 4.5: Drag polars for 777-sized airliner

Landing field length

Rearranging Eq. (4.19) for the wing loading, we get

$$\frac{W}{S} = \frac{(\rho/\rho_{SL})C_{L_{\max}}}{80} (S_{\text{land}} - S_a) \quad (4.45)$$

For the 777-200LR, the maximum landing to maximum takeoff weight ratio is approximately 0.65. We also assume a runway length of 12,000 ft and $\rho/\rho_{SL} = 0.95$ for a hot day near sea-level. To comply with FAR requirements, this runway length is multiplied by 0.6 to get the landing field length, S_{land} . This gives,

$$\frac{W}{S} = \frac{0.95C_{L_{\max}}}{80 \times 0.65} (12000 \times 0.6 - 1000) = 113.27C_{L_{\max}}, \quad (4.46)$$

where we have set $S_a = 1000$ ft (the number appropriate for airliners). Now, we need values for $C_{L_{\max}}$. Assume the following values (Roskam (1989, Table 3.1, Vol. 1) may be used as an initial reference):

- $C_{L_{\max, \text{cruise}}} = 0.9$
- $C_{L_{\max, \text{takeoff}}} = 2.0$
- $C_{L_{\max, \text{landing}}} = 2.6$

Takeoff

From Eqn. (4.15), assuming a field length of 12,000 ft, we get,

$$\text{TOP} = \text{BFL}/37.5 = 12000/37.5 = 320.0 \quad (4.47)$$

Substituting this into Eqn. (4.16), we get,

$$\frac{T}{W} = \frac{W/S}{304.0C_{L_{\max}}} \quad (4.48)$$

which corresponds to a straight line with a slope inversely proportional to the maximum coefficient of lift corresponding to the takeoff configuration.

Climb

Here, we use Eqn. (4.24) and Eqn. (4.25), along with the coefficients of the drag polar equations obtained above, to calculate the required takeoff thrust to weight ratios for the six types of climbs listed in Sec. 4.7.

1. Climb 1 (takeoff climb): The required takeoff thrust to weight ratio is,

$$\frac{T}{W} = \left(\frac{1}{0.8} \right) \left(\frac{2}{1} \right) \left(\frac{1.2^2}{2.2} 0.03597 + \frac{2.2}{1.2^2} 0.04054 + 0.012 \right) \quad (4.49)$$

2. Climb 2 (transition segment climb): The required takeoff thrust to weight ratio is,

$$\frac{T}{W} = \left(\frac{1}{0.8} \right) \left(\frac{2}{1} \right) \left(\frac{1.15^2}{2.2} 0.06097 + \frac{2.2}{1.15^2} 0.04054 + 0.0 \right) \quad (4.50)$$

3. Climb 3 (second segment climb): The required takeoff thrust to weight ratio is,

$$\frac{T}{W} = \left(\frac{1}{0.8} \right) \left(\frac{2}{1} \right) \left(\frac{1.2^2}{2.2} 0.03597 + \frac{2.2}{1.2^2} 0.04054 + 0.024 \right) \quad (4.51)$$

4. Climb 4 (enroute climb): The required takeoff thrust to weight ratio is,

$$\frac{T}{W} = \left(\frac{1}{0.8} \right) \left(\frac{1}{0.94} \right) \left(\frac{2}{1} \right) \left(\frac{1.25^2}{0.9} 0.01597 + \frac{0.9}{1.25^2} 0.03815 + 0.012 \right) \quad (4.52)$$

In this case, we also use the maximum continuous thrust correction factor and use the C_{D_0} and $\frac{1}{\pi A Re}$ values for a configuration with both flaps and gear retracted.

5. Climb 5 (AEO balked landing climb): The required takeoff thrust to weight ratio is,

$$\frac{T}{W} = \left(\frac{1}{0.8} \right) \left(\frac{0.65}{1} \right) \left(\frac{1.3^2}{2.6} 0.11597 + \frac{2.6}{1.3^2} 0.04324 + 0.032 \right) \quad (4.53)$$

In this case, we use a correction factor of 0.65 for the maximum landing weight and we do not use the correction factor for the OEI condition.

6. Climb 6 (OEI balked landing climb): The required takeoff thrust to weight ratio is,

$$\frac{T}{W} = \left(\frac{1}{0.8} \right) \left(\frac{2}{1} \right) \left(\frac{0.65}{1} \right) \left(\frac{1.5^2}{0.85 \times 2.6} 0.08847 + \frac{0.85 \times 2.6}{1.5^2} 0.04324 + 0.021 \right) \quad (4.54)$$

In this case, we use a correction factor of 0.65 for the maximum landing weight and also include the correction factor for the OEI condition. The C_{D_0} value for this case (approach) is approximated as the mean of the takeoff and landing configuration values (with flaps and gear down). Additionally, for approach, $C_{L_{\max}}$ is approximated as $0.85 C_{L_{\max, \text{landing}}}$.

Ceiling

Now, we consider a service ceiling of 42,000 ft, where $\rho_c/\rho_{SL} = 0.2331$. In order to make sure the aircraft is able to reach the ceiling altitude, we set a climb gradient slightly greater than zero. A gradient of 0.001 at ceiling altitude is used. Eqn. (4.30) gives the minimum required thrust-to-weight ratio. In this equation, the thrust must be the sea level static thrust. Therefore, we must consider the thrust lapse of the engine with altitude, which may be estimated by,

$$T = \left(\frac{\rho_c}{\rho_{SL}} \right)^{0.6} T_{SLS} \quad (4.55)$$

Dividing Eqn. (4.30) by the factor in the above equation, we get

$$\frac{T}{W} = \frac{1}{\rho_c/\rho_{SL}^{0.6}} \left(G + 2\sqrt{\frac{C_{D_0}}{\pi AR_e}} \right) = \frac{1}{0.2331^{0.6}} \left(0.001 + 2\sqrt{\frac{0.01597}{\pi \times 9.8 \times 0.85}} \right). \quad (4.56)$$

At some point we should also use Eq. (4.29), the selected wing loading, and the ceiling altitude mentioned above to compute the ceiling speed and make sure it is reasonable.

Cruise

The 777 cruises at Mach 0.84 at 40,000 ft, which corresponds to $q = 228.8 \text{ lbf}/\text{ft}^2$. Using Eqn. (4.34), and accounting for thrust lapse at cruise altitude, we get

$$\frac{T}{W} = \frac{1}{0.2846^{0.6}} \left(\frac{228.8 \times 0.01597}{W/S} + \left(\frac{W}{S} \right) \frac{1}{228.8 \times \pi \times 9.8 \times 0.85} \right) \quad (4.57)$$

T/W–W/S Plot

Plotting each of the constraint functions above, we obtain the various lines shown in Fig. 4.6. The feasible design space is highlighted by the shaded region.

4.12 T–S Plot and Objective Function Contours

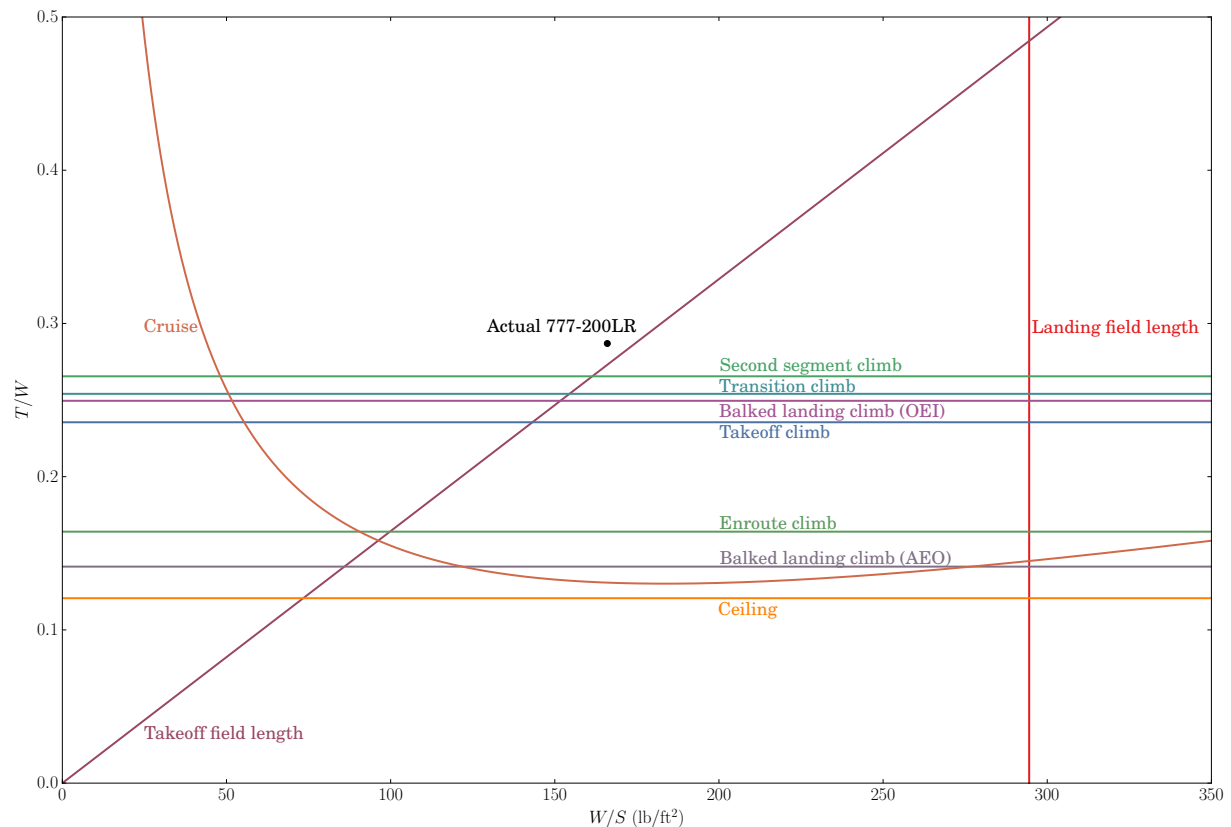
To size the aircraft in terms of the dimensional parameters T and S we will need to modify our weight estimation code to incorporate T and S as variables. Additionally, we will need to reuse the constraint equations used for the T/W – W/S plot but with iteration to find where they lie in dimensional space. This allows us to obtain a T – S plot that will be used to size the aircraft. Fig. 4.7 shows the T – S plot for this example.

4.12.1 Updating the weight estimation

While the T/W – W/S plot is convenient and useful to find the feasible region and establish the critical constraints for your aircraft, they do not include a weight estimation.

To obtain a similar plot where each point corresponds to a sized aircraft with a converged weight estimate, we need to redo the lines in this plot in the space of the actual thrust and reference area—a T – S plot. Then, we will be able to superimpose contours of our objective function (e.g., fuel burn, DOC) and find the best design that is feasible.

First, we need to construct a weight function that depends on T and S , to represent actual tradeoffs. There are two choices for updating your weight estimation code. The preliminary weight

Figure 4.6: T/W - W/S plot for a 777-sized airliner

estimation code can be modified based on an estimate of a baseline T and S using the design point of the $\frac{T}{W}$ vs $\frac{W}{S}$ plot. This process goes as follows...

1. Pick a point on the $\frac{T}{W}$ vs $\frac{W}{S}$ plot as your design point
2. Use the $\frac{T}{W}$ and $\frac{W}{S}$ at your design point with your initial weight estimation to find T and S at that design point
3. Modify your weight estimation code to calculate TOGW as a function of S and T (shown in Algorithm 0)

Additionally, the preliminary weight code can be replaced with the component weight estimate described in Chapter 7. This will be done for the preliminary design anyways.

Algorithm 0 shows how the preliminary weight estimation code can be modified for use in the $T - S$ plot.

Algorithm 2 Iteration for estimating TOGW as a function of T and S

```

 $W_0 = W_{\text{guess}}$                                 ▷ Initial guess
 $\varepsilon = 10^{-6}$                                 ▷ Set the relative convergence tolerance
 $\Delta = 2\varepsilon$                                 ▷ Any value greater than the tolerance
while  $\Delta > \varepsilon$  do
     $\frac{W_e}{W_0} = A W_0^C$                       ▷ Compute empty weight fraction
     $W_e = \frac{W_e}{W_0} W_0$                       ▷ Compute the empty weight
     $W_e = W_e + Dens_{\text{wing}} * (S - S_{\text{Design Point}})$  ▷ Modify wing weight using areaial density from 7.1
     $W_e = W_e + W_{\text{eng}}(T_0) - W_{\text{eng,Design Point}}(T_0)$       ▷ Modify the weight due to the engine
    Compute  $\frac{W_f}{W_0}(S)$                       ▷ Compute fuel fraction as a function of S
     $W_{0\text{new}} = \frac{W_{\text{crew}} + W_{\text{payload}}}{1 - \frac{W_f}{W_0} - \frac{W_e}{W_0}}$           ▷ Compute the new TOGW
     $\Delta = |W_{0\text{new}} - W_0| / |W_{0\text{new}}|$           ▷ Update TOGW value
     $W_0 = W_{0\text{new}}$ 
end while

```

Note that in the above algorithm the fuel fraction is now a function of S . This is because the size of the wings will impact the wetted area and thus C_{D_0} and the $\frac{L}{D}$ of the aircraft at cruise. Additionally, with information about the thrust and weight of the aircraft, the weight fraction at taxi, $\frac{W_1}{W_0}$, and takeoff, $\frac{W_2}{W_1}$, can be estimated more accurately. Although it is unlikely these values will differ significantly from the historical data. Algorithm 0 shows the updated fuel fraction function.

C_{D_0} can be made a function of S by roughly approximating the wing wetted area as $2S$,

$$C_{D_0} = C_f \frac{S_{\text{wet}}}{S} = C_f \frac{(S_{\text{wet,rest}} + 2S)}{S} \quad (4.58)$$

where $S_{\text{wet,rest}}$ is the wetted area of the aircraft excluding the wings.

Algorithm 3 A more detailed fuel fraction calculation

$\frac{W_1}{W_0} = 1 - c_{SL} \frac{15\text{min}}{1\text{hr}} \frac{0.05T}{W_0}$	▷ Fuel burned from running the engine for 15 min at 5% max
$W_1 = \frac{W_1}{W_0} W_0$	
$\frac{W_2}{W_1} = 1 - c_{SL} \frac{1\text{min}}{1\text{hr}} \frac{T}{W_1}$	▷ Fuel burned from running the engine for 1 min at max
$\frac{W_3}{W_2} = \text{historical value}$	▷ Climb segment est. using historical values
Compute $C_{D_0}(S)$	
$C_L = \sqrt{\frac{C_{D_0}}{k}}$	▷ Optimal C_L that maximizes L/D
$\frac{L}{D} = \frac{0.94C_L}{C_{D_0} + kC_L^2}$	▷ L/D calculated for optimal C_L
$\frac{W_4}{W_3} = e^{\frac{-R_c}{V(L/D)}}$	▷ Cruise fuel ratio given by Breguet
$\frac{W_5}{W_4}, \frac{W_6}{W_5} = \text{historical value}$	▷ Descent and landing segment estimate using historical values
$\frac{W_6}{W_0} = \frac{W_6}{W_5} \frac{W_5}{W_4} \frac{W_4}{W_3} \frac{W_3}{W_2} \frac{W_2}{W_1} \frac{W_1}{W_0}$	
$\frac{W_f}{W_0} = 1 - \frac{W_6}{W_0}$	

4.12.2 Solving for the constraint lines

Then the following suggested algorithm can be used for obtaining the curves for the constraints that are expressed as $T/W = f(W/S)$ (e.g., for the takeoff constraint, $\frac{T}{W} = f(W/S) = \frac{W/S}{(\rho/\rho_{SL})C_{L_{max}}\text{TOP}}$).

Algorithm 4 T/W constraint curves for $T-S$ plot

$S = S_{\text{begin}} : \Delta S : S_{\text{end}}$	
for $i = 1 : \text{length}(S)$ do	
$S_0 = S(i)$	▷ Prescribe wing area
$T(i) = T_{\text{guess}}$	▷ Initial thrust guess
tolerance $\leftarrow 0.1$	▷ Convergence tolerance
converged $\leftarrow \text{False}$	
while converged = False do	
$W = W(S_0, T(i))$	▷ Compute TOGW
Compute W/S_0	▷ Compute wing loading
$(T/W)_{\text{new}} = f(W/S_0)$	▷ Compute T/W from constraint equation
$T_{\text{new}} = (T/W)_{\text{new}} \times W$	▷ Compute new total thrust
if $ T_{\text{new}} - T(i) \leq \text{tolerance}$ then	▷ Check for convergence
converged = True	
end if	
$T(i) = T_{\text{new}}$	▷ Update thrust value
end while	
end for	

For constraints like the landing field length that depend on W/S , the procedure needs to be changed. First prescribe T , then guess S , compute W , solve for S_{new} , and iterate until convergence. Repeat for a range of T values.

Bibliography

John D. Anderson Jr. *Aircraft Performance and Design*. McGraw-Hill, 1999.

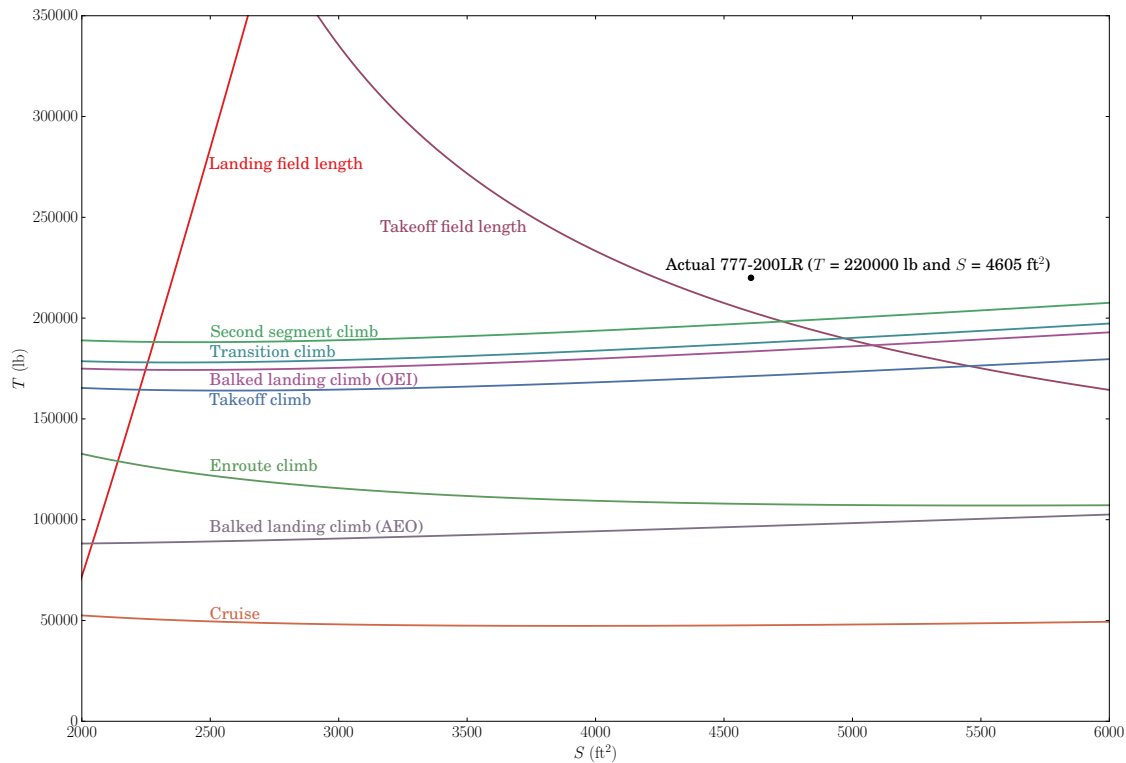


Figure 4.7: T - S plot for a 777-sized airliner

Lloyd R. Jenkinson, Paul Simpkin, and Darren Rhodes. *Civil Jet Aircraft Design*. Arnold, 1999.

Leland M. Nicolai and Grant E. Carichner. *Fundamentals of Aircraft and Airship Design, Vol I — Aircraft Design*. AIAA, Reston, VA, 2010.

Daniel P. Raymer. *Aircraft Design: A Conceptual Approach*. AIAA, 4th edition, 2006.

Daniel P. Raymer. *Aircraft Design: A Conceptual Approach*. AIAA, 5th edition, 2012.

J. Roskam. *Airplane Design, Volumes 1-8*. Roskam Aviation and Engineering Corporation, 1989.

Hendrik Tennekes. *The simple science of flight: from insects to jumbo jets*. MIT press, 2009.

E. Torenbeek. *Synthesis of Subsonic Airplane Design*. Delft University Press and Kluwer Academic Publishers, 6th edition, 1990.

Chapter 5

Fuselage Sizing and Design

For an air transport, the function of the fuselage is to carry crew, passengers and payload safely and (relatively) comfortably, and its sizing is dependent on the requirements related to that function. For low weight and low drag, the designer would like to have the smallest possible fuselage that does the job. Hence, we have the classical tradeoff between performance and comfort.

The dimensions of the fuselage affect the drag in multiple ways. A fuselage with a smaller length to diameter ratio—the *fineness ratio*—has lower wetted area for a given enclosed volume. On the other hand, a fuselage with a larger fineness ratio results in a higher Reynolds number, which reduces the skin friction drag coefficient; the larger moment arm for the empennage also reduces the empennage size and thus weight, although the fuselage itself will be heavier.

5.1 Cross-Section Design

The first decision that needs to be made for a conventional air transport is the size of the cross section. This is an important decision given the tradeoffs we just listed, and also because the cross-section is one of the major parameters that does not change when new derivatives of a given aircraft are made.

The circular fuselage cross-section is predominant in air transports since it efficiently reacts to the cabin pressurization loads with hoop tension, instead of bending. The circular shape also minimizes the wetted area for a given enclosed volume. In spite of these advantages, a few non-circular cross-sections are in use. Examples of non-circular cross-sections include the Boeing 747 and the Airbus A380, although these cross-sections still exhibit a rounded shape that is formed with circular arcs. Other options for cross-sectional shapes are being considered for future aircraft.

An additional advantage of the rounded fuselage cross section is aerodynamic: the absence of corners encourages the flow to remain attached at moderate angles of attack or sideslip angle.

The typical airliner houses the passengers in the upper portion of the cross section, with the luggage and cargo placed below the cabin floor. The main decision to be made is the number of seats to have across a row and the aisle arrangement. This determines both the size of the cross section and the number of rows (and thus the length of the cabin) for the specified number of passengers. Fig. 5.2 shows how this decision affects the fuselage fineness ratio.

Although the designer sizes the cross section with a seat size in mind, the ultimate choice is that of the operator. Typical seat widths are listed in Table 5.1.

When it comes to aisle width, FAR 25.815 quotes: minimum aisle widths of 15 in and 20 in, respectively below and above a reference height of 25 in above the floor. However, most airlines choose aisles wider than this to avoid congestion when the service carts are in use.

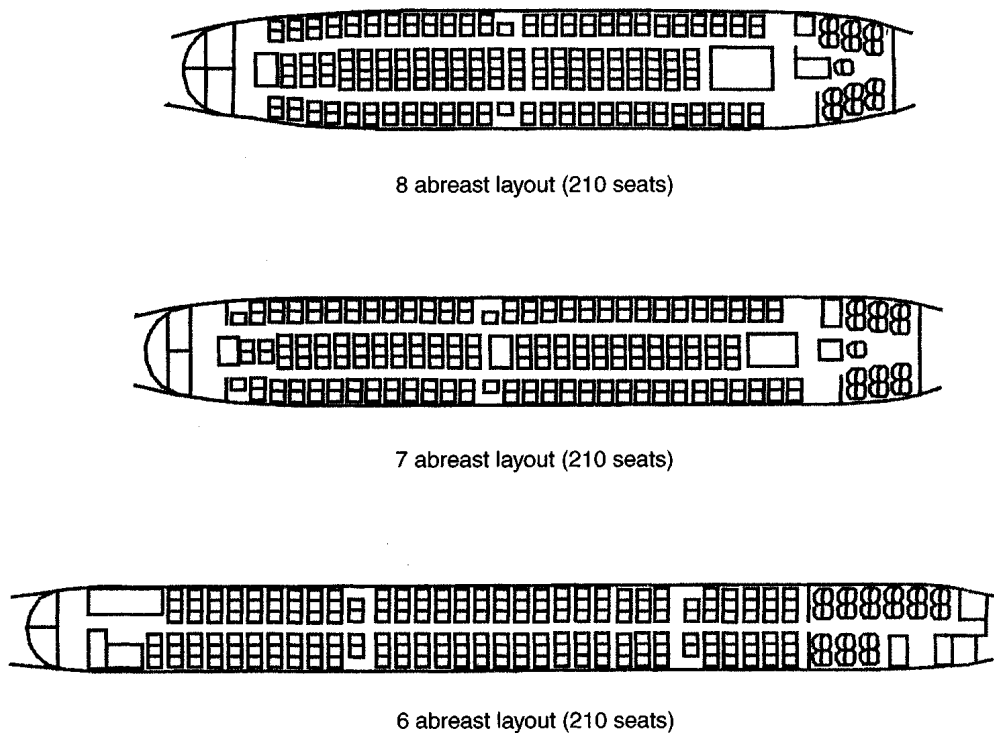


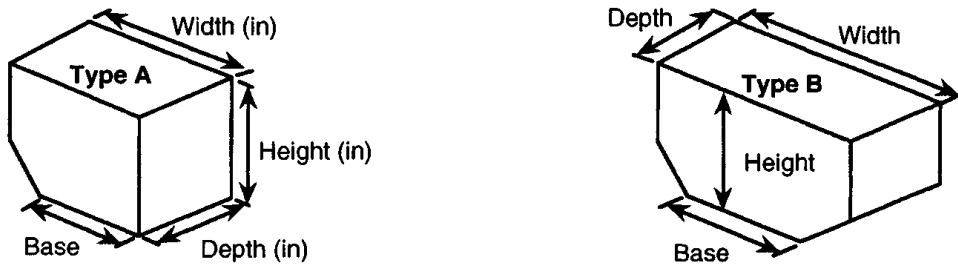
Figure 5.1: Three possibilities for a 210 passenger cabin ([Jenkinson et al., 1999](#), Fig. 5.4)

Class	Seat width (in)
Charter	16–17
Economy	19–21
Business	23–25
First	25–28

Table 5.1: Typical seat widths ([Jenkinson et al., 1999](#), Table 5.2)

When dimensioning the cross section, it is important to provide adequate headroom to the window passengers. We also need to account for the fuselage frame, stringers and insulation thickness, all of which reduce the available cabin space. For small commercial aircraft, 1.5 in on each side is typical; for large transports, you can use $0.02 \times D + 1$, where D is the fuselage diameter (Roskam, 1989). An additional clearance of about 3/4 in should also be added to account for fuselage deflection, seat width tolerances, and seat track location tolerances.

To estimate the volume needed for the luggage (and potentially cargo: airlines get some revenue from this), we need the average density of those items. For passenger luggage this is 12.5 lb/ft³, while for cargo it is 10 lb/ft³(Torenbeek, 1990). Luggage and cargo are typically packages onto pallets or put into containers. The International Air Transport Association (IATA) has specified sizes for standard containers. Some of these specifications relate to the frequently used LD- designations shown in Table 5.2. Containers LD-I, LD-2, LD-3, LD-4 and LD-8 are the most common types. Data from this table can be used in the layout of the fuselage shape and to predict cargo capacity in the design of a new aircraft. Fig. 5.2 shows the container arrangement for three Boeing aircraft.



Designation	Width	Height	Depth	Base	Maximum load (lb)	Notes
LD-1	92.0	64.0	60.4	61.5	3500	Type A
LD-2	61.5	64.0	60.4	47.0	2700	Type A
LD-3	79.0	64.0	60.4	61.5	3500	Type A
LD-4	96.0	64.0	60.4	—	5400	Rectangular
LD-5	125.0	64.0	60.4	—	7000	Rectangular
LD-6	160.0	64.0	60.4	125.0	7000	Type B
LD-7	125.0	64.0	80.0	—	13 300	Rect/Contoured
LD-8	125.0	64.0	60.4	96.0	5400	Type B
LD-9	125.0	64.0	80.0	—	13 300	Rect/Contoured
LD-10	125.0	64.0	60.4	—	7000	Contoured
LD-11	125.0	64.0	60.4	—	7000	Rectangular
LD-29	186.0	64.0	88.0	125.0	13 300	Type B

Table 5.2: Standard sizes for cargo containers(Jenkinson et al., 1999, Table 5.1)

5.2 Cabin Planform Layout

Once the cross section has been sized, we can find out the number of rows needed in each class to accommodate the specified number of passengers. The crucial choice now is the pitch of the seats in each class, which will determine the cabin length. Typical seat pitches are listed in Table 5.3.

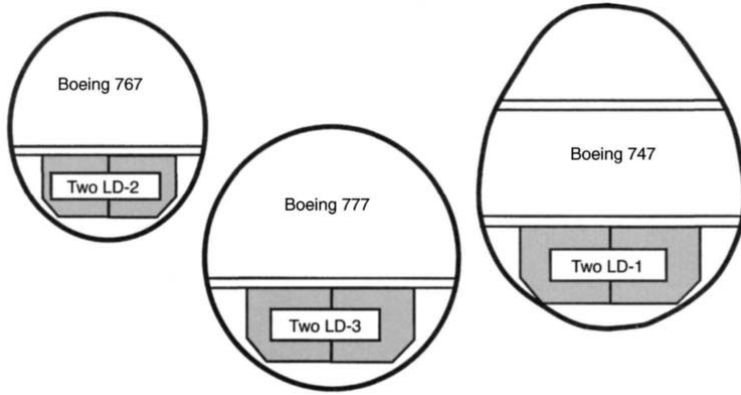


Figure 5.2: Typical standard container arrangements([Jenkinson et al., 1999](#), Fig. 5.6)

Class	Seat pitch (in)
Charter	28–31
Economy	31–34
Business	36–38
First	38–42+

Table 5.3: Typical seat pitch ([Jenkinson et al., 1999](#), Table 5.3)

The cabin length is also affected by the number and type of emergency exits—see FAR 25.807 for more details.

Extra seats must also be provided for flight attendants, which are required adjacent to door exits and may be stowed upright, but clear of exit paths. Service modules (galleys, lavatories and closets) must be provided in the cabin layout. Depending on the class of ticket, there will be one galley per 10–60 passengers, and one lavatory per 15–40 passengers. Typical sizes for the galleys are 30×36 in and lavatories are either 36×36 in or 34×38 in. Closets are usually installed in business and first class cabins, and take up to 2 in per passenger.

5.3 Nose and Tail Cone

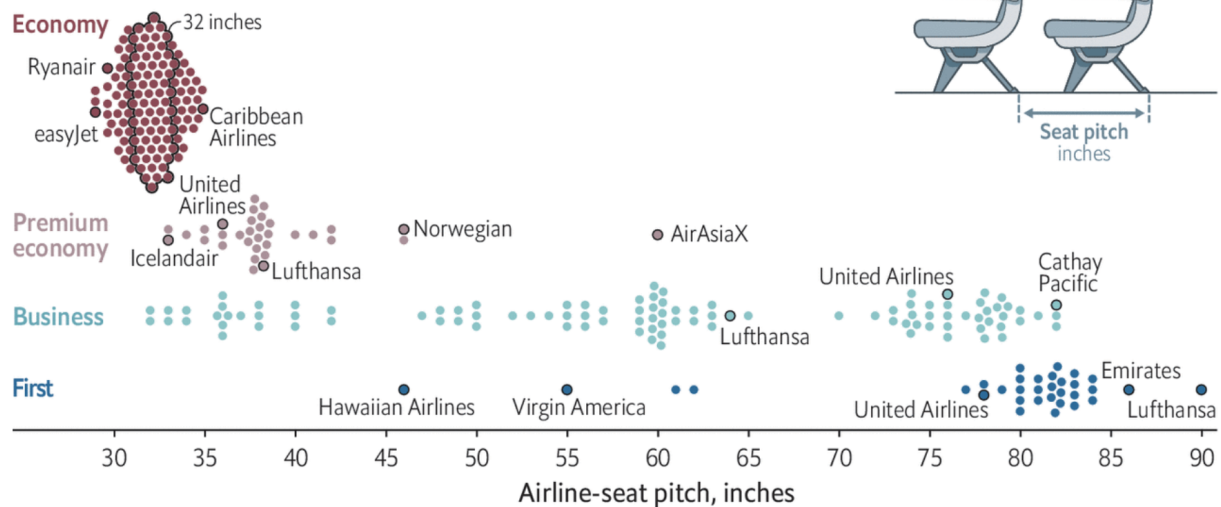
Once the cabin has been sized, we can proceed to shape the rest of the fuselage planform. The cockpit needs to be placed in front, and a tapered tail cone is required in the back for aerodynamic reasons. The fuselage shape must be such that separation and shock waves are avoided. For low Mach numbers, constraints on fuselage pressure gradients limit the nose length to fuselage diameter ratio to about 1.5. Higher values of the nose fineness ratio might be required for higher Mach numbers to avoid shock waves that would add wave drag. The tail cone taper is chosen to avoid separation that would add profile drag, and is typically 1.8–2.0. The transition from nose and tail cone to the constant diameter section must be smooth, with no discontinuities in slope (kinks) and with low curvature. Otherwise, the resulting unfavorable pressure gradients can cause separation. Also, the closure angle at the very end should not be too large, with a half angle less than 14–20°.

The shape of the tail cone in side view is determined based on ground clearance of the tail cone. Usually aft-fuselage upsweep is required to provide the capability of rotating to high angles of attack on the ground (often about 14°). The upsweep cannot be set without estimating the

Legroom on planes has been shrinking for decades. It'll probably get worse

Pitch perfect

Distribution of airline-seat pitch* by ticket class, inches
December 2019



Source: Skytrax

*Distance between a row of seats. Measurement from the same position on two seats, one behind the other

The Economist

Figure 5.3: Airline seat pitch

length and position of the main landing gear, but this can be done early in the design process by comparison with similar aircraft.

5.4 Cockpit

The overall length of the cockpit varies according to aircraft type from about 110 in for smaller aircraft to 150 in for larger ones. The larger space can accommodate a third crew member if required.

The shape of the nose side view and the geometry of the windscreens are determined based on visibility requirements for the cockpit. The pilot's seat and controls must be adjustable to suit pilots between 5 ft 2 in and 6 ft 3 in tall, allowing the pilot's eye to be positioned at a specified design location around which the designer lays out the windscreen. Either pilot must be able to fly the aircraft and therefore the windscreen and front geometry should be symmetrical about the aircraft longitudinal centerline. The pilots must have good visibility in all flight and ground manoeuvres. They must be able to see below the horizon in the approach attitude and at least 10° below the horizon when climbing. In turning flight they should be able to see upwards at about 20° and sideways 110°. On the ground the pilots must be able to see the aircraft wing tips (although they might have to lean forward and sideways).

5.5 Relevant Federal Aviation Regulations

The following FARs are relevant to the cabin layout and fuselage design:

Sec. 25.801 Ditching

Sec. 25.803 Emergency evacuation

Sec. 25.807 Emergency exits

Sec. 25.809 Emergency exit arrangement

Sec. 25.810 Emergency egress assist means and escape routes

Sec. 25.813 Emergency exit access

Appendix J: Emergency Evacuation Demonstration

Bibliography

Lloyd R. Jenkinson, Paul Simpkin, and Darren Rhodes. *Civil Jet Aircraft Design*. Arnold, 1999.

J. Roskam. *Airplane Design, Volumes 1-8*. Roskam Aviation and Engineering Corporation, 1989.

E. Torenbeek. *Synthesis of Subsonic Airplane Design*. Delft University Press and Kluwer Academic Publishers, 6th edition, 1990.

Chapter 6

Wing Design

This chapter deals with some of the considerations involved in wing design, especially the selection of basic sizing parameters. There are a number of important trade-offs associated with these parameters, each one of which affects drag, structural weight, stalling characteristics, fuel volume, off-design performance, and other characteristics.

There are two approaches to wing design:

1. Find planform and twist distribution that minimize a combination of drag and weight, while satisfying $C_{L_{\max}}$ constraints.
2. Select a desirable lift distribution and then compute the twist, taper, and thickness distributions to achieve it.

The latter approach is only viable when the designer has enough experience to know what constitutes a desirable lift distribution. The first approach is often combined with numerical optimization.

Wing lift distribution is an important consideration in wing design. The spanwise lift distribution is closely related to the wing geometry and determines wing performance characteristics such as induced drag, structural weight, and stalling characteristics. A reasonable lift and C_l distribution provides a good starting point in the design of a wing.

6.1 Wing Design Parameters

The major wing design parameters can be divided into two levels. The first level design parameters are generally more influential and should be determined first. They are:

- Span
- Area
- Thickness
- Sweep

The second level design parameters are important, but they can be determined at a later stage because the trade-offs between the first level design parameters and the rest of the aircraft are more crucial, and can be made assuming that a set of second level parameters can be determined such that the wing performs as expected. The second level parameters are:

- Taper

- Airfoil shape(s)
- Twist
- Tip shape

In this section, we will discuss the effect that each of these variables has on drag, structural weight, etc., before describing a procedure for performing the actual design. Some of these parameters are illustrated in Fig. 6.1.

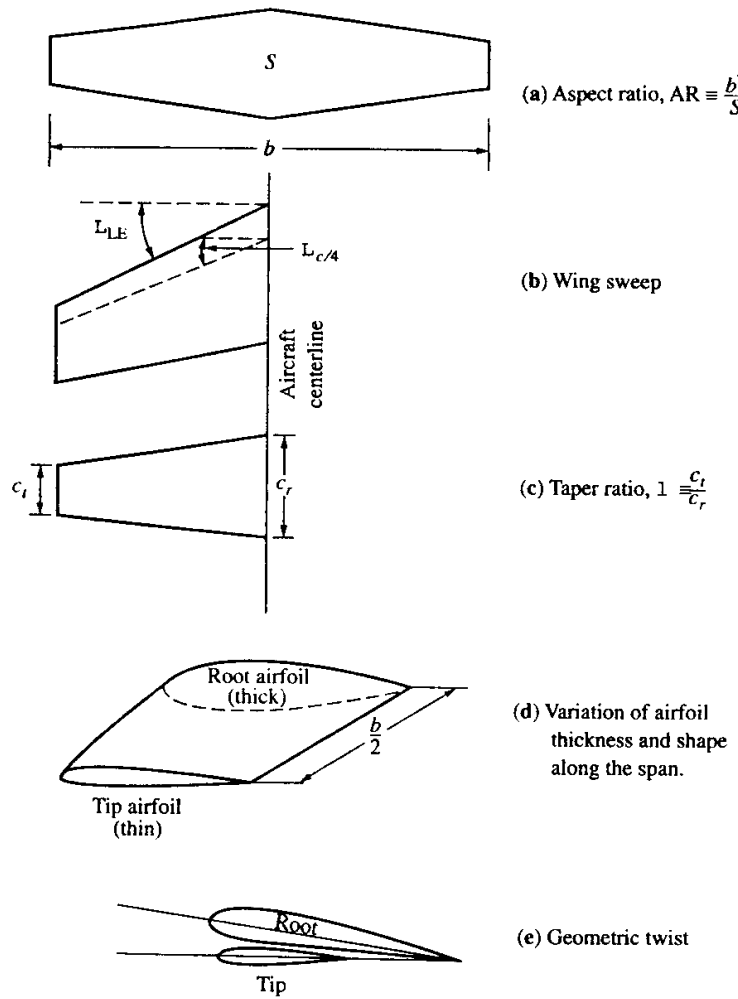


Figure 6.1: Wing planform design parameters (Anderson Jr., 1999, Fig. 8.6)

6.1.1 Span

Selecting the wing span is one of the most basic decisions to made in the design of a wing. The span is sometimes constrained by contest rules, hangar size, or ground facilities but when it is not we might decide to use the largest span consistent with structural dynamic constraints (flutter). This would reduce the induced drag directly.

However, as the span is increased, the wing structural weight also increases and at some point the weight increase offsets the induced drag savings. This point is rarely reached, though, for several reasons:

1. The optimum is quite flat and one must stretch the span a great deal to reach the actual optimum.
2. As span is increases, so does wing bending which can negatively affect stability and flutter characteristics.
3. The cost of the wing itself increases as the structural weight increases.
4. The volume of the wing in which fuel can be stored is reduced.
5. It becomes more difficult to locate the main landing gear at the root of the wing.
6. The Reynolds number of wing sections is reduced, increasing parasite drag and reducing
7. Span might be restricted by the infrastructure (airport gates, hangars) maximum lift capability.

6.1.2 Area

The wing area, like the span, is chosen based on several considerations including:

- Cruise drag
- Stalling speed and field length requirements
- Wing structural weight
- Fuel volume

These considerations often lead to a wing with the smallest area allowed by the constraints. But this is not always true; sometimes the wing area must be increased to obtain a reasonable C_L at the selected cruise conditions.

Selecting cruise conditions is also an integral part of the wing design process. It should not be dictated a priori because the wing design parameters will be strongly affected by the selection, and an appropriate selection cannot be made without knowing some of these parameters. But the wing designer does not have complete freedom to choose these, either. Cruise altitude affects the fuselage structural design and the engine performance as well as the aircraft aerodynamics. The best C_L for the wing is not the best for the aircraft as a whole. An example of this is seen by considering a fixed C_L , fixed Mach design. If we fly higher, the wing area must be increased by the wing drag is nearly constant. The fuselage drag decreases, though; so we can minimize drag by flying very high with very large wings. This is not feasible because of considerations such as engine performance.

Aspect ratio is directly related to the wing area and wing span and is defined as:

$$AR = \frac{b^2}{S_{\text{ref}}}, \quad (6.1)$$

where S_{ref} should be the same as the one used in the definition of C_L and C_D .

6.1.3 Sweep

Sweep is the angle between the $c/4$ line and the spanwise axis. Wing sweep is mainly used for reducing transonic wave drag. There are cases, however, when sweep is used to improve stability (as in the case of flying wings).

Sweep has the following consequences:

- It permits higher cruise Mach number, greater airfoil thickness or higher C_L at a given Mach number without drag divergence.
- It increases the additional loading at the tip,
- It increases the structural weight, because of the increased tip loading, and also because of the increased structural span.
- It stabilizes the wing aeroelastically but is destabilizing to the airplane.
- Too much sweep makes it difficult to accommodate the main gear in the wing.

Much of the effect of sweep varies as the cosine of the sweep angle, making forward and aft-swept wings similar. There are, however, important differences in other characteristics.

6.1.4 Thickness

The distribution of thickness from wing root to tip is selected by considering the following:

- We would like to make t/c as large as possible to reduce wing weight
- Greater t/c tends to increase $C_{L_{max}}$ up to a point, depending on the high-lift system, but gains above about 12% are small if there at all.
- Greater t/c increases fuel volume and wing stiffness.
- Increasing t/c increase incompressible drag slightly by increasing the velocities and the adiabaticity of the pressure gradients.
- Increasing t/c shifts the transonic drag rise towards lower the Mach numbers, limiting the speed and C_L at which the airplane may fly efficiently.

6.1.5 Taper

Wing taper is the ratio of tip chord to root chord, i.e.,

$$\lambda = \frac{c_{tip}}{c_{root}} \quad (6.2)$$

The wing taper ratio (and planform shape in general) is determined from the following considerations:

- The planform shape should not give rise to an additional lift distribution that is so far from elliptical that the required twist for low cruise drag results in large off-design penalties.
- The chord distribution should be such that with the cruise lift distribution, the distribution of lift coefficient is compatible with the section performance. Avoid high C_{ls} which may lead to buffet, drag rise, or separation.

- The chord distribution should produce a load distribution which is compatible with the high-lift system and desired stalling characteristics.
- Lower taper ratios lead to lower wing weight.
- Lower taper ratios result in increased fuel volume.
- The tip chord should not be too small as Reynolds number effects cause reduced C_l capability.
- Larger root chords more easily accommodate landing gear.

The major design goal is to keep the taper ratio as small as possible (to keep the wing weight down) without excessive C_l variation or unacceptable stalling characteristics. Since the lift distribution elliptical, the chord distribution should be nearly elliptical for a uniform C_l distribution.

6.1.6 Twist

The twist must be chosen so that the cruise drag is low.

Other considerations include:

- Extra washout (negative twist towards the wing tip) helps the stalling characteristics.
- Twist changes the structural weight by modifying the moment distribution over the wing.
- Twist on swept-back wings also produces a positive pitching moment which has a small effect on trimmed drag.

The selection of wing twist is therefore accomplished by examining the trades between cruise drag, drag in second segment climb, and the wing structural weight. The selected washout is then just a bit higher to improve stall.

6.2 Lift Distributions

It is easier to relate the wing geometry to its performance through the intermediary of the lift distribution. Wing design often proceeds by selecting a desirable wing lift distribution and then finding the geometry that achieves this distribution. In this section, we describe the lift and lift coefficient distributions, and relate these to the wing geometry and performance.

6.2.1 Lift and C_l Distributions

The distribution of lift on the wing affects the wing performance in many ways. The lift per unit length $l(y)$ may be plotted from the wing root to the tip as shown below.

In this case the distribution is roughly elliptical. In general, the lift goes to zero at the wing tip. The area under the curve is the total lift. The section lift coefficient is related to the section lift by

$$C_l(y) = \frac{l(y)}{qc(y)}. \quad (6.3)$$

Thus, if we know the lift distribution and the planform shape, we can find the C_l distribution: The lift and lift coefficient distributions are directly related by the chord distribution.

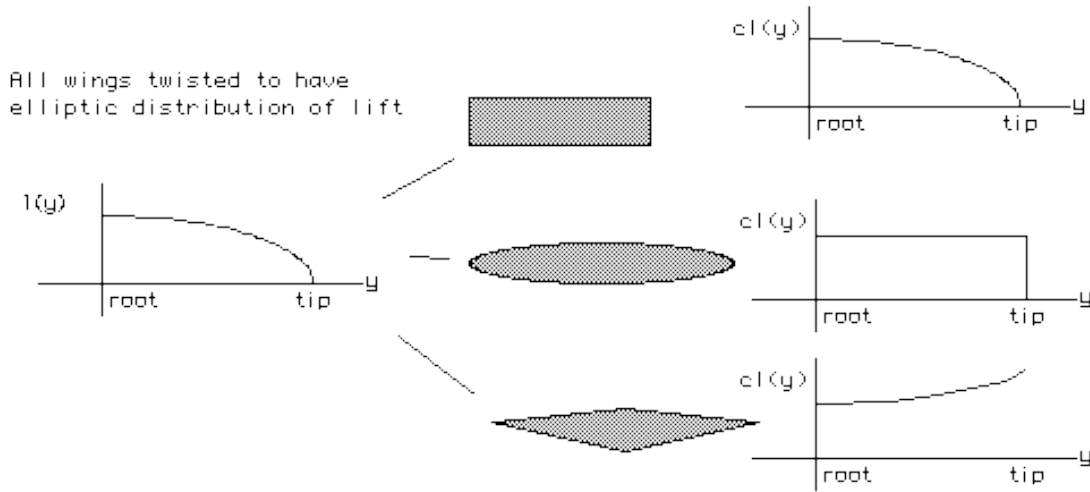
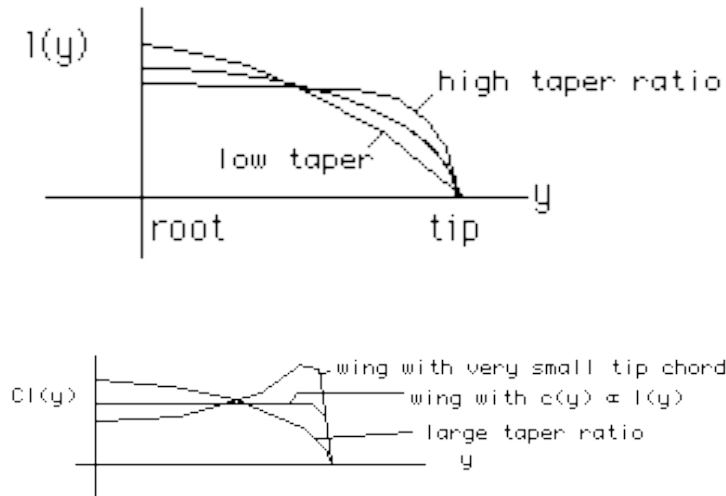


Figure 6.2: Relating lift and lift coefficient distributions: The lift distribution on the left can yield all three lift coefficient distributions on the left, depending on the chord distribution.

6.2.2 Wing Geometry and Lift Distributions

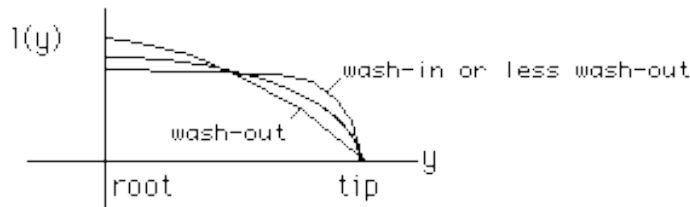
The wing geometry affects the wing lift and C_l distributions in ways that are intuitive for the most part.

Increasing the taper ratio (making the tip chords larger) produces more lift at the tips, just as one might expect, but because the section C_l is the lift divided by the local chord, taper has a very different effect on the C_l distribution.

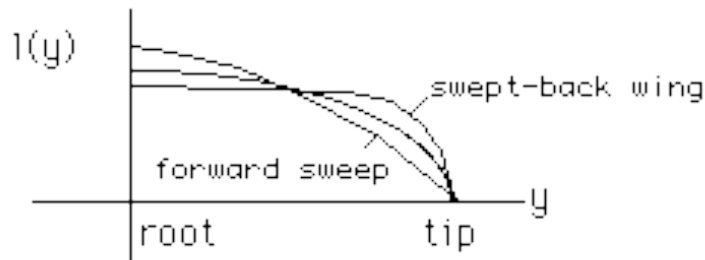


When it comes to wing twist, increasing the tip incidence with respect to the root is called wash-in. Wings often have less incidence at the tip than the root (wash-out) to reduce structural weight and improve stalling characteristics. Since changing the wing twist does not affect the chord distribution, the effect on lift and C_l is similar.

Wing sweep produces a less intuitive change in the lift distribution of a wing. Because the downwash velocity induced by the wing wake depends on the sweep, the lift distribution is affected.



The result is an increase in the lift near the tip of a swept-back wing and a decrease near the root (as compared with an unswept wing). This effect can be quite large and causes problems for swept-back wings. The greater tip lift increases structural loads and can lead to stalling problems.



Note that many of these effects are similar and by combining the right twist and taper and sweep, we can achieve desirable distributions of lift and lift coefficient. For example: Although a swept back wing tends to have extra lift at the wing tips, wash-out tends to lower the tip lift. Thus, a swept back wing with washout can have the same lift distribution as an unswept wing without twist.

Lowering the taper ratio can also cancel the influence of sweep on the lift distribution. However, then the C_l distribution is different. Today, we can relate the wing geometry to the lift and C_l distributions with panel methods. Yet, this more intuitive understanding of the impact of wing parameters on the distributions remains an important skill.

6.2.3 Lift Distributions and Performance

Wing design has several goals related to the wing performance and lift distribution. One would like to have a distribution of C_l that is relatively flat so that the airfoil sections in one area are not “working too hard” while others are at low C_l . In such a case, the airfoils with C_l much higher than the average will likely develop shocks sooner or will start stalling prematurely.

The induced drag depends solely on the lift distribution, so one would like to achieve a nearly elliptical distribution of section lift.

On the other hand structural weight is affected by the lift distribution as well, so the ideal shape depends on the relative importance of induced drag and wing weight.

By varying taper, sweep, and twist, these goals can be easily achieved at a given design point. The difficulty appears when the wing must perform well over a range of conditions. One of the more interesting tradeoffs that is often required in the design of a wing is that between drag and structural weight. This may be done in several ways. Some of the optimization problems that have been solved include:

- Minimum induced drag with given span (Prandtl)
- Minimum induced drag with given root bending moment (Jones, Lamar, and others)
- Minimum induced drag with fixed wing weight and constant thickness (Prandtl, Jones)
- Minimum induced drag with given wing weight and specified thickness-to-chord ratio (Ward, McGeer, Kroo)
- Minimum total drag with given wing span and planform – Kuhlman
- Maximum range and other problems based on the Breguet range equation

There are many problems of this sort left to solve and many approaches to the solution of such problems. These include some closed-form analytic results, analytic results together with iteration, and finally numerical optimization.

The best wing design will depend on the construction materials, the arrangement of the high-lift devices, the flight conditions (C_L , Re , M) and the relative importance of drag and weight.

All of this is just to say that it is difficult to design just a wing without designing the entire airplane. If we were just given the job of minimizing cruise drag the wing would have a very high aspect ratio.

If we add a constraint on the wing structural weight based on a trade-off between cost and fuel savings then the problem is somewhat better posed but we would still select a wing with very small taper ratio.

High t/c and high sweep are often suggested by studies that include only weight and drag. The high lift characteristics of the design force the taper ratio and sweep to more usual values and therefore must be a fundamental consideration at the early stages of wing design. Unfortunately the estimation of $C_{L_{max}}$ is one of the more difficult parts of the preliminary design process.

6.3 Winglets and Other Nonplanar Wings

Increasing the wing span redistributes the spanwise vorticity such that induced drag is reduced. Winglets have a similar effect.

However, when the wing-winglet combination is optimized for minimum drag at fixed span, it achieves about the same drag as a planar wing with a span increased by about 45% of the winglet height.

The same approach may be taken for general nonplanar wake shapes. The figure below summarizes some of these results.

Several points should be made about the preceding results:

- The result that the sidewash on the winglet is zero for minimum induced drag means that the self-induced drag of the winglet just cancels the winglet thrust associated with wing sidewash. Optimally-loaded winglets thus reduce induced drag by lowering the average downwash on the wing, not by providing a thrust component.
- The results shown here deal with the inviscid flow over nonplanar wings. There is a slight difference in optimal loading in the viscous case due to lift-dependent viscous drag.
- Other potentially important factors not considered in this study are: stability and control, structures, and a number of practical issues.

More details on the design of nonplanar wings may be found in various papers (Jansen et al., 2010; Kroo, 2005; Kroo et al., 1998; Verstraeten and Slingerland, 2009; ?).

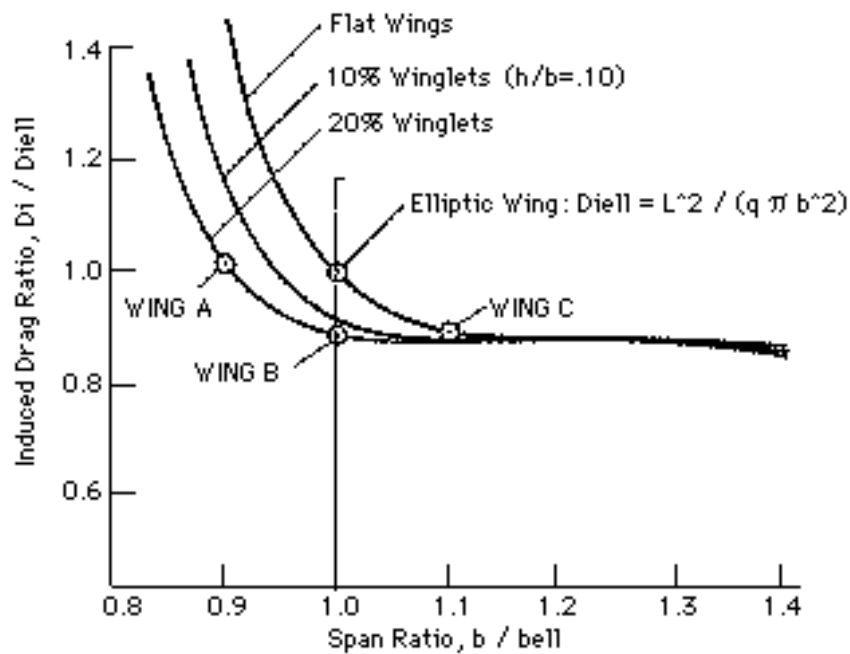


Figure 6.3: Span efficiency of different wings for varying span

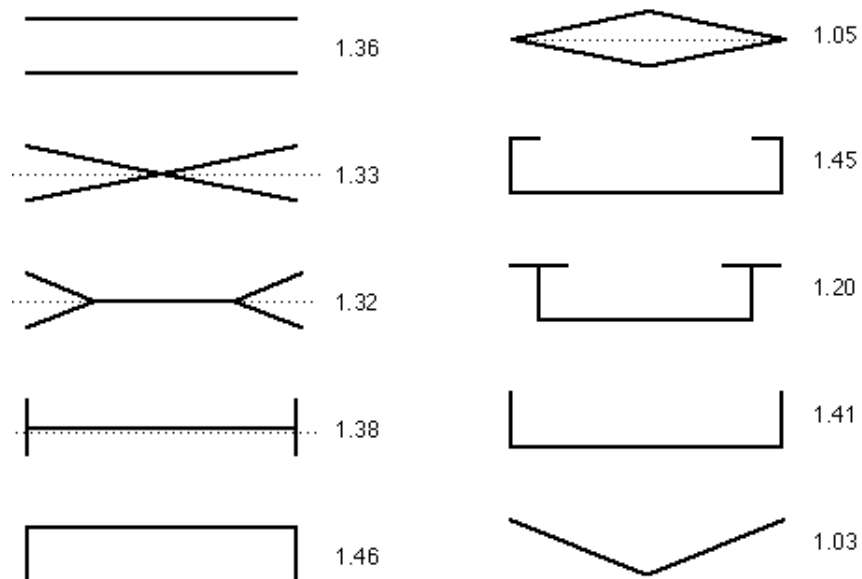


Figure 6.4: Maximum span efficiency for nonplanar wings of various shapes with a height to span ratio of 0.2

6.4 Transonic Wave Drag

We now present an alternative approach to Raymer (2006, Figs. 12.28–12.33). This approach relies on the prediction of wave drag, rather than directly deciding the design parameters. It uses the three-dimensional version of the Korn equation, which can be used to predict the wave drag of swept wings (Malone and Mason, 1995). The Korn equation connects the drag divergence Mach number with airfoil performance, wing sweep and thickness-to-chord ratio by the following relation:

$$M_{DD} = \frac{\kappa}{\cos \Lambda} - \frac{t/c}{\cos^2 \Lambda} - \frac{C_L}{10 \cos^3 \Lambda} \quad (6.4)$$

where M_{DD} is the drag divergent Mach number, C_L is the wing lift coefficient in cruise, Λ is the wing sweep at the quarter chord, t/c is the average wing thickness-to-chord ratio, and κ is an *airfoil technology factor*. This factor varies from $\kappa = 0.87$ for a NACA 6-series airfoil section, to $\kappa = 0.95$ for a supercritical section (Mason, 1990).

The critical Mach number is the minimum Mach number for which there is sonic flow over any portion of the wing, and is determined empirically by

$$M_{crit} = M_{DD} - \left(\frac{0.1}{80} \right)^{1/3} \quad (6.5)$$

The wave drag coefficient can then be estimated by:

$$C_{Dwave} = 20(M - M_{crit})^4 \quad (6.6)$$

which is valid if $M > M_{crit}$. If $M < M_{crit}$, there are no shocks and the wave drag is zero.

6.5 Airfoil Design

6.5.1 Airfoil Geometry

Airfoil geometry can be characterized by the coordinates of the upper and lower surface. It is often summarized by a few parameters such as: maximum thickness, maximum camber, position of maximum thickness, position of max camber, and nose radius. One can generate a reasonable airfoil section given these parameters. This was done by Eastman Jacobs in the early 1930's to create a family of airfoils known as the NACA Sections.

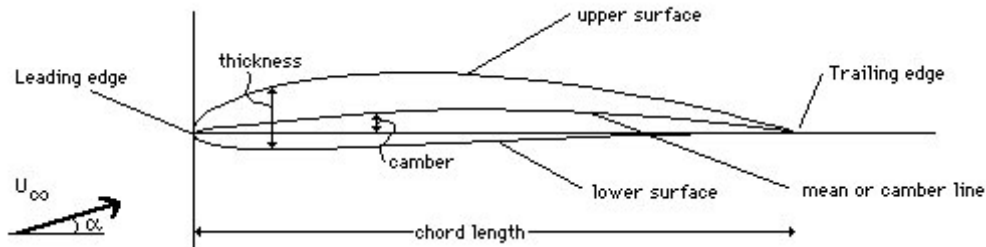


Figure 6.5: Airfoil geometry parameters

The NACA 4 digit and 5 digit airfoils were created by superimposing a simple meanline shape with a thickness distribution that was obtained by fitting a couple of popular airfoils of the time:

$$\pm y \equiv \frac{t}{0.2} \left(.2969x^{1/2} - .126x - .3537x^2 + .2843x^3 - .1015x^4 \right) \quad (6.7)$$

Table 6.1: NACA 4-Digit Series

4 max camber in % in c	4 position of max camber in 1/10 of c	12 max t/c in %
-----------------------------------	--	-------------------------

Table 6.2: NACA 5-Digit Series

2 approx max camber in % in c	30 position of max camber in 2/100 of c	12 max t/c in %
--	--	-------------------------

The camberline of 4-digit sections was defined as a parabola from the leading edge to the position of maximum camber, then another parabola back to the trailing edge.

After the 4-digit sections came the 5-digit sections such as the famous NACA 23012. These sections had the same thickness distribution, but used a camberline with more curvature near the nose. A cubic was faired into a straight line for the 5-digit sections.

The 6-series of NACA airfoils departed from this simply-defined family. These sections were generated from a more or less prescribed pressure distribution and were meant to achieve some laminar flow.

After the 6-series sections, airfoil design became much more specialized for the particular application. Airfoils with good transonic performance, good maximum lift capability, very thick sections, very low drag sections are now designed for each use. Often a wing design begins with the definition of several airfoil sections and then the entire geometry is modified based on its 3-dimensional characteristics.

6.5.2 Airfoil Pressure Distributions

The aerodynamic performance of airfoil sections can be studied most easily by reference to the distribution of pressure over the airfoil (just like referring to the spanwise lift distribution to study the effect of planform variables on the wing aerodynamic performance). This distribution is usually expressed in terms of the pressure coefficient (C_p), which is the difference between local static pressure and freestream static pressure, nondimensionalized by the freestream dynamic pressure, i.e.,

$$C_p = \frac{p - p_\infty}{\frac{1}{2} \rho U_\infty^2}. \quad (6.8)$$

What does an airfoil pressure distribution look like? We generally plot C_p vs. x/c .

x/c varies from 0 at the leading edge to 1.0 at the trailing edge. C_p is plotted “upside-down” with negative values (suction), higher on the plot. (This is done so that the upper surface of a

Table 6.3: NACA 6-Digit Series

6 Six- series	3 location of min C_p in 1/10 c	2 half width of low drag bucket in 1/10 of C_l	– ideal C_l in tenths	12 max t/c in %
---------------------	--	---	-------------------------------	-------------------------

conventional lifting airfoil corresponds to the upper curve.)

The C_p starts from about 1.0 at the stagnation point near the leading edge. It rises rapidly (pressure decreases) on both the upper and lower surfaces, and finally recovers to a small positive value of C_p near the trailing edge.

Various parts of the pressure distribution are depicted in the figure below and are described in the following sections.

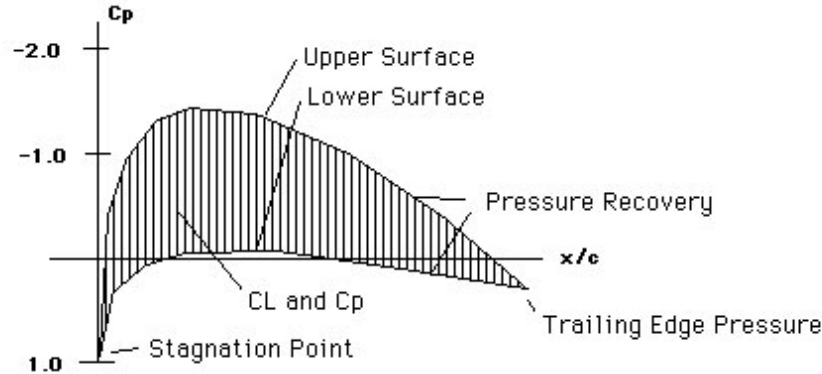


Figure 6.6: Airfoil pressure coefficient

Upper Surface: The upper surface pressure is lower (plotted higher on the usual scale) than the lower surface C_p in this case. But it doesn't have to be.

Lower Surface: The lower surface sometimes carries a positive pressure, but at many design conditions is actually pulling the wing downward. In this case, some suction (negative C_p results in downward force on lower surface) is present near the midchord.

Pressure Recovery: This region of the pressure distribution is called the pressure recovery region. The pressure increases from its minimum value to the value at the trailing edge. This area is also known as the region of adverse pressure gradient. As discussed in other sections, the adverse pressure gradient is associated with boundary layer transition and possibly separation, if the gradient is too severe.

Trailing Edge Pressure: The pressure at the trailing edge is related to the airfoil thickness and shape near the trailing edge. For thick airfoils the pressure here is slightly positive (the velocity is a bit less than the freestream velocity). For infinitely thin sections $C_p = 0$ at the trailing edge. Large positive values of C_p at the trailing edge imply more severe adverse pressure gradients.

C_L and C_p : The section lift coefficient is related to the C_p by:

$$C_l = \int_0^1 (C_{p_l} - C_{p_u}) d\left(\frac{x}{c}\right) \quad (6.9)$$

This represents the area between the curves.

Stagnation Point: The stagnation point occurs near the leading edge. It is the place at which $U = 0$. Note that in incompressible flow $C_p = 1.0$ at this point. In compressible flow it may be somewhat larger.

We can get a more intuitive picture of the pressure distribution by looking at some examples and this is done in some of the following sections in this chapter.

6.5.3 Airfoil Pressures and Performance

The shape of the pressure distribution is directly related to the airfoil performance as indicated by some of the features shown in the Fig. 6.7.

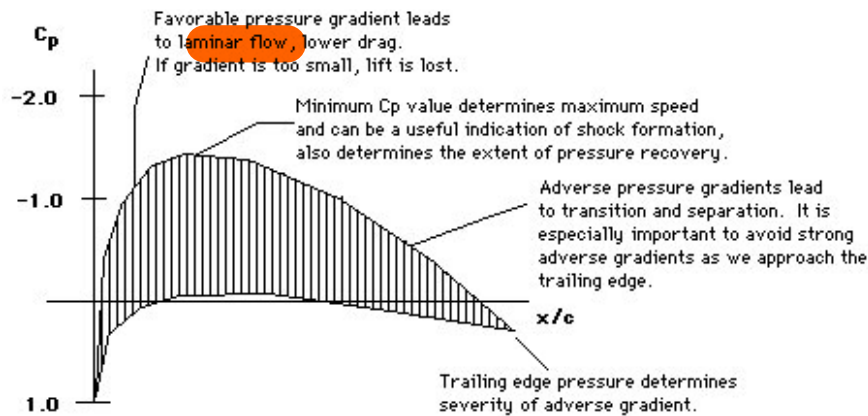


Figure 6.7:

Most of these considerations are related to the airfoil boundary layer characteristics which we will take up later, but even in the inviscid case we can draw some conclusions. We may compute the maximum local Mach numbers and relate those to lift and thickness; we can compute the pitching moment and decide if that is acceptable.

Whether we use the inviscid pressures to form qualitative conclusions about the section, or use them as input to a more detailed boundary layer calculation, we must first investigate the close relation between the airfoil geometry to these pressures.

Relating Airfoil Geometry and Pressures

The relationship between airfoil geometry and airfoil pressure distributions can be predicted numerically solving the relevant field equations. But it can also be understood in an intuitive way.

Let's consider, in more detail the relationship between airfoil geometry and airfoil pressure distributions. The next few examples show some of the effects of changes in camber, leading edge radius, trailing edge angle, and local distortions in the airfoil surface.

6.5.4 Airfoil Design Methods

The process of airfoil design proceeds from a knowledge of the boundary layer properties and the relation between geometry and pressure distribution. The goal of an airfoil design varies. Some airfoils are designed to produce low drag (and may not be required to generate lift at all.) Some sections may need to produce low drag while producing a given amount of lift. In some cases, the drag doesn't really matter — it is maximum lift that is important. The section may be required to achieve this performance with a constraint on thickness, or pitching moment, or off-design

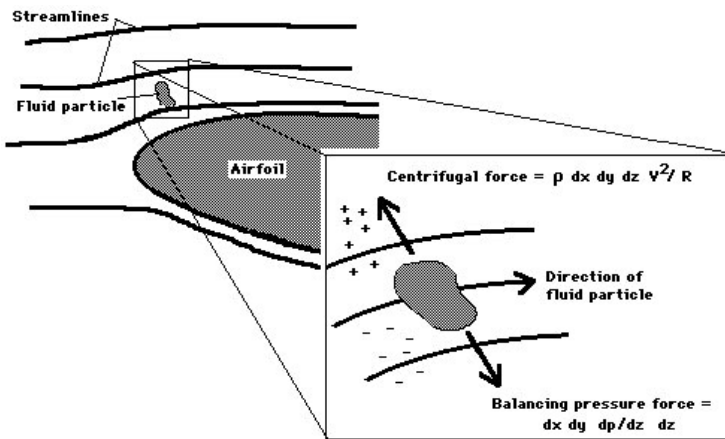


Figure 6.8: Effect of changes in surface curvature

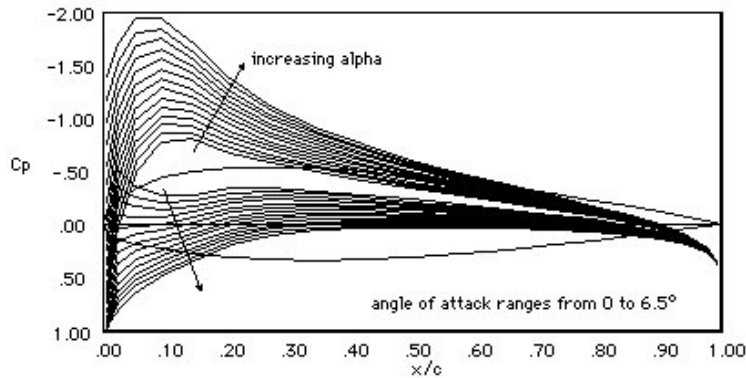


Figure 6.9: Variation of C_p with angle of attack. Note that the “nose peak” becomes more extreme as the angle increases

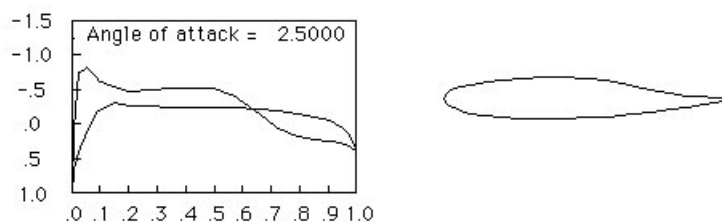


Figure 6.10: A reflexed airfoil section has reduced camber over the aft section producing less lift over this region. and therefore less nose-down pitching moment. In this case the aft section is actually pushing downward and C_{m_0} is positive

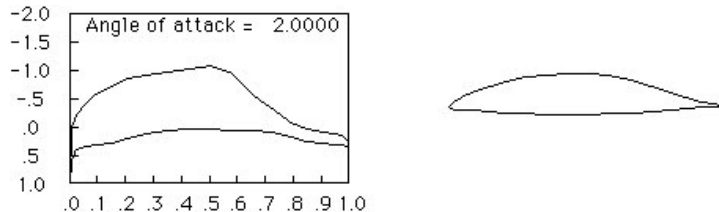


Figure 6.11: A natural laminar flow section has a thickness distribution that leads to a favorable pressure gradient over a portion of the airfoil. In this case, the rather sharp nose leads to favorable gradients over 50% of the section.

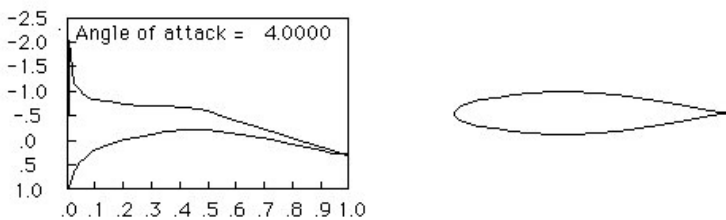


Figure 6.12: Symmetrical section at 4° angle of attack. Note the pressure peak near the nose. A thicker section would have a less prominent peak.

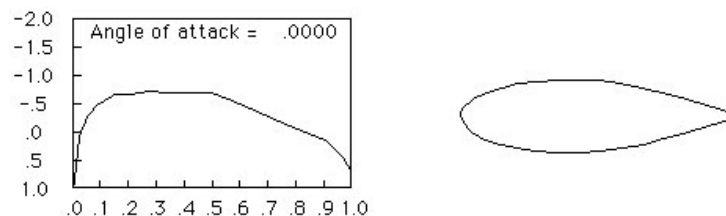


Figure 6.13: Thicker section at 0° . Only one line is shown on the plot because at zero lift, the upper and lower surface pressure coincide.

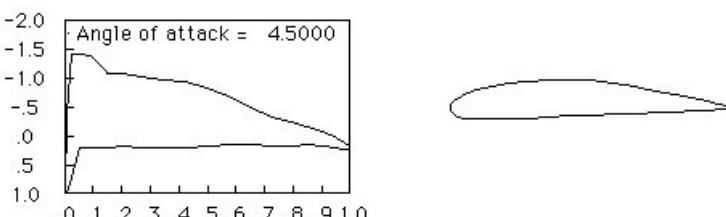


Figure 6.14: A conventional cambered section.

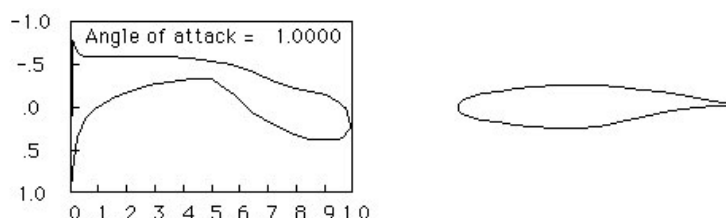


Figure 6.15: Aft-loaded section, the opposite of a reflexed airfoil carries more lift over the aft part of the airfoil. Supercritical airfoil sections look similar to this.

performance, or other unusual constraints. Some of these are discussed further in the section on historical examples.

One approach to airfoil design is to use an airfoil that was already designed by someone who knew what they were doing. This “design by authority” works well when the goals of a particular design problem happen to coincide with the goals of the original airfoil design. This is rarely the case, although sometimes existing airfoils are good enough. In these cases, airfoils may be chosen from catalogs such as Abbott and Von Doenhoff (1959), Althaus and Wortmann (1981), Selig et al. (1989).

The advantage to this approach is that there is test data available. No surprises, such as a unexpected early stall, are likely. On the other hand, available tools are now sufficiently refined that one can be reasonably sure that the predicted performance can be achieved. The use of “designer airfoils” specifically tailored to the needs of a given project is now very common. This section of the notes deals with the process of custom airfoil design.

Methods for airfoil design can be classified into two categories: direct and inverse design.

Direct Methods for Airfoil Design

The direct airfoil design methods involve the specification of a section geometry and the calculation of pressures and performance. One evaluates the given shape and then modifies the shape to improve the performance.

The two main subproblems in this type of method are:

1. The identification of the measure of performance
2. The approach to changing the shape so that the performance is improved

The simplest form of direct airfoil design involves starting with an assumed airfoil shape (such as a NACA airfoil), determining the characteristic of this section that is most problematic, and fixing this problem. This process of fixing the most obvious problems with a given airfoil is repeated until there is no major problem with the section. The design of such airfoils, does not require a specific definition of a scalar objective function, but it does require some expertise to identify the potential problems and often considerable expertise to fix them.

Sometimes the objective of airfoil design can be stated more positively than, “fix the worst things”. We might try to reduce the drag at high speeds while trying to keep the maximum C_L greater than a certain value. This could involve slowly increasing the amount of laminar flow at low C_l s and checking to see the effect on the maximum lift. The objective may be defined numerically. We could actually minimize C_d with a constraint on $C_{l_{\max}}$. We could maximize L/D or $C_l^{3/2}/C_d$ or $C_{l_{\max}}/C_{d@ \text{design } C_l}$. The selection of the figure of merit for airfoil sections is quite important and generally cannot be done without considering the rest of the airplane. For example, if we wish to build an airplane with maximum L/D we do not build a section with maximum L/D because the section C_l for best C_l/C_d is different from the airplane C_L for best C_L/C_D .

Inverse Design

Another type of objective function is the target pressure distribution. It is sometimes possible to specify a desired C_p distribution and use the least squares difference between the actual and target C_ps as the objective. This is the basic idea behind a variety of methods for inverse design. As an example, thin airfoil theory can be used to solve for the shape of the camberline that produces a specified pressure difference on an airfoil in potential flow.

The second part of the design problem starts when one has somehow defined an objective for the airfoil design. This stage of the design involves changing the airfoil shape to improve the performance. This may be done in several ways:

1. By hand, using knowledge of the effects of geometry changes on C_p and C_p changes on performance.
2. By numerical optimization, using shape functions to represent the airfoil geometry and letting the computer decide on the sequence of modifications needed to improve the design.

Bibliography

Ira Herbert Abbott and Albert Edward Von Doenhoff. *Theory of wing sections, including a summary of airfoil data*. Dover Publications, New York, 1959.

Dieter Althaus and Franz Xaver Wortmann. *Stuttgarter Profilkatalog*. F. Vieweg, Braunschweig, Germany, 1981.

John D. Anderson Jr. *Aircraft Performance and Design*. McGraw-Hill, 1999.

Peter Jansen, Ruben. E. Perez, and Joaquim R. R. A. Martins. Aerostructural optimization of nonplanar lifting surfaces. *Journal of Aircraft*, 47(5):1491–1503, September 2010. doi:[10.2514/1.44727](https://doi.org/10.2514/1.44727).

Ilan Kroo. Nonplanar wing concepts for increased aircraft efficiency. In *VKI lecture series on Innovative Configurations and Advanced Concepts for Future Civil Aircraftecture series on Innovative Configurations and Advanced Concepts for Future Civil Aircraft*, 2005.

Ilan Kroo, John McMasters, and Stephen C. Smith. Highly nonplanar lifting systems. In *Transportation Beyond 2000: Technologies Needed for Engineering Design*, pages 331–370, September 1998.

B. Malone and W.H. Mason. Multidisciplinary optimization in aircraft design using analytic technology models. *Journal of Aircraft*, 32(2):431–438, mar-apr 1995. doi:[10.2514/3.46734](https://doi.org/10.2514/3.46734).

W. H. Mason. Analytic models for technology integration in aircraft design. In *AIAA/AH-S/ASEE Aircraft Design, Systems and Operations Conference*, Dayton, OH, September 1990. doi:[10.2514/6.1990-3262](https://doi.org/10.2514/6.1990-3262). AIAA 1990-3262.

Daniel P. Raymer. *Aircraft Design: A Conceptual Approach*. AIAA, 4th edition, 2006.

Michael S Selig, John Francis Donovan, and David B Fraser. *Airfoils at low speeds*, volume 8. H.A. Stokely, Virginia Beach, Va., USA (1504 Horseshoe Cir., Virginia Beach 23451), 1989.

Joram G. Verstraeten and Ronald Slingerland. Drag characteristics for optimally span-loaded planar, wingletted, and C wings. *Journal of Aircraft*, 46(3):962–971, 2009.

Chapter 7

Weights

7.1 Introduction

Weight estimation is of critical importance in aircraft design, and thus it is no coincidence that the very first step in aircraft design is the estimation of the takeoff weight. The initial weight estimation method, described in Chapter 2, is based purely on historical data for the aircraft type in question. This chapter presents a more detailed method that takes into account the geometry of the components and other more detailed information that has been determined by sizing the wing, fuselage, and control surfaces. The overall approach is to estimate the weight of each major component and add them up to estimate the total. The actual weight of the aircraft will not be known until the aircraft flies because it is difficult to predict the weight of every component in advance. However, it is crucial to continuously improve the weight estimate to ensure that the design is on track to meeting the requirements. In addition, this chapter also describes how to estimate the position of the center of gravity (CG) of the aircraft, which is critical for stability and control, as we will see in the next chapter.

The component weights are usually grouped in the following categories:

Structures: e.g., wing, vertical tail, horizontal tail, fuselage, main landing gear, nose landing gear, engine mounts, and firewall.

Propulsion: e.g., installed engines, exhaust system, engine oil, engine controls, starter, fuel system, and tank.

Equipment: e.g., flight controls, APU, instruments, hydraulics, pneumatics, electrical, avionics, furnishings, air conditioning, and anti-icing.

Useful load: e.g., crew, usable fuel, trapped fuel, oil, passengers, baggage, and other cargo.

7.2 Preliminary Empty Weight and Center of Gravity Calculation

As an intermediate weight estimation, the weights for various components of the aircraft can be estimated based on their surface areas by assuming an average weight per unit area for each component based on historical data. Typical weights per unit area are listed in Table 7.1. Weights for engines or motors can be found for existing models or using the estimates discussed in Section 7.3.3.

	Fighters		Transport & Bomber		General aviation		Multiplier	Approximate location
	lb/ft ²	kg/m ²	lb/ft ²	kg/m ²	lb/ft ²	kg/m ²		
Wing	9	44	10	49	2.5	12	$S_{\text{exposed planform}}$	40% MAC
Horizontal tail	4	20	5.5	27	2	10	$S_{\text{exposed planform}}$	40% MAC
Vertical tail	5.3	26	5.5	27	2	10	$S_{\text{exposed planform}}$	40% MAC
Fuselage	4.8	23	5	24	1.4	7	$S_{\text{wetted area}}$	40–50% length
	Weight ratio		Weight ratio		Weight ratio			
Landing gear*	0.033		0.043		0.057		TOGW	centroid
Landing gear—Navy	0.045		—		—		TOGW	centroid
Installed engine	1.3		1.3		1.4		Engine weight	centroid
"All-else empty"	0.17		0.17		0.1		TOGW	40–50% length

*15% to nose gear, 85% to main gear; reduce gear weight by 0.014 W_0 if fixed gear.

Table 7.1: Typical weights per unit area various aircraft components using the approximate empty weight buildup (Raymer, 2006, Table 15.2)

To obtain a preliminary estimate of the aircraft CG location, we need the approximate CG locations of each component. Table 7.1 also lists the approximate CG locations for the major aircraft components.

The position of the aircraft CG is then given by,

$$x_{\text{CG}} = \frac{\sum_i W_i x_{\text{CG},i}}{\sum_i W_i} \quad (7.1)$$

where the CG positions can be measured with respect to any reference point, as long as it is used consistently. This equation can also be used with the more detailed component weight estimates described in Section 7.3.

Example 7.1: Preliminary Weight and CG for a Long Range Transport

This example is based on the Boeing 777-200LR. The weights for each component are estimated using the factors listed in Table 7.1. The first step is to estimate the 40 % mean aerodynamic chord (MAC) location of the wing, horizontal stabilizers, and vertical stabilizer. For a trapezoidal planform, Eqn. (7.2) can be used to estimate the MAC.

$$\text{MAC} = \frac{2}{3} \left(c_{\text{root}} + c_{\text{tip}} - \frac{c_{\text{root}} c_{\text{tip}}}{c_{\text{root}} + c_{\text{tip}}} \right) \quad (7.2)$$

The location of the mean aerodynamic chord relative to the nose can be calculated using Raymer (2006, Fig. 4.17).

$$x_{\text{MAC}} = x_{\text{RLE}} + \frac{b}{6} \frac{c_{\text{root}} + 2 c_{\text{tip}}}{c_{\text{root}} + c_{\text{tip}}} \tan(\Lambda_{\text{LE}}) \quad (7.3)$$

where x_{MAC} is the position of the leading edge of the MAC, x_{RLE} is the position of the leading edge of the root chord, and Λ_{LE} is the sweep angle of the leading edge. The location of the 40% MAC point can then be calculated as

$$x_{40\% \text{ MAC}} = x_{\text{MAC}} + 0.4 \text{ MAC} \quad (7.4)$$

Table 7.2 lists the approximate geometric parameters for equivalent trapezoidal planforms corresponding to the 777-200LR. For the wing, the MAC is

	c_{root} (ft)	c_{tip} (ft)	x_{RLE} (ft)	b (ft)	Λ_{LE} (deg)
Wing	41.3	4.7	64.0	206.0	33.7
Horizontal Tail	23.0	8.2	173.4	71.0	38.7
Vertical Tail	27.8	8.2	166.2	33.6	44.4

Table 7.2: 777-200LR wing, horizontal tail, and vertical tail geometric parameters

$$\text{MAC}_W = \frac{2}{3} \left(41.3 + 4.7 - \frac{41.3 \times 4.7}{41.3 + 4.7} \right) = 27.9 \text{ ft} \quad (7.5)$$

and the position of the 40 % MAC point measured relative to the nose is

$$x_{40\% \text{ MAC}, W} = 64.0 + \frac{206}{6} \frac{41.3 + 2 \times 4.7}{41.3 + 4.7} \tan(33.7) + 0.4 \times 27.9 = 100.4 \text{ ft} \quad (7.6)$$

Similarly, for the horizontal tail, the position of the 40 % MAC point measured relative to the nose can be calculated to be

$$x_{40\% \text{ MAC}, \text{HT}} = 192.1 \text{ ft} \quad (7.7)$$

For the vertical tail, the MAC is calculated using the same method described above.

$$\text{MAC}_{\text{VT}} = \frac{2}{3} \left(27.8 + 8.2 - \frac{27.8 \times 8.2}{27.8 + 8.2} \right) = 19.8 \text{ ft} \quad (7.8)$$

However, for the position of the 40% MAC point, twice the span of the vertical tail must be used in Eq. 7.3.

$$x_{40\% \text{ MAC}, \text{VT}} = 166.2 + \frac{2 \times 33.6}{6} \frac{27.8 + 2 \times 8.2}{27.8 + 8.2} \tan(44.4) + 0.4 \times 19.8 = 187.6 \text{ ft} \quad (7.9)$$

Now, we can use the factors listed in Table 7.1 to estimate the weights for the different components. Table 7.3 lists the weight estimates and their approximate CG locations (measured relative to the nose). Note that the multipliers for the wing and tail weights are the exposed planform areas. These are the planform areas of the portions of the wing and tail surfaces that are exposed to the air.

	Ratio	Multiplier	Weight	CG location	Moment
Wing	10 lb/ft ²	3,923 ft ²	39,230 lb	100.4 ft	3,938,692 lb-ft
Horizontal tail	5.5 lb/ft ²	903 ft ²	4,967 lb	192.1 ft	954,161 lb-ft
Vertical tail	5.5 lb/ft ²	604 ft ²	3,322 lb	187.6 ft	623,207 lb-ft
Fuselage	5 lb/ft ²	13,125 ft ²	65,625 lb	93 ft	6,103,125 lb-ft
Nose landing gear	0.043 × 0.15	766,000 lb	4,941 lb	19.3 ft	95,361 lb-ft
Main landing gear	0.043 × 0.85	766,000 lb	27,997 lb	103.9 ft	2,908,888 lb-ft
Installed engine	1.3	36,520 lb	47,476 lb	77.3 ft	3,669,895 lb-ft
All-else empty	0.17	766,000 lb	130,220 lb	93 ft	12,110,460 lb-ft
Total			323,778 lb		30,403,789 lb-ft

Table 7.3: Empty weight buildup and moment estimates for the 777-200LR

Table 7.4 compares the empty weight estimates obtained using the two different methods covered so far. In the case of the 777-200LR, this quick and dirty estimate is more accurate than the initial

empty weight estimate. Once we have the empty weights and moments calculated, we can also obtain the empty aircraft CG location.

$$x_{CG} = \frac{\sum_i W_i x_{CG,i}}{\sum_i W_i} = \frac{30,403,789}{323,778} = 93.9 \text{ ft} \quad (7.10)$$

777-200LR W_e	First estimate W_e	% Difference	Weight buildup estimate W_e	% Difference
320,000 lb	349,993 lb	9.4%	323,778 lb	1.2%

Table 7.4: Comparison of actual and estimated empty weights of the 777-200LR

7.3 Detailed Component Weights Method

A more refined weights group estimate also uses regression analysis performed on historical data, but takes into account more details. For a wing, for example, instead of accounting only for its reference area, it will account for its geometry (aspect ratio, taper ratio, thickness to chord ratio, and sweep) as well as the dynamic pressure and load factor at the operating conditions.

The various regressions are often aircraft dependent, as one would expect. For a given component, different regressions exist, both in the literature and within companies. Weight estimation methods within a company are closely guarded trade secrets. It is a good idea to try different estimates that are applicable to your type of aircraft to get an idea of the uncertainty bounds of the estimate.

Pay particular attention to the units of the result and the numbers you use in the formulas.

Note that for non-conventional aircraft, the estimates will not work as well.

7.3.1 Load Factor

The weights of some aircraft components obviously depend on the magnitude of the loads the aircraft is designed to sustain. The greatest loads come from generation of lift during high-g maneuvers. A load factor n is number of g's experienced in a given maneuver. Raymer (2006, Table 14.2) lists typical load factors for various types of aircraft (typically between 3 and 4 for transport aircraft). See section 11.3.3 for the FAR requirements.

7.3.2 Wing

The wing weight estimate is particularly important because it is a major factor in the aerostructural tradeoff. In particular, the variation of wing weight with reference area, aspect ratio, sweep and thickness-to-chord ratio is important, because these same variables have a direct effect on the aerodynamic performance. Typical wing weights are 20–30% of the OEW.

For cargo/transport aircraft, Raymer (2006, Eqn.(15.25)) gives

$$W_{wing} = 0.0051(W_{dg}N_z)^{0.557}S_w^{0.649}AR^{0.5}(t/c)_{root}^{-0.4}(1+\lambda)^{0.1}(\cos\Lambda)^{-1}S_{csw}^{0.1}, \quad (7.11)$$

where W_{dg} is the flight design gross weight in lb, N_z is the ultimate load factor ($1.5 \times$ limit load factor, see Section 11.3.3 for the limit load factor), S_w is the trapezoidal wing area in ft^2 , AR is the aspect ratio, $(t/c)_{root}$ is the thickness to chord ratio at the root, λ is the taper ratio, Λ is the wing sweep at 25 % MAC, and S_{csw} is the wing mounted control surface area (including flaps) in ft^2 .

Kroo, Component Weights gives

$$W_{\text{wing}} = 4.22S_{\text{wing}} + 1.642 \times 10^{-6} \frac{n b^3 \sqrt{W_0 W_{ZF}} (1 + 2\lambda)}{S_{\text{wing}}(t/c) \cos^2 \Lambda_{EA}(1 + \lambda)}, \quad (7.12)$$

where S_{wing} is the gross wing area (in ft^2 with chords extended to the aircraft centerline), W_0 is the maximum takeoff weight in lb, W_{ZF} is the zero fuel weight in lb, n is the ultimate load factor, b is the span in ft, t/c is the thickness to chord ratio, Λ_{EA} is the sweep angle of the structural elastic axis, and λ is the taper ratio.

Torenbeek (1990, Eq. (8.12)) and Nicolai and Carichner (2010, Eq. (20.2)) present other estimates that is appropriate for jet transports.

7.3.3 Engine/Motor

Jet engines

The engine weight regression is another important component as it measures the tradeoff of maximum sea level static thrust to engine weight. In particular the engine weight is the weight of the dry engine, along with oil, thrust reverser, control, and starting system weights. These weights depend only on the maximum thrust of each engine, T_0 , in lbs, as seen below, Roskam:

$$W_{\text{eng dry}} = 0.521(T_0)^{0.9} \quad (7.13)$$

$$W_{\text{eng oil}} = 0.082(T_0)^{0.65} \quad (7.14)$$

$$W_{\text{eng rev}} = 0.034(T_0) \quad (7.15)$$

$$W_{\text{eng control}} = 0.26(T_0)^{0.5} \quad (7.16)$$

$$(7.17)$$

The starting system weight for aircraft with 1 or 2 jet engines using a pneumatic system according to Roskam is

$$W_{\text{eng start}} = 9.33 \left(\frac{W_{\text{eng dry}}}{1000} \right)^{1.078} \quad (7.18)$$

The total weight of a single engine is then:

$$W_{\text{engine}} = W_{\text{eng dry}} + W_{\text{eng oil}} + W_{\text{eng rev}} + W_{\text{eng control}} + W_{\text{eng start}} \quad (7.19)$$

Turboprop engines

From Roskam (1989, Part V, Fig. 6.2) we get the following relation based on existing turboprop engines from 1985:

$$W_{\text{eng}} = P^{0.9306} 10^{-0.1205}, \quad (7.20)$$

where P is the rated shaft horsepower (for one engine) and W_{eng} is the weight of the engine in lbs. Alternatively, using the power and weights of more up-to-date engines, we can develop our own regression. To account for the weight of other components (such as fuel, oil, and control systems) that are required when the engine is installed onto the aircraft, including the propeller, we can use the following formula from Torenbeek (1990, Section 8.4.2):

$$W_{\text{pg}} = k_{\text{pg}}(W_{\text{eng}} + 0.24P_{\text{TO}}), \quad (7.21)$$

where W_{pg} is the weight of the propulsion group for each engine (including the engine) in lbs, k_{pg} is a factor that depends on the aircraft type (1.16 for single tractor propeller in the fuselage and 1.35 for multi-engine propeller aircraft), and P_{TO} is the rated takeoff horsepower.

Electric motors

Electric motors are a relatively scale-free technology. This means that their power-to-weight ratio does not change significantly with rated power. Power-to-weight ratios can be found for existing electric motors and motors under development. For example, Siemens¹ has developed motors with a power-to-weight ratio of 5.2 kW/kg and are looking to further improve this for their motor that will be used on the Airbus E-fan X test platform.

7.3.4 Fudge factors

Since the above weight estimates are based on databases of existing aircraft, they may provide poor predictions for aircraft using advanced materials and novel configurations. To account for this it is common to use reasonable fudge factors. Raymer (2006, Section 15.4) recommends the factors in Table 7.5 to account for advanced composites.

Weight group	Fudge factor (multiplier)
Wing	0.85 – 0.90
Tails	0.83 – 0.88
Fuselage/nacelle	0.90 – 0.95

Table 7.5: Fudge factors to account for composite materials (Raymer, 2006)

7.3.5 Other Components

The estimates for other components are given by Kroo, (Component Weights section), Raymer (2006, Sec. 15.3), Torenbeek (1990, Sec. 8.4), and Nicolai and Carichner (2010, Sec.20.2).

7.3.6 A More Sophisticated Weight Estimate

Below is an example of the previous weight estimate algorithm updated with the new component breakdown methods introduced this chapter. Note that empty weight regression has been dropped in lieu of the individual component weights. With this new weight approximation it is now possible to account for the trade-off in weight for a larger wing or more engine thrust. Also note that we do not use Table 7.1 to the engine weight instead using Roskam (1989, Eqn.(8.15)) to better capture the importance engine design on take off weight.

Bibliography

Ilan M. Kroo. Aircraft design: Synthesis and analysis. URL <http://adg.stanford.edu/aa241/AircraftDesign.html>.

¹<https://www.siemens.com/innovation/en/home/pictures-of-the-future/mobility-and-motors/the-future-of-mobility-e-fan-x.html>

Algorithm 5 A more detailed weight estimate

Leland M. Nicolai and Grant E. Carichner. *Fundamentals of Aircraft and Airship Design, Vol I — Aircraft Design*. AIAA, Reston, VA, 2010.

Daniel P. Raymer. *Aircraft Design: A Conceptual Approach*. AIAA, 4th edition, 2006.

J. Roskam. *Airplane Design, Volumes 1-8*. Roskam Aviation and Engineering Corporation, 1989.

E. Torenbeek. *Synthesis of Subsonic Airplane Design*. Delft University Press and Kluwer Academic Publishers, 6th edition, 1990.

Chapter 8

Stability and Control

When an airplane is stable, it tends to return to its equilibrium position after being disturbed without any action from the pilot.

8.1 Preliminary Empennage Sizing

For the initial layout, we use an approach based on historical data to size the empennage. The effectiveness of the vertical and horizontal tails can be quantified using the *tail volume coefficients*,

$$c_{VT} = \frac{L_{VT}S_{VT}}{b_W S_W} \quad (8.1)$$

$$c_{HT} = \frac{L_{HT}S_{HT}}{\bar{c}_W S_W} \quad (8.2)$$

Fig. 8.1 shows the definitions of the various moment arms and areas involved.

The preliminary empennage sizing methods consists in choosing the tail volume coefficients based on historical data and then compute the required tail area given the moment arm available in the configuration. The historical tail volume coefficient can be estimated for a given aircraft type by estimating lengths and areas from scale drawings. Alternatively, [Raymer \(2012, Table 6.4\)](#) lists typical coefficients for different types of aircraft.

Example 8.1: Preliminary Empennage Sizing for a Long Range Transport

We base this calculation on the drawings of a Boeing 777-200LR, and likewise, you should base your calculation on the drawings of your own aircraft.

Based on the 777-200LR drawings, we can find the following data: the vertical tail moment arm is $L_{VT} = 104.5 \text{ ft}$, the horizontal tail moment arm is $L_{HT} = 114.9 \text{ ft}$, the wing area is $S_W = 4,605 \text{ ft}^2$, the wing mean chord $\bar{c}_W = 27.9 \text{ ft}$ and the wing span is $b_W = 199 \text{ ft}$.

The typical horizontal and vertical tail volume coefficients for jet transports, according to [Raymer \(2012, Table 6.4\)](#) are $c_{VT} = 0.09$ and $c_{HT} = 1$, respectively.

Now we can use the tail volume coefficient equations (8.1, 8.2) to obtain the required planform areas,

$$S_{VT} = \frac{c_{VT}b_W S_W}{L_{VT}} = \frac{0.09 \times 199 \times 4,605}{104.5} = 789.2 \text{ ft}^2 \quad (8.3)$$

$$S_{HT} = \frac{c_{HT}\bar{c}_W S_W}{L_{HT}} = \frac{1.00 \times 27.9 \times 4,605}{114.9} = 1,118.2 \text{ ft}^2 \quad (8.4)$$

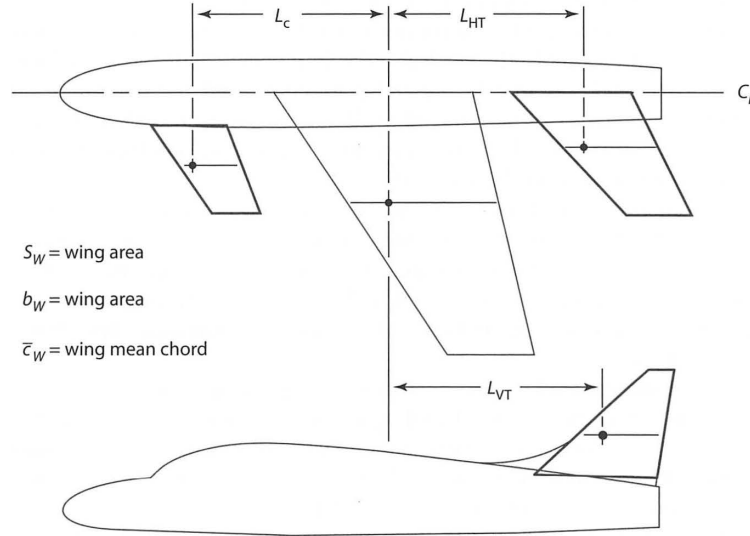


Figure 8.1: Areas and moment arms in the tail volume coefficient formulas (Raymer, 2012, Fig. 6.2)

The Boeing 777-200LR actual vertical tail area is 573.0 ft^2 and a horizontal tail surface area of $1,090 \text{ ft}^2$, so there is some discrepancy between the initial sizing and the actual tail sizes.

8.2 Longitudinal Static Stability

8.2.1 Center of Pressure of an Airfoil

The pitching moment of an airfoil is an important quantity when considering the longitudinal equilibrium and stability. For a given angle of attack, this moment varies with the longitudinal position within the airfoil about which the moment is computed, as shown in Figure 8.2. There is a particular point about which the moment is zero, and this is called the *center of pressure*.

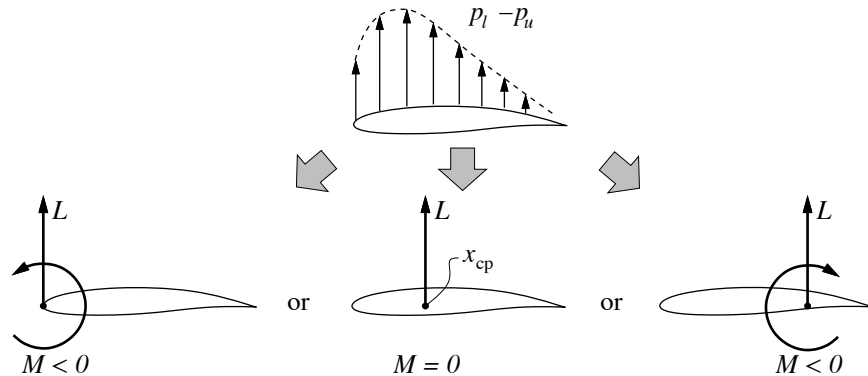


Figure 8.2: The airfoil center of pressure, x_{cp} is the point in the about which the moment is zero(Drela, 2003).

The center of pressure for a symmetric airfoil is located at about $0.25c$ and does not change with angle of attack or thickness distribution. This can be shown using thin-airfoil theory in

incompressible flow. However, the center of pressure moves wildly with the angle of attack, as seen in Figure 8.3. For an airfoil with positive camber, this position tends to $+\infty$ as the lift tends to zero. Given this movement, the center of pressure is not useful as a reference point in longitudinal stability. Instead, we use the *aerodynamic center*, which is explained below.

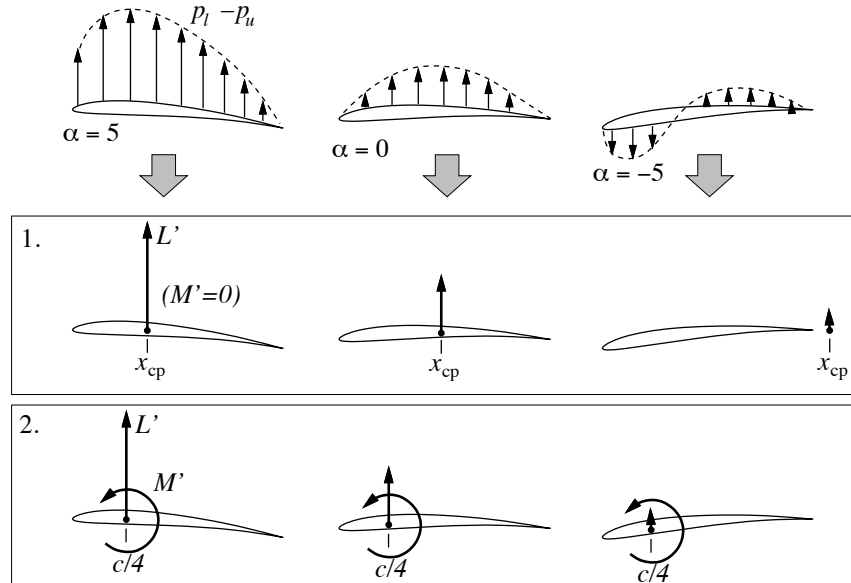


Figure 8.3: The airfoil center of pressure, x_{cp} is the point in the about which the moment is zero(Drela, 2003).

8.2.2 Aerodynamic Center

One surprising feature of airfoil aerodynamics is that there is one position on the chord line where the magnitude of the pitching moment does not change significantly with the angle of attack. This point is called the *aerodynamic center* and is coincided with the center of pressure for symmetric airfoils ($0.25c$). This is a useful reference point for longitudinal trim and stability computations.

8.2.3 Mean Aerodynamic Chord

The notion of aerodynamic center introduced above is for an airfoils, but can be extended to wings by defining the *mean aerodynamic chord* (\bar{c} , or MAC). The MAC of a wing is defined as,

$$\bar{c} = \frac{1}{S} \int_{-b/2}^{b/2} c(y)^2 dy \quad (8.5)$$

which mathematically is the root-mean-square chord. The geometric representation of the mean aerodynamic chord for a trapezoidal wing is shown in Fig. 8.4. For a trapezoidal wing, the MAC can be computed using,

$$\bar{c} = \frac{2}{3} c_{root} \frac{1 + \lambda + \lambda^2}{1 + \lambda} \quad (8.6)$$

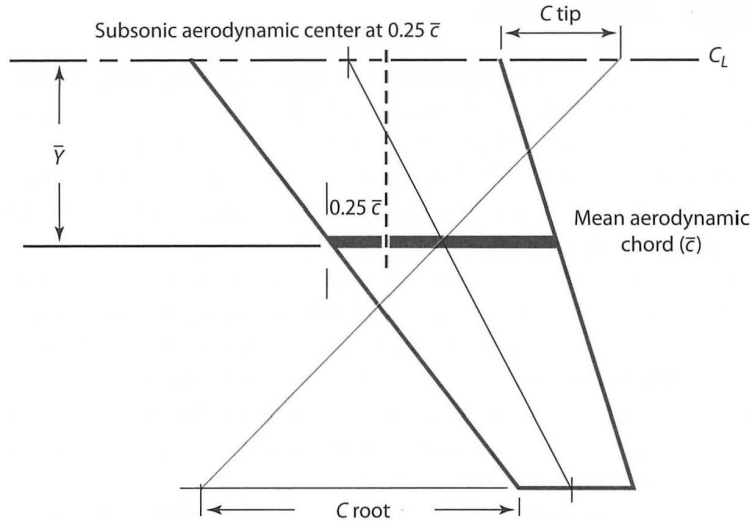


Figure 8.4: Geometric interpretation of the mean aerodynamic chord for a trapezoidal wing (Raymer, 2012, Fig. 4.13)

The MAC is also characterized by a spanwise position, \bar{Y} , whose geometric representation is also shown in Fig. 8.4. For a trapezoidal wing, the \bar{Y} can be computed using,

$$\bar{Y} = \frac{b}{6} \left(\frac{1 + 2\lambda}{1 + \lambda} \right). \quad (8.7)$$

This spanwise position ends up defining the longitudinal position of the MAC, which has a physical meaning: the quarter point of the MAC is the approximate aerodynamic center of the wing (at least for subsonic conditions). The longitudinal position of the quarter MAC will be important in the longitudinal stability computations. Also, MAC is the reference chord of choice for non-dimensionalizing longitudinal moment coefficients.

8.2.4 Equations for Trim Static Stability

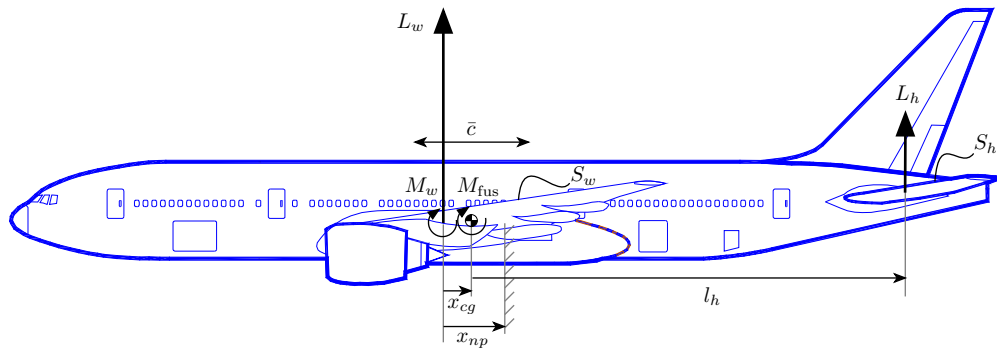


Figure 8.5: Forces and moments for longitudinal trim and static stability; arrows show positive quantities. Note that M_w and L_h are usually negative.

The analysis of longitudinal stability and trim begins with expressions for the pitching moment

about the airplane CG,

$$C_{m_{cg}} = \frac{x_{cg}}{\bar{c}} C_{L_w} - \frac{l_h}{\bar{c}} \frac{S_h}{S_w} C_{L_h} + C_{m_w} + C_{m_{fus}} \quad (8.8)$$

Where:

x_{cg}	= distance from wing aerodynamic center back to the CG
\bar{c}	= mean aerodynamic chord
C_{L_w}	= wing lift coefficient
l_h	= distance from CG back to tail
S_h	= horizontal tail reference area
S_w	= wing reference area
C_{L_h}	= tail lift coefficient
C_{m_w}	= wing pitching moment coefficient (about the wing aerodynamic center)
$C_{m_{fus}}$	= pitching moment of fuselage, nacelles, and other components (about CG)

For equilibrium in level flight, in addition to the lift being equal to the weight, the moment must be zero ($C_{m_{cg}} = 0$). If both these conditions are met, the aircraft is said to be *trimmed*.

For stability, if we displace the wing or airplane from its equilibrium flight condition to a higher angle of attack and thus higher lift coefficient, we would like the airplane to naturally return to the lower lift coefficient, otherwise, the angle of attack will keep increasing until the airplane stalls. This requires that the pitching moment about the rotation point, $C_{m_{cg}}$, to become negative as we increase C_L , i.e.,

$$\frac{\partial C_{m_{cg}}}{\partial C_L} < 0 \quad (8.9)$$

We can approximate this derivative by differentiating the pitching moment coefficient equation (8.8) with respect the angle of attack:

$$\frac{\partial C_{m_{cg}}}{\partial \alpha} = \frac{x_{cg}}{\bar{c}} C_{L_{\alpha w}} - \frac{l_h S_h}{\bar{c} S_w} C_{L_{\alpha h}} + \frac{\partial C_{m_{fus}}}{\partial \alpha} \quad (8.10)$$

where $C_{L_{\alpha w}}$ and $C_{L_{\alpha h}}$ are the lift curve slopes for the wing and the horizontal stabilizer, respectively. This derivative of the total moment with respect to angle of attack is called the *pitch stiffness*.

The *neutral point*, x_{np} is the position of CG that would achieve neutral stability ($\partial C_{m_{cg}} / \partial \alpha = 0$) for a given configuration. This can be found by setting Eq. (8.10) to zero, and yielding:

$$\frac{x_{np}}{\bar{c}} = \frac{l_h S_h}{\bar{c} S_w} \frac{C_{L_{\alpha h}}}{C_{L_{\alpha w}}} - \frac{1}{C_{L_{\alpha w}}} \frac{\partial C_{m_{fus}}}{\partial \alpha} \quad (8.11)$$

where we replace x_{cg} with x_{np} , by definition.

The distance from the neutral point to the actual CG position, normalized with respect to the MAC is called the *static margin*:

$$\text{static margin} = \frac{x_{np} - x_{cg}}{\bar{c}} = \frac{l_h S_h}{\bar{c} S_w} \frac{C_{L_{\alpha h}}}{C_{L_{\alpha w}}} - \frac{1}{C_{L_{\alpha w}}} \frac{\partial C_{m_{fus}}}{\partial \alpha} - \frac{x_{cg}}{\bar{c}} \quad (8.12)$$

By comparing Eq. (8.12) with Eq.(8.10), we see that

$$-\frac{\partial C_{m_{cg}}}{\partial \alpha} \frac{1}{C_{L_{\alpha w}}} = -\frac{\partial C_{m_{cg}}}{\partial C_{L_w}} \quad (8.13)$$

Note that this is approximate because the static margin is really the derivative of $C_{m_{cg}}$ with respect to the lift coefficient of the entire airplane.

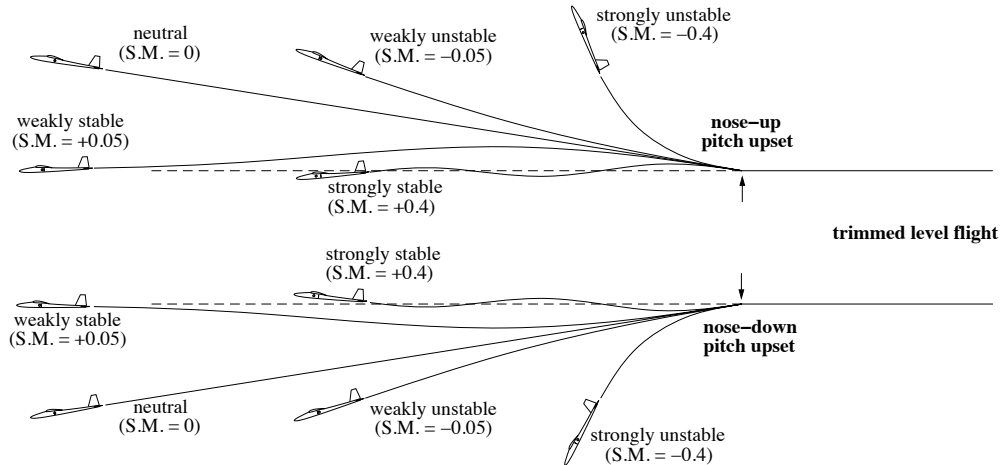


Figure 8.6: Possible flight trajectories for various static margin values (Drela, 2006).

The tail lift curve slope, $C_{L_{\alpha h}}$, is affected by the presence of the wing and the fuselage. In particular, the wing and fuselage produce downwash on the tail, and the fuselage boundary layer and contraction reduce the local velocity of flow over the tail. Thus we write,

$$C_{L_{\alpha h}} = C_{L_{\alpha h0}} \left(1 - \frac{\partial \varepsilon}{\partial \alpha} \right) \eta_h \quad (8.14)$$

where $C_{L_{\alpha h0}}$ is the isolated tail lift curve slope.

The isolated wing and tail lift curve slopes may be determined from experiments, simple codes such as the wing analysis program in these notes, or even from analytical expressions such as the DATCOM formula:

$$C_{L_{\alpha}} \approx \frac{2\pi AR}{2 + \sqrt{(AR/\eta)^2(1 + \tan^2 \Lambda - M^2) + 4}} \quad (8.15)$$

where the often-used constant η accounts for the difference between the theoretical section lift curve slope of 2π and the actual value. A typical value is $\eta = 0.97$.

The value of the downwash at the tail is affected by fuselage geometry, flap angle wing planform, and tail position. It is best determined by measurement in a wind tunnel, but lacking that, lifting surface computer programs do an acceptable job. For advanced design purposes it is often possible to approximate the downwash at the tail by the downwash far behind an elliptically-loaded wing:

$$\varepsilon \approx \frac{2C_{L_w}}{\pi AR_w} \quad \Rightarrow \quad \frac{\partial \varepsilon}{\partial \alpha} \approx \frac{2C_{L_{\alpha w}}}{\pi AR_w} \quad (8.16)$$

We have now most of the pieces required to predict the airplane stability. The last and important factor is the fuselage contribution. The fuselage produces a pitching moment about the CG which depends on the angle of attack. It is influenced by the fuselage shape and interference of the wing on the local flow. Additionally, the fuselage affects the flow over the wing. Thus, the destabilizing effect of the fuselage depends on: L_f , the fuselage length, w_f , the fuselage width, the wing sweep, aspect ratio, and location on the fuselage.

Gilruth (NACA TR711) developed an empirically-based method for estimating the effect of the fuselage:

$$\frac{\partial C_{m_{fus}}}{\partial C_L} = \frac{K_f w_f^2 L_f}{S_w \bar{c} C_{L_{\alpha w}}}, \quad (8.17)$$

wing 1/4 chord position	K_f
.1	.115
.2	.172
.3	.344
.4	.487
.5	.688
.6	.888
.7	1.146

Table 8.1: Values of K_f for different position quarter root chord on body as fraction of body length

where,

$C_{L_{\alpha w}}$ is the wing lift curve slope per radian

L_f is the fuselage length

w_f is the maximum width of the fuselage

K_f is an empirical factor discussed in NACA TR711 and developed from an extensive test of wing-fuselage combinations in NACA TR540.

K_f is found to depend strongly on the position of the quarter chord of the wing root on the fuselage. In this form of the equation, the wing lift curve slope is expressed in radians and K_f is given below. The data shown in Table 8.1 is taken from [Jacobs and Ward \(1936\)](#) and [Schlichting and Truckenbrodt \(1979\)](#):

Finally, nacelles and pylons produce a change in static margin. On their own nacelles and pylons produce a small destabilizing moment when mounted on the wing and a small stabilizing moment when mounted on the aft fuselage.

With these methods for estimating the various terms in the expression for pitching moment, we can satisfy the stability and trim conditions. Trim can be achieved by setting the incidence of the tail surface (which adjusts C_{L_h}) to make $C_{m_{cg}} = 0$:

Thus, given a stability constraint and a trim requirement, we can determine where the CG must be located and can adjust the tail lift to trim. We then know the lifts on each interfering surface and can compute the combined drag of the system.

Example 8.2: Static Margin Estimation for a Long Range Transport

Following up on Example 1, we calculate the static margin for the Boeing 777-200LR. The first step is to compute the neutral point of the aircraft. We begin with the lift slope curve of the main wing. For the 777-200LR, we already have wing geometry ($AR = 8.7$, $\Lambda = 33.7$ deg) and the cruise speed ($M = 0.84$). Assuming a section lift curve difference coefficient $\eta = 0.97$, we can use DATCOM formula (8.15) to compute the lift curve slope,

$$C_{L_{\alpha w}} \approx \frac{2\pi AR}{2 + \sqrt{(AR/\eta)^2(1 + \tan^2 \Lambda - M^2) + 4}} = 5.48 \text{ per radian} \quad (8.18)$$

Similarly, we can compute the lift curve slope for the horizontal tail, given that $AR_h = 4.5$, $\Lambda_h = 35$ deg.

$$C_{L_{\alpha h0}} \approx \frac{2\pi AR}{2 + \sqrt{(AR/\eta)^2(1 + \tan^2 \Lambda - M^2) + 4}} = 4.30 \text{ per radian} \quad (8.19)$$

Since the tail would be affected by the downwash from the main wing, we calculate the downwash using Eq. (8.14),

$$\frac{\partial \varepsilon}{\partial \alpha} \approx \frac{2C_{L_{\alpha w}}}{\pi AR_w} = 0.401 \text{ per radian} \quad (8.20)$$

and then correct the tail lift curve slope by assuming a free stream downwash by an elliptically-loaded wing using Eq. (8.16),

$$C_{L_{\alpha h}} = C_{L_{\alpha h 0}} \left(1 - \frac{\partial \varepsilon}{\partial \alpha} \right) \eta_h = 2.32 \text{ per radian} \quad (8.21)$$

where we used a tail efficiency of $\eta_h = 0.9$, which is typical for low tails.

Now, we also need to consider the contribution from the fuselage using the empirically-based method given by Eq. (8.17). The width of fuselage is $w_f = 20.4$ ft, the length of fuselage is $L_f = 209$ ft, the wing area is $S_w = 4605 \text{ ft}^2$ and the mean chord is $\bar{c} = 27.9$ ft. The empirical factor, K_f , is 0.487.

$$\frac{\partial C_{m_{\text{fuselage}}}}{\partial C_L} = \frac{K_f w_f^2 L_f}{S_w \bar{c} C_{L_{\alpha w}}} = 0.0602 \quad (8.22)$$

Finally, we can put everything together using Eq. (8.12) to compute static margin.

$$-\text{static margin} \approx \frac{\partial C_m}{\partial C_{L_w}} = \frac{x_{CG} - x_{25\%MAC}}{\bar{c}} - \frac{C_{L_{\alpha h}} S_h l_h}{C_{L_{\alpha w}} S_w \bar{c}} + \frac{\partial C_{m_{\text{fuselage}}}}{\partial C_L} \quad (8.23)$$

$$-\text{static margin} = \frac{93.9 - 96.24}{27.9} - \frac{2.32 \times 1,090 \times 97.2}{5.48 \times 4,605 \times 27.9} + 0.0602 = -0.0839 - 0.349 + 0.0602 = -0.3727 \quad (8.24)$$

Therefore, we get the static margin is 37.27% for 700-200LR example. Due the accuracy of the quick weight buildup method used to estimate of the CG location, the static margin is on the high side of the desired range between 5% to 40%. The Boeing 777-200LR actually has a very low static margin to increase the cruise performance. According to the Boeing article (www.boeing.com/commercial/aeromagazine/aero_02/textonly/fo01txt.html), Boeing 777 use digital flight control computers to provide positive stability. The actual CG location of 777-200 is between 7.5% to 44%. Our CG estimate is very close to the most stable CG location of the 777-200. Due to the advance digital flight control on the 777, airliners often set the CG close to the aft limit in order to save fuel. With CG at 30% of MAC, the static margin is about 23%. At the aft CG limit, the static margin is about 9.9%.

8.3 Dynamic Stability

8.3.1 Introduction

The evaluation of static stability provides some measure of the airplane dynamics, but only a rather crude one. The dynamic response of the aircraft is of greater relevance, especially for lateral motion. It is possible for an airplane to be statically stable, yet dynamically unstable, resulting in unacceptable characteristics.

Just what constitutes acceptable characteristics is often not obvious, and several attempts have been made to quantify pilot opinion on acceptable handling qualities. Subjective flying qualities evaluations such as Cooper–Harper ratings are used to distinguish between “good-flying” and

difficult-to-fly aircraft. New aircraft designs can be simulated to determine whether they are acceptable. Such real-time, pilot-in-the-loop simulations are expensive and require a great deal of information about the aircraft. Earlier in the design process, flying qualities estimate may be made on the basis of various dynamic characteristics. One can correlate pilot ratings to the frequencies and damping ratios of certain types of motion as is done in the U.S. Military Specifications governing airplane flying qualities. The figure below shows how the short-frequency longitudinal motion of an airplane and the load factor per radian of angle of attack are used to establish a flying qualities estimate. In Mil Spec 8785C, level 1 handling is considered “clearly adequate” while level 3 suggests that the airplane can be safely controlled, but that the pilot workload is excessive or the mission effectiveness is inadequate.

Rather than solve the relevant equations of motion, we describe here some of the simplified results obtained when this is done using linearized equations of motion.

When the motions are small and the aerodynamics can be assumed linear, many useful, simple results can be derived from the 6 degree-of-freedom equations of motion. The first simplification is the decoupling between symmetric, longitudinal motion, and lateral motion. (This requires that the airplane be left/right symmetric, a situation that is often very closely achieved.) Other decoupling is also observed, with 5 decoupled modes required to describe the general motion. The stability of each of these modes is often used to describe the airplane dynamic stability.

Modes are often described by their characteristic frequency and damping ratio. If the motion is of the form:

$$x = A e^{(n+i\omega)t}, \quad (8.25)$$

then the period is given by $T = 2\pi/\omega$, while the time to double or halve the amplitude of a disturbance is t_{double} or $t_{\text{half}} = 0.693/|n|$. Other parameters that are often used to describe these modes are the undamped circular frequency: $\omega_n = (\omega^2 + n^2)^{1/2}$ and the damping ratio, $\xi = -n/\omega_n$.

8.3.2 Longitudinal Dynamic Modes

When the aircraft is not perturbed about the roll or yaw axis, only the longitudinal modes are required to describe the motion. These modes usually are divided into two distinct types of motion.

Short-Period

The first, short period, motion involves rapid changes to the angle of attack and pitch attitude at roughly constant airspeed. This mode is usually highly damped; its frequency and damping are very important in the assessment of aircraft handling. For a 747, the frequency of the short-period mode is about 7 seconds, while the time to halve the amplitude of a disturbance is only 1.86 seconds. The short period frequency is strongly related to the airplane’s static margin, in the simple case of straight line motion, the frequency is proportional to $\sqrt{C_{m\alpha}/C_L}$.

Phugoid

The long-period of phugoid mode involves a trade between kinetic and potential energy. In this mode, the aircraft, at nearly constant angle of attack, climbs and slows, then dives, losing altitude while picking up speed. The motion is usually of such a long period (about 93 seconds for a 747) that it need not be highly damped for piloted aircraft. This mode was studied (and named) by Lanchester in 1908. He showed that if one assumed constant angle of attack and thrust equals drag, the period of the phugoid could be written as $T = 1.414\pi U/g$ ($= 0.138U$, with U in ft/sec).

That is, the period is independent of the airplane characteristics and altitude, and depends only on the trimmed airspeed. With similarly strong assumptions, it can be shown that the damping varies as $\xi = .7071/(L/D)$.

8.3.3 Lateral Dynamic Modes

Three dynamic modes describe the lateral motion of aircraft. These include the relatively uninteresting roll subsidence mode, the Dutch-roll mode, and the spiral mode.

The roll mode consists of almost pure rolling motion and is generally a non-oscillatory motion showing how rolling motion is damped.

Of somewhat greater interest is the spiral mode. Like the phugoid motion, the spiral mode is usually very slow and often not of critical importance for piloted aircraft. A 747 has a non-oscillatory spiral mode that damps to half amplitude in 95 seconds under typical conditions, while many airplanes have unstable spiral modes that require pilot input from time to time to maintain heading.

The Dutch-roll mode is a coupled roll and yaw motion that is often not sufficiently damped for good handling. Transport aircraft often require active yaw dampers to suppress this motion.

High directional stability (C_{n_β}) tends to stabilize the Dutch-roll mode while reducing the stability of the spiral mode. Conversely large effective dihedral (rolling moment due to sideslip, C_{l_β}) stabilizes the spiral mode while destabilizing the Dutch-roll motion. Because sweep produces effective dihedral and because low wing airplanes often have excessive dihedral to improve ground clearance, Dutch-roll motions are often poorly damped on swept-wing aircraft.

Bibliography

Mark Drela. Fluids—lecture 3 notes. (lecture notes), 2003.

Mark Drela. Lab 8 notes—basic aircraft design rules. (lecture notes), April 2006.

Eastman N. Jacobs and Kenneth E. Ward. Interference of wing and fuselage from tests 209 combinations in the naca variable-density tunnel. Technical Report TR-540, NASA Langley Research Center, 1936.

Daniel P. Raymer. *Aircraft Design: A Conceptual Approach*. AIAA, 5th edition, 2012.

Hermann T. Schlichting and Erich A. Truckenbrodt. *Aerodynamics of the Aeroplane*. McGraw Hill Higher Education, 2nd edition, 1979.

Chapter 9

Landing Gear

9.1 Preliminary Landing Gear Positioning

To determine the preliminary position and height of a tricycle type landing gear, the following requirements must be met:

Rotation angle clearance: The height and position of the landing gear must be such the tail does not hit the ground on landing or takeoff. The required angle can be estimated by finding the angle of attack that achieves 90% of the maximum lift. Typically, the rotation clearance angle is between 10 to 16 degrees.

Tipback angle: At the maximum rotation angle for landing or takeoff, the CG must not move behind a vertical line originating from the main gear point of contact (otherwise, there is a risk that the aircraft will tip back on its tail).

Tipover angle clearance: This is required for the event of an imperfect landing, to avoid the nacelles or wing hitting the ground.

Overtur angle: This is to avoid tip over when the aircraft is turning during taxiing. The angle should be no greater than 60 degrees ([Kundu, 2010](#), Ch. 7).

Example 9.1: Preliminary landing gear disposition for a long range transport

We will use the 777-200LR drawings to demonstrate the disposition of the landing gear. The landing gear location and length satisfy the following requirements:

- The rotation angle clearance is greater than 10 degrees, as shown in Fig. 9.1.
- The tipback angle is greater than the rotation angle, as shown in Fig. 9.1.
- The tipover angle is greater than 5 degrees, as shown in Fig. 9.2.
- The overturn angle is less than 60 deg, a show in Fig. 9.3.

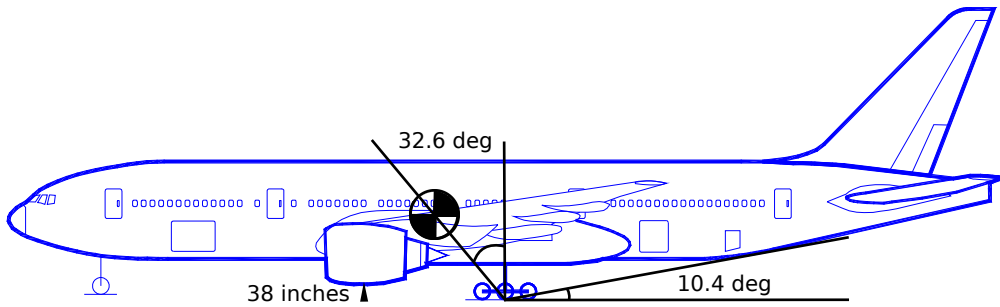


Figure 9.1: Rotation angle clearance and tipback angle for the Boeing 777-200LR

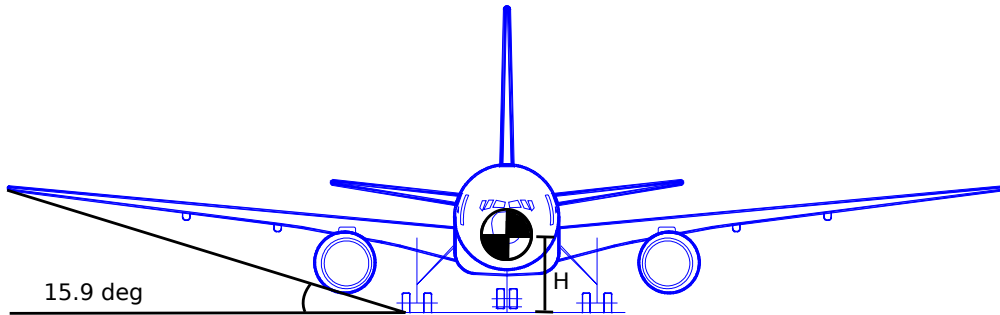


Figure 9.2: Tipover angle for the Boeing 777-200LR

9.2 Landing Gear Sizing

For more details on the disposition of the landing gear, tire sizing and strut sizing, see [Raymer \(2012, Ch. 11\)](#). [Kundu \(2010, Ch. 7\)](#) provides one of the most detailed descriptions of landing gear design that can be found in aircraft design text books. Note that in British English, the landing gear is called the “undercarriage”.

Example 9.2: Preliminary landing gear sizing for a long range transport We will use the 777-200LR to demonstrate the landing gear sizing.

Step 1: Landing Gear System

The first step is to determine the type of landing gear system to use. 777-200LR has a cruise more than 150kts. Therefore, a retractable landing gear is certainly more appropriate to avoid a drag penalty.

Step 2: Overall Landing Gear Configuration

Based on the aircraft geometry and its intent usage, we choose tricycle landing gear layout.

Step 3: Preliminary landing gear and strut disposition

777-200LR has a MTOW more than 400,000lbs. Based on [Raymer \(2012\)](#), we would choose four bogey each with four or six wheels. Boeing decided to fit 777-200LR with two bogey each with six wheels in order to main a clearer landing gear sizing. The resulting landing gear is the largest ever incorporated into a commercial airplane.

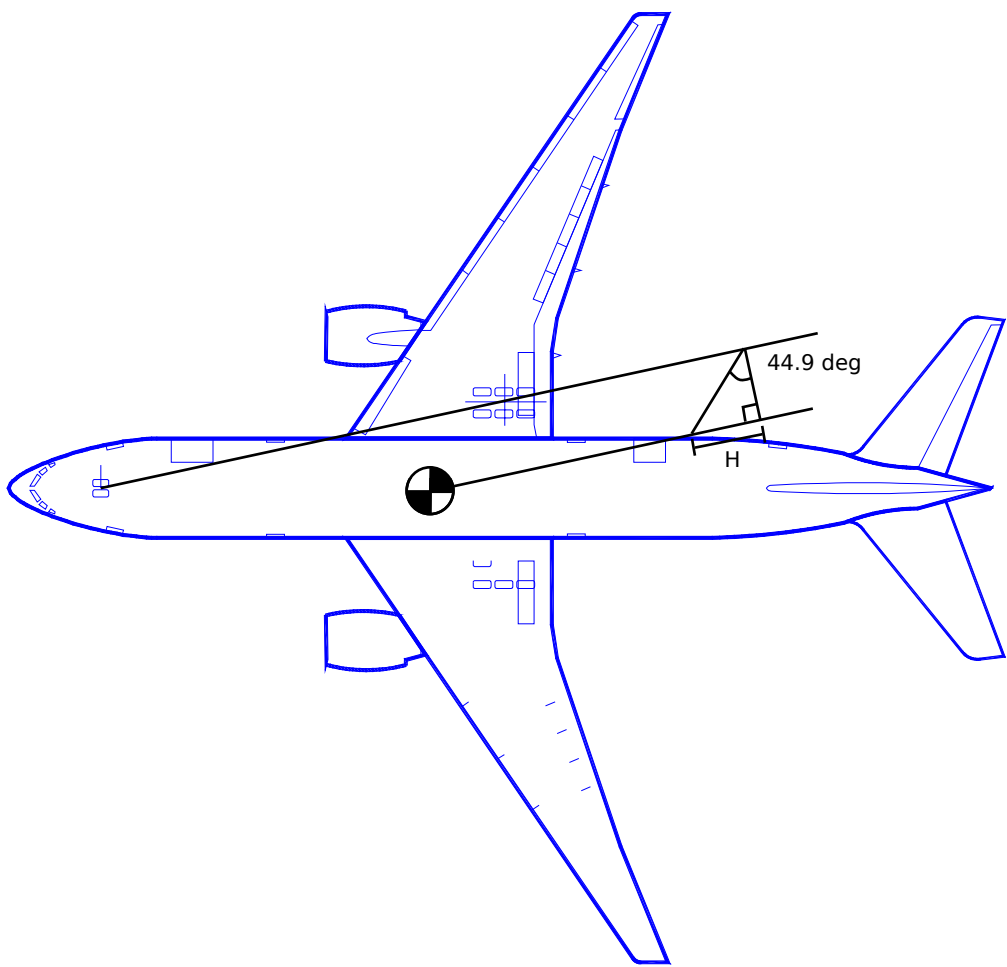


Figure 9.3: Overturn angle for the Boeing 777-200LR

Please see the previous example for landing gear disposition.

Step 4: Tire Size

Using the methods in [Raymer \(2012\)](#), we need to determine the loading on the landing gears. From the calculations in the previous chapters, we have the fwd and aft CG locations. Based on the aircraft drawings, we can determine the CG location with respect to the nose and main landing gear. In our example, $N_f = 79.9$ ft, $N_a = 81.1$ ft, $M_f = 2.6$ ft, $M_a = 1.4$ ft, $B = 82.5$ ft, $H = 16.2$ ft. Thus, we can obtain the landings on the nose and main landing gears:

$$(\text{Max Static Load}) = W \frac{N_a}{B} = 766,800 \frac{81.1}{82.5} = 753,388 \text{ lbs} \quad (9.1)$$

$$(\text{Max Static Load})_{\text{nose}} = W \frac{M_f}{B} = 766,800 \frac{2.6}{82.5} = 24,166 \text{ lbs} \quad (9.2)$$

$$(\text{Min Static Load})_{\text{nose}} = W \frac{M_a}{B} = 766,800 \frac{1.4}{82.5} = 13,012 \text{ lbs} \quad (9.3)$$

$$(\text{Dynamic Braking Load})_{\text{nose}} = \frac{10 H W}{g B} = \frac{10 \cdot 16.2 \cdot 766,800}{32.2 \cdot 82.5} = 46,761 \text{ lbs} \quad (9.4)$$

To ensure the nose gear can support this loading, M_a/B is greater than 0.05, and M_f/B is less than 0.20.

We can then choose the appropriate tires to carry those loads. The main landing gear has a total of 12 wheels, and the nose gear has two wheels. FAR 25 requires a safety factor of 7%, and 25% for further growth. We can obtain the loads per wheel:

$$(\text{wheel load}) = 1.07 \cdot 1.25 \frac{(\text{Max Static Load})}{\text{no. of wheels}} = 1.07 \cdot 1.25 \frac{753,388}{12} = 78,478 \text{ lbs/wheel} \quad (9.5)$$

$$(\text{wheel load})_{\text{nose}} = 1.07 \frac{(\text{Dynamic Braking Load})_{\text{nose}}}{\text{no. of wheels}} = 1.07 \cdot 1.25 \frac{46,761}{2} = 31,271 \text{ lbs/wheel} \quad (9.6)$$

Then, we can choose the tires using a tire books (eg: http://www.goodyearaviation.com/resources/pdf/db_airdatabook.pdf). Based on the calculations, we choose H54x21.0-24 for the main wheels and 41x15.0-18 for the nose gear. The actual tires that are used on 777-200LR are relatively close to the tires we calculated. 777-200LR uses 50x20.0R22 for the main wheels and 42x17.0R18 for the nose wheels. As we can see, the main wheel is slightly over-sized and the nose wheel is slightly under-sized.

In addition, we also need to calculate the kinetic energy of braking to ensure the brakes are able to absorb the kinetic energy of the aircraft. 777-200LR has a stall speed of 136 knots.

$$KE_{\text{braking}} = \frac{1}{2} \frac{W_{\text{landing}}}{g} V_{\text{stall}}^2 \frac{1}{\text{no. of wheels}} = 42 \times 10^6 \text{ ft-lb/s} \quad (9.7)$$

As we can see from [Raymer \(2012, Fig. 11.8\)](#), the chosen wheel diameter is more than the required diameter for the purpose of radiating heat. Therefore, the wheels satisfy the requirements.

Steps 5 and 6: Retraction Kinematics and Volume, Dimensioned Drawing

Those steps will be based on the CAD drawing of the aircraft.

Bibliography

Ajoy Kumar Kundu. *Aircraft Design*. Cambridge University Press, 2010.

Daniel P. Raymer. *Aircraft Design: A Conceptual Approach*. AIAA, 5th edition, 2012.

Chapter 10

Propulsion

10.1 Introduction

The purpose of all aircraft propulsion devices is to add momentum to fluid in order to produce thrust according to Newton's second law. The fluid could be air, air and combustion products, or combustion products.

Propulsion systems differ in how they add this momentum to the stream tube. A broad classification of these systems is listed below and is illustrated in Fig. 10.1.

Propellers are driven by piston engines, gas turbines (turboprops), or electric motors. Propellers impart a relatively small change in velocity to a large mass of air. They are limited to tip velocities less than sonic due to shock formation.

Turbojets impart a large velocity change to a small mass of air, and can operate at speeds up to Mach 3.5.

Turbofans can be considered a hybrid between turbojets and a turboprop, where the "prop" is shrouded.

Ramjets do without the compressor because at higher Mach numbers, the inlet can perform the compression efficiently. The combustion can be subsonic or supersonic.

Rockets carry their own oxidizer and thus impart a very high velocity to a very small mass of combusted propellant products.

Diagrams for the turbojet, turboprop and turbofan engines are shown in Fig. 10.2.

10.2 The Tradeoff Between Thrust and Efficiency

The choice of the propulsive system for aircraft hinges on a compromise between thrust and efficiency. Generally speaking, propellers produce relatively low thrust with great efficiency, while turbojets produce higher thrust with lower efficiency, and the rocket engine produces a massive amount of thrust with poor efficiency. Thus, the greater the required thrust, the lower the efficiency will be.

To understand the physical reason behind this tradeoff, consider a device flying at a speed of V_∞ , with an air-breathing propulsion system that ejects the air at V_j . We draw a stream tube

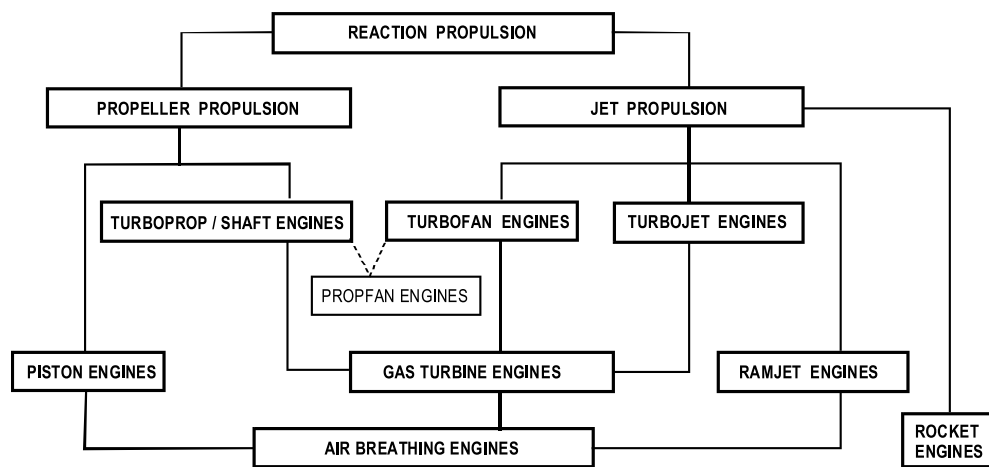


Figure 10.1: Classification of propulsion systems

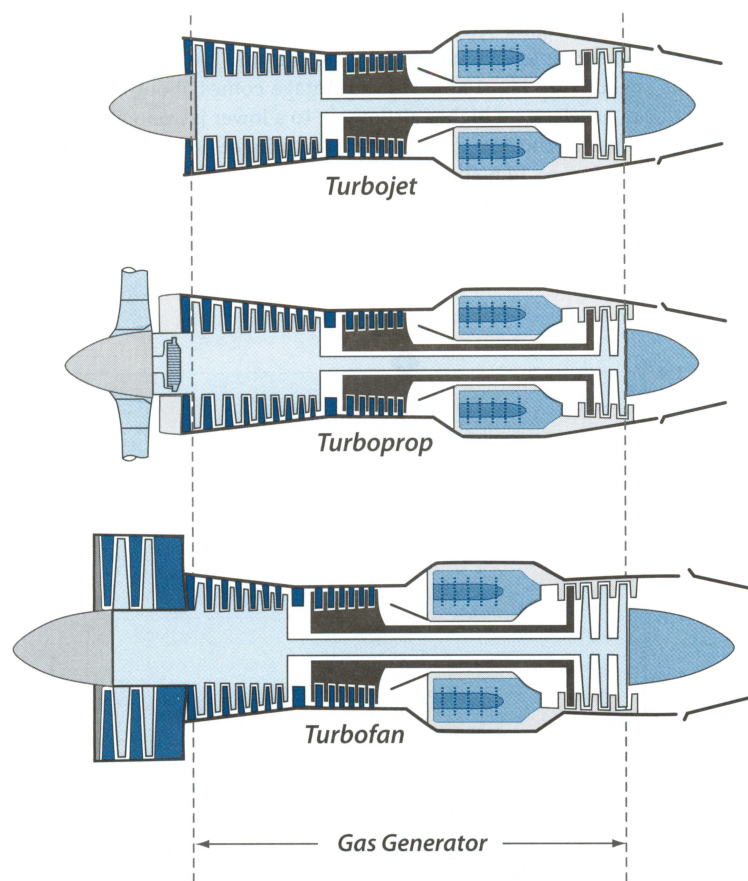


Figure 10.2: Diagrams showing the components for the turbojet, turboprop and turbofan; note that all three have a gas generator in common.

control volume and assume that the pressure integral on its faces is negligible, and so is the mass of fuel added to the system. The thrust is then given by

$$T = \dot{m}(V_j - V_\infty), \quad (10.1)$$

where \dot{m} is the mass flow rate of air going through the stream tube.

The propulsive efficiency, is defined as the ratio of useful power over total power produced. The useful power produced by the thrust is

$$P_{\text{av}} = TV_\infty \quad (10.2)$$

which is called the *power available*.

The propulsive system is actually putting out more power than the power available because it is adding kinetic energy to the air left behind. The energy per unit time equal to $1/2\dot{m}(V_j - V_\infty)^2$, which represents the power that is wasted.

Hence the propulsive efficiency is

$$\eta_p = \frac{\text{useful power available}}{\text{total power produced}} = \frac{TV_\infty}{TV_\infty + \frac{1}{2}\dot{m}(V_j - V_\infty)^2} \quad (10.3)$$

(Alternatively, the total power produced can be written as the variation in the kinetic energy $\dot{m}(V_j^2/2 - V_\infty^2/2)$.) Substituting the thrust (10.1) into this equation and simplifying we get

$$\eta_p = \frac{2}{1 + V_j/V_\infty}. \quad (10.4)$$

The tradeoff between thrust and efficiency can now be clearly seen by looking at Eqns. (10.1) and (10.4). For maximum propulsive efficiency, we would want $V_j = V_\infty$ in Eqn. (10.4), but in that case, no thrust is produced, according to Eqn. (10.1). For high efficiency with nonzero thrust, we would want V_j/V_∞ close to 1.

We can then obtain the required thrust by having a large mass flow rate, which is given by $\dot{m} = \rho A_j V_j$. Since we want to keep V_j small, our only option is to increase the area, and hence the use of a propeller. The problem with propellers is that they become inefficient above a Mach number of about 0.75, as the tip flow becomes supercritical, shocks form and wave drag dramatically increases the required torque to drive the propeller. Jet engines can overcome this limit in thrust by adding much more velocity to a smaller mass of air. Turbofans and turboprops are compromises between these two extremes. This is part of the reason for the SFC trends in Fig. 2.3.

10.3 The Turbojet Engine

The basic components of the turbojet engine are shown in Fig. 10.3, together with typical variations in pressure p , temperature T , and axial velocity V . The air enters the diffuser essentially at freestream velocity (actually a little less, depending on conditions). The air is slowed in the diffuser (to about Mach 0.4) and thus p and T before the air enters the compressor. In the compressor, work is done on the air greatly increasing p and T further. This hot, high-pressure air then enters the combustor, where it mixed with fuel and burned at constant pressure. The fuel-air mixture then expands through a turbine, which extracts the work that is used to drive the compressor through a shaft. Finally, the fuel-air mixture expands through the nozzle to ambient pressure with velocity V_j .

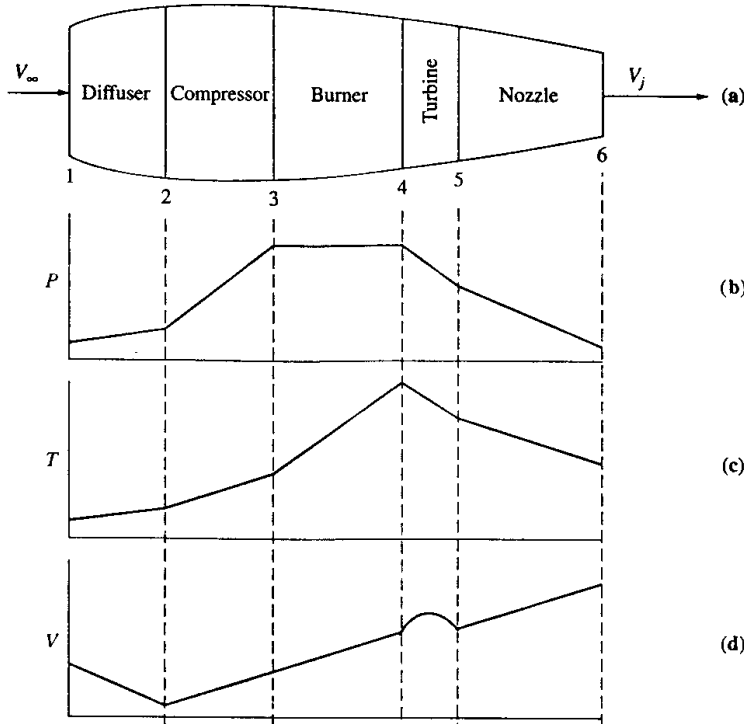


Figure 10.3: Distribution of (a) components, (b) pressure, (c) temperature, and (d) velocity (Anderson Jr., 1999, Fig. 3.10).

As mentioned previously, Eqn. (10.1) ignores the pressures and mass flow rate of fuel added. A more detailed derivation yields,

$$T = (\dot{m} + \dot{m}_{\text{fuel}})V_j - \dot{m}V_\infty + (p_e - p_\infty)A_e. \quad (10.5)$$

The specific fuel consumption (SFC) for a turbojet — introduced in Sec. 2.3.2 — is based on thrust, since this is its primary measurable output (as opposed to power in piston engines). To make this distinction clear, this is often called the *thrust* specific fuel consumption (TSFC). It is the weight of fuel burned per unit thrust per unit time.

One important question in the context of aircraft design is how the thrust and TSFC vary with flight velocity and altitude.

Examining Eqn. (10.5), we see that there are two main terms: the mass flow rate $\dot{m} = \rho_\infty A_1 V_\infty$ and the velocity difference $(V_j - V_\infty)$. The jet velocity V_j is more a function of the jet engine itself than anything else, and tends to stay the same. Hence as the aircraft velocity V_∞ increases, the velocity difference decreases. However, the mass flow rate also increased linearly, and these two effect more or less cancel each other. The result is that *the thrust of a turbojet is more or less independent of the aircraft velocity*.

The TSFC for turbojets increases linearly with Mach number below Mach 1, i.e.,

$$c = 1 + kM_\infty \quad (10.6)$$

where k is a function of altitude and throttle setting (engine rpm).

There is a strong dependence of thrust on altitude that can be inferred from Eqn. (10.5). The air mass flow rate is directly proportional to the air density ρ_∞ , which of course decreases with

altitude. Since T is almost directly proportional to \dot{m} , thrust decreases with altitude and this variation can be approximated by

$$T = T_{SLS} \frac{\rho}{\rho_0} \quad (10.7)$$

where T_{SLS} is the sea-level-static thrust at standard conditions and ρ_0 is the air density at sea-level.

The effect of altitude on TSFC is very small, hence we can assume that *the TSFC of a turbojet is constant with altitude*.

Note that all these trends are applicable only to subsonic speeds. For details on the supersonic regime, see [Anderson Jr. \(1999, Sec. 3.4.1\)](#).

10.4 The Turbofan Engine

The turbofan engine strives to strike a balance in thrust-efficiency trade-off by achieving the high thrust of a turbojet with the high efficiency of the propeller. As shown in Fig. 10.4, the turbofan has a core that is essentially a turbojet engine. The turbine of the core drives not only the core compressor, but a large fan in front of the core. The fan is enclosed in a shroud and acts as a propeller. Part of the flow it compresses *bypasses* the core generating a lower speed jet around the higher speed jet that is ejected from the core. The overall propulsive efficiency of the turbofan is a compromise between the propeller and the turbojet. The vast majority of jet-propelled aircraft today are powered by turbofan engines.

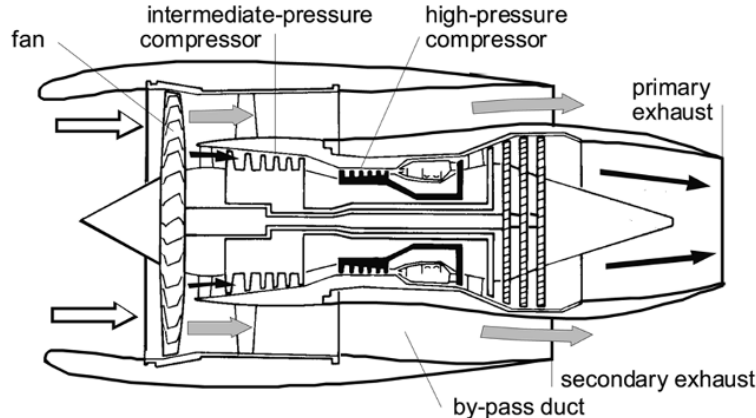


Figure 10.4: Turbofan engine arrangement ([Torenbeek and Wittenberg, 2009, Fig. 5.22](#))

The *bypass ratio* (BPR) is an important parameter for turbofans. It is the ratio of mass flow passing through the fan externally to the core divided by the mass flow passing through the core. The higher the bypass ratio, the higher the propulsive efficiency.

We now discuss the variation in the performance of turbofans with bypass ratio of around 5. In contrast with the turbojet, for which the thrust remained essentially constant with velocity, the thrust of turbofans decreases with V_∞ .

$$T = T_{SLS} A M_\infty^{-n} \quad (10.8)$$

where A and n are functions of altitude.

Although T varies with V_∞ for these turbofans, T is relatively constant for Mach numbers in the range from 0.7 to 0.85 ([Anderson Jr., 1999, Sec. 3.5.1](#)), which corresponds to the cruise Mach numbers of typical civil transports.

The variation of T with altitude for a given velocity can be approximated by

$$T = T_0 \left(\frac{\rho}{\rho_0} \right)^m. \quad (10.9)$$

where T_0 is the thrust at sea-level for that velocity.

The variation of TSFC with velocity follows the relation ([Anderson Jr., 1999](#), Eqn. (3.26))

$$c = B(1 + kM_\infty) \quad (10.10)$$

where B and k are empirical constants round by correlating the data, and c is in units of lb/(lbf-h). This is valid only for $0.7 < M_\infty < 0.85$.

[Mattingly \(1996, Eqn. \(1.36a\)\)](#) gives the following relationship for high-bypass-ratio turbofans,

$$c = (0.4 + 0.45M)\sqrt{\theta} \quad (10.11)$$

where θ is the dimensionless temperature ratio between the chosen altitude and the standard temperature at sea level, using degrees Kelvin. This is equivalent to having $B = 0.4$ and $k = 1.125\sqrt{\theta}$ in Eq. (10.10).

A much more involved estimate for TSFC as a function of altitude and Mach number is presented by [Hill and Peterson \(1991, Ch. 5\)](#).

[Nicolai and Carichner \(2010, Appendix J\)](#) include various tables and graphs with data for real engines. Table 10.1 list data for the GE 90 turbofan taken from that appendix. From this data, it is possible to use the above trends to fit reasonable estimates of the performance for this engine at various conditions.

Bibliography

John D. Anderson Jr. *Aircraft Performance and Design*. McGraw–Hill, 1999.

Philip Hill and Carl Peterson. *Mechanics and Thermodynamics of Propulsion*. Prentice Hall, 2nd edition, 1991.

Jack D. Mattingly. *Elements of Gas Turbine Propulsion*. McGraw–Hill, 1996.

Leland M. Nicolai and Grant E. Carichner. *Fundamentals of Aircraft and Airship Design, Vol I — Aircraft Design*. AIAA, Reston, VA, 2010.

E. Torenbeek and H. Wittenberg. *Flight Physics*. Springer, 2009.

Manufacturer: General Electric					
Application: Boeing 777					
Specification: Uninstalled					
SLS thrust: Ranges from 76,000 lb (777-200) to 115,000 lb (777-300ER)					
SLS SFC: 0.29–0.31					
Weight = 17,300 lb					
Length = 287 in.					
Maximum diameter = 134 in.					
OPR = 40					
Takeoff Thrust: Uninstalled thrust/SFC, limited to 5 minutes					
Altitude	M = 0	M = 0.1	M = 0.2		
SL	98,000/0.29	87,762/0.32	79,585/0.356		
2000	92,908/0.289	83,569/0.322	75,929/0.358		
4000	87,390/0.292	7877/0.325	71,741/0.361		
Climb Thrust: Uninstalled thrust/SFC					
Altitude	M = 0.4	M = 0.5	M = 0.6	M = 0.7	
5,000	53,071/0.417	49,185/0.459	45,899/0.502	—	
10,000	—	44,660/0.459	42,091/0.495	—	
15,000	—	39,268/0.461	37,509/0.497	—	
20,000	—	33,138/0.463	32,364/0.50	31,798/0.532	
25,000	—	—	26,886/0.50	26,971/0.534	
30,000	—	—	21,777/0.492	22,177/0.532	
35,000	—	—	17,282/0.482	17,581/0.52	
40,000	—	—	13,699/0.486	13,936/0.524	
Cruise Partial Power: Uninstalled thrust/SFC					
Altitude	M = 0.75				
30,000	22,568/0.551	20,275/0.523	18,300/0.51	16,514/0.51	14,904/0.51
35,000	17,888/0.539	16,538/0.512	14,925/0.50	13,469/0.497	12,156/0.50
40,000	14,170/0.542	13,077/0.513	11,801/0.50	10,651/0.497	9610/0.499
45,000	11,238/0.55	10,199/0.515	9204/0.502	8307/0.5	7497/0.503
50,000	8777/0.55	7948/0.518	7173/0.506	6474/0.504	5843/0.507
55,000	6840/0.553	6172/0.521	5570/0.509	5027/0.509	4539/0.512

Table 10.1: GE 90 turbofan engine data (Nicolai and Carichner, 2010, Table J.6) Note: there seem to be typos in the last row of Mach numbers.

Chapter 11

Structures and Loads

11.1 Introduction

Structural design is of critical importance to aircraft safety, but also plays a key role in aircraft cost and performance. The airplane cost is related to the structural design in complex ways, but typically aircraft end up costing \$200-\$500 per pound (with sailplanes and military aircraft such as the B-2 being the extreme examples — the B-2 reportedly costs more per unit weight than gold).

In addition to its direct impact on aircraft cost, the aircraft structural weight affects performance. Every pound of airplane structure means one less pound of fuel when the take-off weight is specified. This can be quantified using the Breguet range equation.

We have already estimated the aircraft weights using historical data for the various components in Ch. 7. The next step would be to analyze the structure for all the relevant loads and design it such that it can support those loads.

11.2 Preliminary Structural Arrangement

The very first stage of structural design takes place at the configuration layout stage. This is to make sure that the configuration can accommodate the major structural components. These major structural components are responsible for carrying the most significant loads the aircraft is subjected to: lift, weight, and landing loads. A good structural layout of these major components increases the likelihood of successfully designing a light structure, while a poor structural layout will incur weight penalties and might even make the configuration infeasible.

The lift is mostly provided by the wing, and the fuselage contributes most of the weight. These two forces counteract each other in level flight and add up to zero, but they are not applied in the same area. This generates internal forces and moments that must be sustained by the structure.

The main objective in deciding on the structural arrangement is to provide efficient “load paths”. These load paths are the major structural components that transmit the loads throughout the structure, such as the wingbox, fuselage frames, and bulkheads. The basic principle is to find the shortest and straightest path to carry the load between opposing forces. Another way to increase the structural efficiency is to use a given structural component to carry load from multiple sources. For example, it is advantageous to attach the landing gear to the wingbox, instead of designing a separate structure to take the landing gear loads.

Fig. 11.1 shows an example of a structural arrangement for a fighter aircraft. The wingbox carries the shear force and moments generated by the wing as one continuous structure from tip to tip. Two frames are positioned on the center wingbox to transmit the loads to the fuselage. The

landing gears attach to either fuselage frames or reinforced points on the wingbox. The engine is mounted on fuselage frames, and the tail also attaches to those same frames.

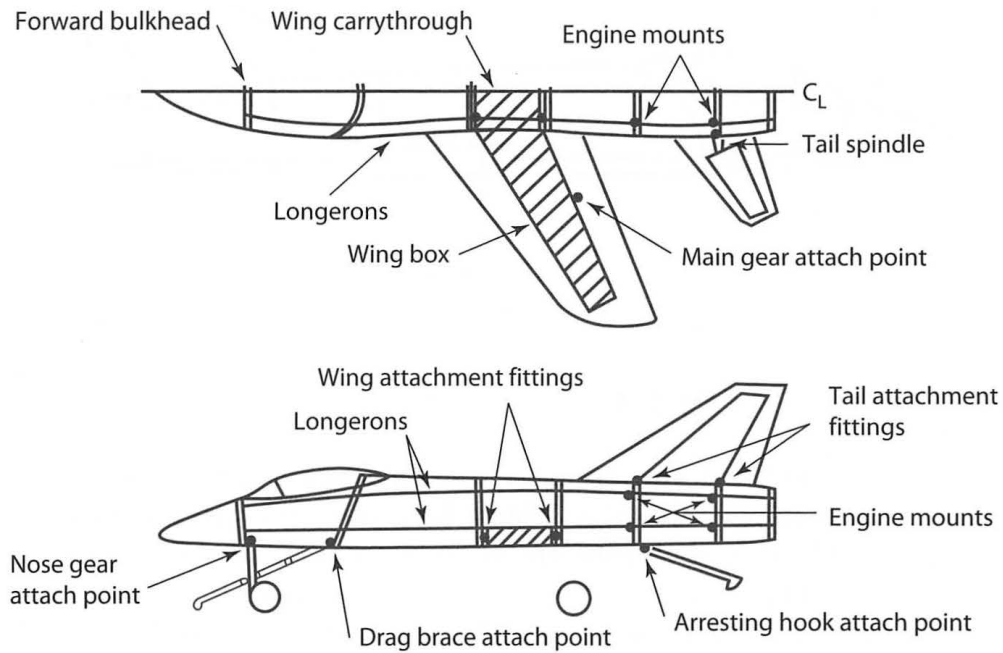


Figure 11.1: Structural arrangement showing the major load paths ([Raymer, 2012](#), Fig. 8.9)

Cutaway drawings, such as the one shown in Fig. 11.2, show a lot more structural details and describe the materials used. These are valuable references for how aircraft structures are arranged.

More details on the structural arrangement can be found in [Raymer \(2012, Secs. 8.3\)](#).

11.3 Aircraft Structural Loads

Before the structure can be designed, we need to determine the loads that will be imposed on the aircraft. This section deals with the general issue of aircraft loads and how they are predicted at the early stages of the design process.

Each part of the aircraft is subject to many different loads. In the final design of an aircraft structure, one might examine tens of thousands of loading conditions of which several hundred may be critical for some part of the airplane. In addition to the obvious loads such as wing bending moments due to aerodynamic lift, many other loads must be considered. These include items such as inertia relief, the weight and inertial forces that tend to reduce wing bending moments, landing loads and taxi-bump loads, pressurization cycles on the fuselage, local high pressures on floors due to high-heeled shoes, and many others.

These loads can be predicted using aerodynamic analysis, wind tunnel tests, or various heuristics. Static and dynamic load tests on structural components are carried out to assure that the predicted strength can be achieved. The definition of strength requirements for commercial aircraft is specified in FAR Part 25 and this section deals with those requirements.

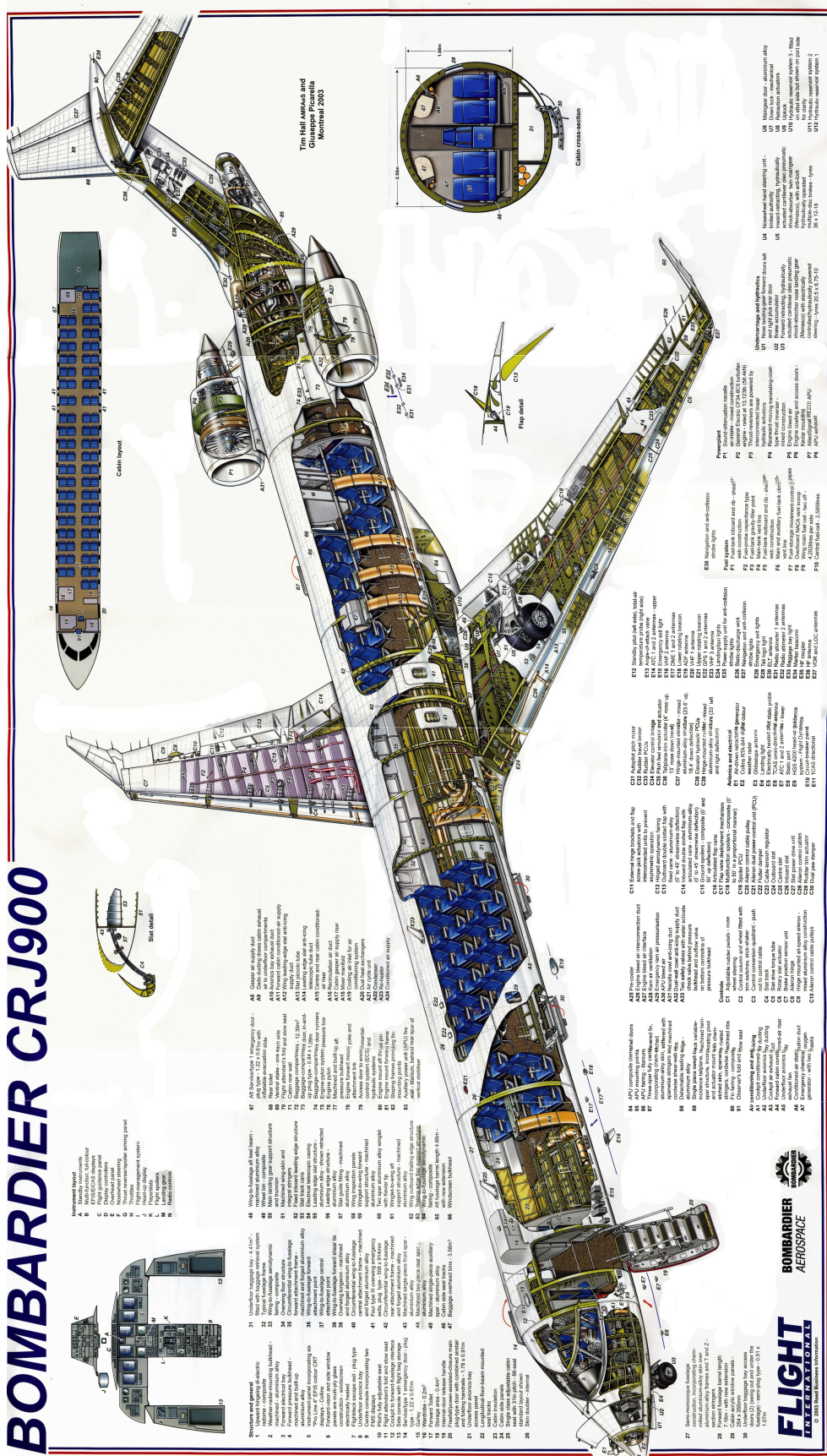


Figure 11.2: Cutaway drawing for the Bombardier CRJ900 [Flight International]

11.3.1 Operating and Design Flight Envelopes

The designer must ensure the structural integrity of the aircraft at all points on and within its operating envelope. The structural design envelope represents more severe conditions than the operating envelope. The flight envelope is represented by a range in the combination of two variables: the *equivalent airspeed* (EAS), and the normal acceleration (or load) factor n . The equivalent air speed is a surrogate for dynamic pressure, as explained below. These two parameters are significant for structural design because the load factor directly affects the inertial and lift loads, and the dynamic pressure directly affects the loads in the longitudinal direction and also influences the load factor limits.

The equivalent airspeed is the speed at sea level that would yield the same incompressible dynamic pressure as the *true airspeed* (TAS) at which the aircraft is flying. This can be calculated using,

$$V_{\text{EAS}} = V_{\text{TAS}} \sigma^{1/2}, \quad (11.1)$$

where $\sigma = \rho/\rho_{\text{SL}}$ is the density ratio at the given altitude at which the TAS was measured relative to sea level density ($\sigma \leq 1$).

The load factor n , represents the acceleration parallel to the lift vector. In level flight, $n = 1$, in level inverted flight $n = -1$, and $n > 1$ when performing a turn or a pitch up maneuver. Assuming the angle of attack is not large, $n = L/W$. This is the effective perpendicular acceleration of the airplane in units of g , the acceleration due to gravity.

11.3.2 Design Airspeeds

As previously mentioned, all speeds are equivalent air speeds. Several airspeeds are important in the definition of the aircraft's operating envelope:

V_S is the stalling speed at normal level flight.

V_A is the design maneuver speed, or corner speed. It is the lowest speed at which the aircraft can achieve the maximum limit normal maneuver load factor n_1 .

V_B is the design speed for maximum gust intensity and is the airspeed at which the required vertical gust produces maximum C_L on the aircraft.

V_C is the design EAS. It is intended to cover the maximum normal operating conditions. V_C must be sufficiently greater than the gust design speed, V_B , to provide for inadvertent speed increases resulting from turbulence.

V_{MO} is the maximum operating EAS (or Mach number, M_{MO}). A good guess for this is about 6% above V_C (Kroo, Sec. 10.1.1).

V_D is the design diving speed (or M_D). It is the EAS that should not be exceeded. It must be sufficiently greater than V_C to provide for safe recovery from inadvertent upsets at V_C . For transonic aircraft, V_D is usually 7% higher than V_{MO} (Kroo, Sec. 10.1.1). At high altitude, V_D may be limited by the onset of high-speed flutter. For slower aircraft, $V_D = 1.25V_C$.

More detailed information on design speeds can be found in Howe (2004, Sec. 2.6).

11.3.3 Limit and Ultimate Load Factors

The FAA establishes two kinds of load conditions:

Limit loads are the maximum loads expected in service. FAR Part 25 (and most other regulations) specifies that there be no permanent deformation of the structure at limit load. For FAR Part 25 aircraft, the positive limit load limit may not be less than 2.5 g (and need not be greater than 3.8) and the negative one may not be less than -1 g.

Ultimate loads are defined as the limit loads times a safety factor. In Part 25 the safety factor is specified as 1.5. For some research or military aircraft the safety factor is as low as 1.20, while composite sailplane manufacturers may use 1.75. The structure must be able to withstand the ultimate load for at least 3 seconds without failure. The factor of safety also covers variations in material properties and manufacturing.

11.3.4 V-n Diagram

The *V-n* diagram—also called the *n-V* diagram, flight envelope or maneuver diagram—shows the variation of load factor limits with airspeed. First we must draw the basic flight envelope and then consider the additional loads due to gusts to draw the final envelope.

Basic Flight Envelope

At low speeds, the maximum load factor is constrained by the aircraft's maximum C_L , i.e.,

$$n = \frac{L}{W} = \frac{\rho_{SL} V_{EAS}^2 C_{L\max}}{2W/S} \quad (11.2)$$

This defines the positive stall line in the *V-n* diagram. One of the most common issues when using Eq. (11.2) is using the correct units. The result must be dimensionless, so it is easy to check.

At higher speeds, the maneuver load factor is restricted as specified by FAR Part 25, defining a horizontal line in the *V-n* diagram. The minimum limit maneuver load factor for civil transports is +2.5 g for airplanes weighing more than 50,000 lbs. If the airplane weighs less than 50,000 lbs, the limit load factor must be given by:

$$n_{\text{limit}} = 2.1 + \frac{24000}{W + 10000} \quad (11.3)$$

where, n need not be greater than 3.8. This is the required maneuver load factor at all speeds up to V_C , unless the maximum achievable load factor is limited by stall. An example of the basic flight envelope is shown in Fig. 11.3.

The point where the positive-stall and the limit load factor lines intersect, is at the maneuvering speed V_A , which can be shown to be $V_A = V_S \sqrt{n_{\text{limit}}}$. The negative value of n is -1.0 at speeds up to V_C decreasing linearly to 0 at V_D .

Gust Envelope

Loads associated with vertical gusts must also be evaluated over the range of speeds. Gusts are horizontal and vertical variations in velocity in the atmosphere. Gusts are seldom encountered in the stratosphere but occur frequently in the lower atmosphere (in thunderstorms, near mountains, and in areas where thermal gradients exist). Crossing the wake of another aircraft has a similar effect to that of a gust.

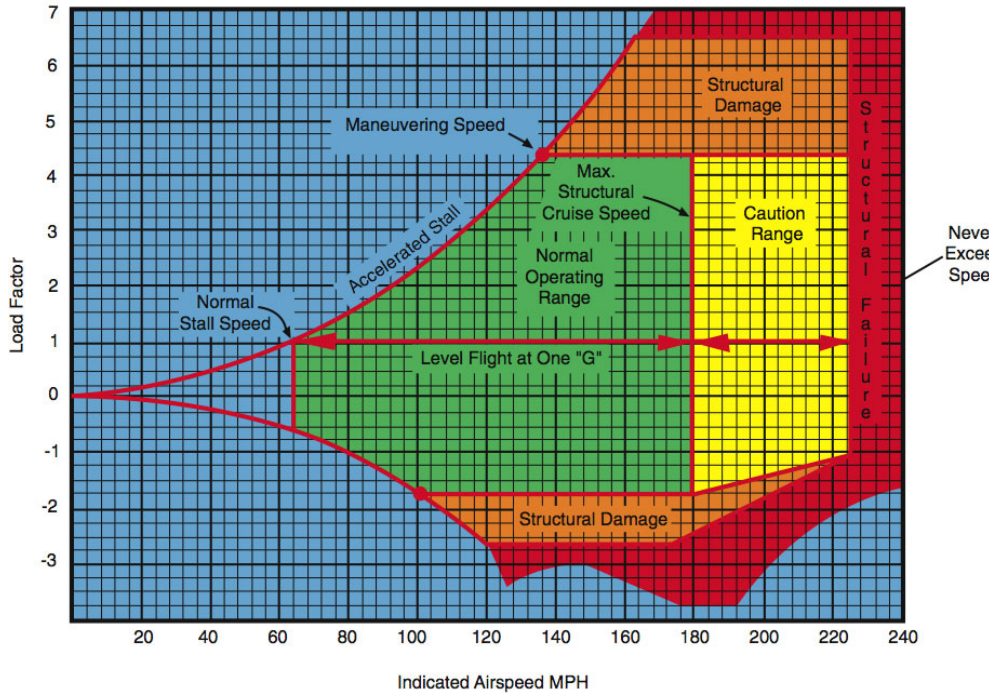


Figure 11.3: Example V - n diagram (Note: for your diagram, use EAS in knots; the indicated airspeed above is closely related to EAS)

A horizontal gust causes a change in dynamic pressure over the wing, which does result in change of lift, but since it does not change the angle of attack, the resulting change in the load factors is relatively small and can be ignored. A vertical gust, on the other hand, changes angle of attack, as shown in Fig. 11.4, and results in a significant change in load factor.

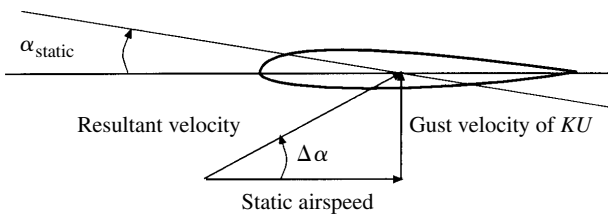


Figure 11.4: Effect of gust on angle of attack

The FARs describe the calculation of these loads in detail. Here is a summary of the method for constructing the V - n diagram. Pilots must fly at lower speeds if high turbulence is encountered. The gust load may be computed from the expression given in FAR Part 25, which is based on the work of Pratt and Walker (1954):

$$n = 1 \pm \frac{K_g C_{L\alpha} U_e V_{EAS}}{498 W/S} \quad (11.4)$$

where,

K_g =	gust alleviation factor
U_e =	equivalent gust velocity (in ft/sec)
V_{EAS} =	equivalent airspeed (in knots)
W/S =	wing loading (in lbs/ft ²)

$$K_g = \frac{0.88\mu}{5.3 + \mu}, \quad \text{with} \quad \mu = \frac{2(W/S)}{\rho \bar{c} C_{L\alpha} g} \quad (11.5)$$

where \bar{c} is the mean geometric chord, also known as the standard mean chord, defined as S/b . The result from this equation should be dimensionless. Check your units, as it is easy to make a mistake when using this equation.

This formula is the result of considering a vertical gust of specified speed and computing the resulting change in lift. The associated incremental load factor is then multiplied by a load alleviation factor that accounts primarily for the aircraft dynamics in a gust.

The FAA specifies the magnitude of the gusts to be used as a function of altitude and speed, as shown in Table 11.1. These are based on statistical observations and are specified as equivalent airspeeds. They can be linearly interpolated between 20,000 and 50,000 ft, as shown in Fig. 11.5.

	Altitudes 20,000 ft and below	Altitudes 50,000 ft and above
V_B (rough air gust)	66 ft/s	38 ft/s
V_C (gust at max design speed)	50 ft/s	25 ft/s
V_D (gust at max dive speed)	25 ft/s	12.5 ft/s

Table 11.1: FAR-specified gust velocities; between 20,000 and 50,000 ft, the velocities vary linearly

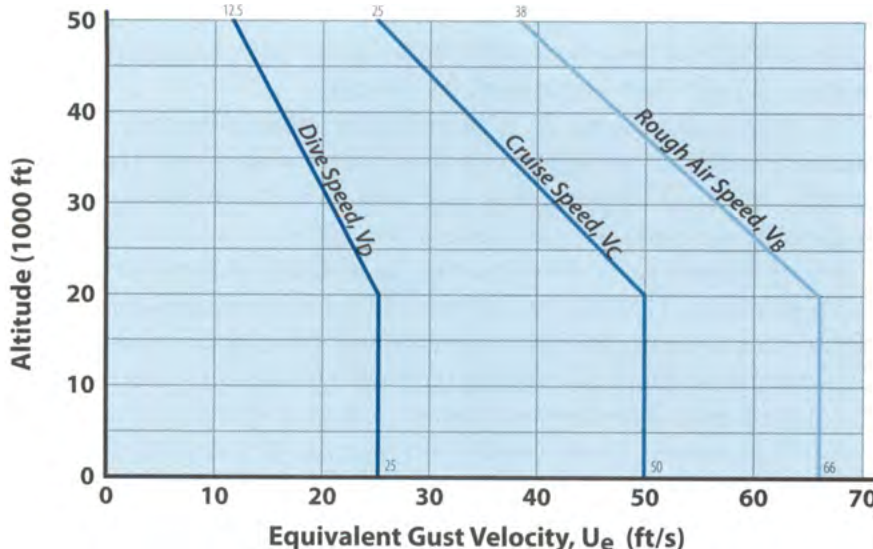


Figure 11.5: Equivalent gust velocity as a function of altitude for the various design speeds (Nicolai and Carichner, 2010, Fig. 19.2)

So, to construct the $V-n$ diagram at a particular aircraft weight and altitude, we start with the maximum achievable load factor curve from the maneuver diagram. We then vary the airspeed and compute the gust load factor associated with the V_B gust intensity. The intersection of these two lines defines the velocity V_B .

Next we compute the gust load factor at V_C and V_D from the FAR formula, using the appropriate gust velocities. A straight line is then drawn from the V_B point to the points at V_C and V_D . Fig. 11.6 shows the resulting diagram.

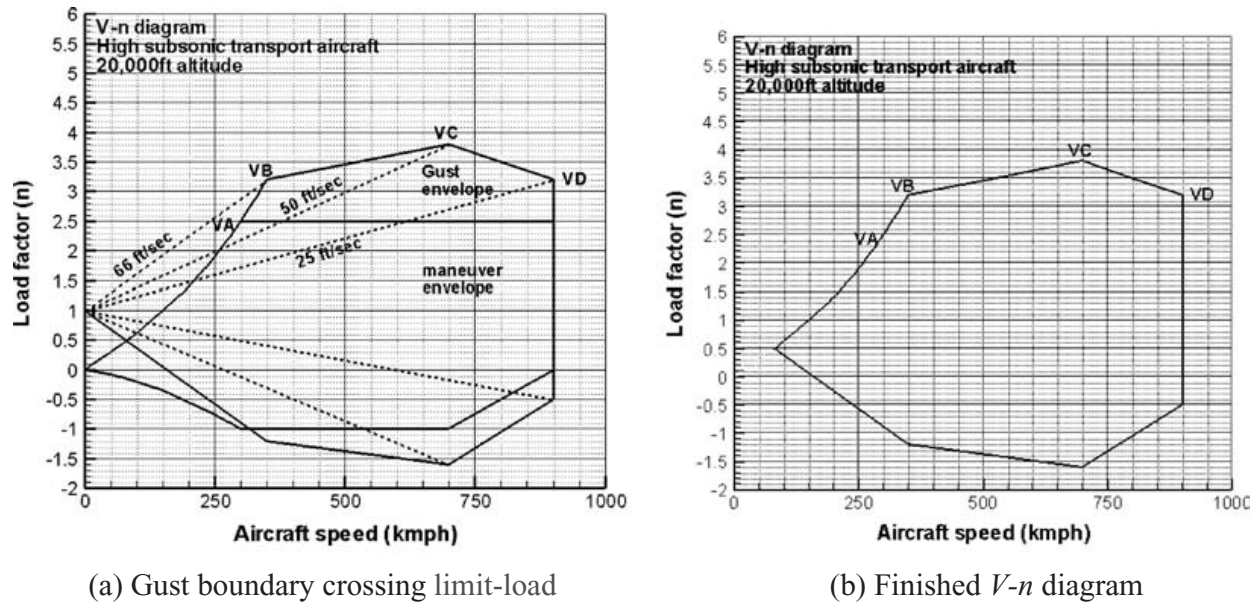


Figure 11.6: Example of a V - n diagram with a an FAR 25 gust envelope (Kundu, 2010, Fig. 5.4). Note that the gust lines should be symmetric about the $n = 1$ line.

Note on Lift Curve Slope The lift curve slope may be computed from the DATCOM expression:

$$C_{L\alpha} = \frac{2\pi AR}{2 + \sqrt{AR^2 \left(\frac{\beta}{\kappa}\right)^2 \left(1 + \frac{\tan^2 \Lambda_c/2}{\beta^2}\right) + 4}} \quad (11.6)$$

where β is the Prandtl–Glauert factor,

$$\beta = \sqrt{1 - M^2} \quad (11.7)$$

and κ is an empirical correction factor that accounts for section lift curve slopes different from 2π . In practice κ is approximately 0.97. This expression provides a reasonably good low-speed lift curve slope even for low aspect ratio wings.

Example 11.1: V - n Diagram for a Commercial Transport

This section details an example of how to construct a V - n diagram for a long range transport aircraft. This example is based on the Boeing 777-200ER.

Maneuver loads for maximum weight at 20,000 ft In order to determine the maneuver loads, we must calculate the required equivalent airspeeds. Assume that this aircraft is designed to fly at a maximum Mach number of 0.84, or about 490 knots TAS at 35,000 ft, under normal operating conditions. V_C is calculated by converting this true airspeed to EAS, V_{MO} is approximated as 106% V_C , and V_D is approximated as 107% V_{MO} . This gives, $V_C = 273.0$ knots, $V_{MO} = 289.4$ knots, and $V_D = 309.7$ knots (EAS).

First, we will consider the diagrams for flight at 20,000 ft. Assuming $C_{L_{\max}} = 1.4$ and $C_{L_{\min}} = -0.7$ (without high-lift devices), and using Eq. (11.2) with a wing loading equal to 0.96×142.0 lbs/ft² (96% of the maximum wing loading to account for fuel burn during takeoff and climb) and a sea level air density of 0.002377 slugs/ft³, the stall curves are given by,

$$n = \frac{\rho_{SL} V_{EAS}^2 C_{L_{\max}}}{2W/S} = \frac{0.002377 \times (1.688 V_{EAS})^2 \times 1.4}{2 \times 0.96 \times 142.0} \quad (11.8)$$

and

$$n = \frac{\rho_{SL} V_{EAS}^2 C_{L_{\min}}}{2W/S} = \frac{0.002377 \times (1.688 V_{EAS})^2 \times (-0.7)}{2 \times 0.96 \times 142.0}. \quad (11.9)$$

Since we are using V_{EAS} values in knots, a factor of 1.688 is included to convert the values to ft/s. Using a limit load factor of $n = 2.5$, we get a design maneuver speed $V_A = 268.1$ knots. Using a normal load factor of $n = 1.0$, we get a normal stall speed $V_S = 169.6$ knots. These speeds are summarized in Table 11.2.

Design Speed	Value (knots)
V_S	169.6
V_A	268.1
V_C	273.0
V_{MO}	289.4
V_D	309.7

Table 11.2: Design speeds for jet transport example

The maneuver part of the V - n is now complete and shown in Fig. 11.7. The horizontal line on the top is given by $n = 2.5$ between V_A and V_D . The right side is bounded by V_D between $n = 2.5$ to $n = 0$. There is a linear relation between V_D at $n = 0$ and V_C at $n = -1$.

Gust loads for maximum weight at 20,000 ft The gust loads at 20,000 ft will be considered now. In order to find the gust loads, we use Eqs. (11.4) and (11.5). The table below gives the values needed for Eq. (11.5).

Parameter	Value
W/S	136.3 lbs/ft ²
\bar{c}	21.72 ft
$\rho_{20,000}$	0.001267 slugs/ft ³
$C_{L_{\alpha}}$	5.64

Table 11.3: Data for gust line calculation

From Eq. (11.5), at 20,000 ft, μ is 54.61. This gives $K_g = 0.802$. For these parameters, Eq. (11.4) becomes

$$n = 1 \pm \frac{0.802 \times 5.64 U_e V_{EAS}}{498 \times 136.3} \quad (11.10)$$

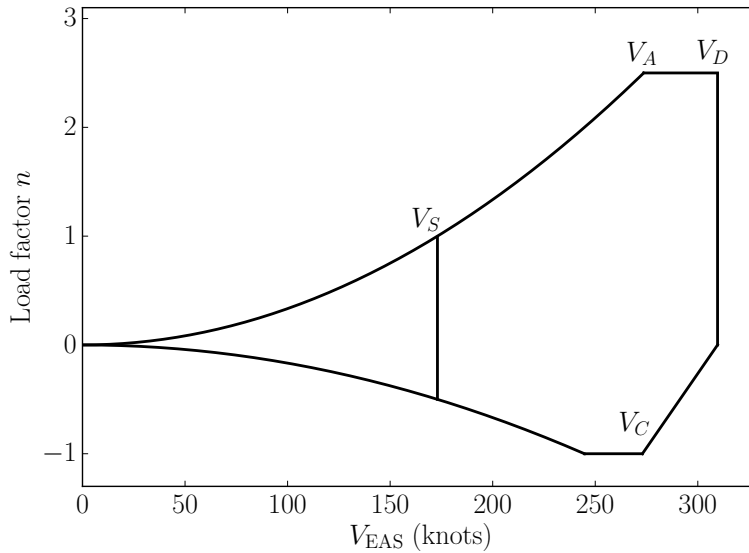


Figure 11.7: Maneuver V - n diagram for max. weight at 20,000 ft.

Note that, in this equation, U_e must be in ft/s and V_{EAS} must be in knots. At 20,000 ft, $U_{eD} = 25$ ft/s, $U_{eC} = 50$ ft/s, and $U_{eB} = 66$ ft/s. Using these gust speeds, we can obtain the gust lines shown in Fig. 11.8. The upper rough air gust line intersects the stall curve at $V_B = 244.18$ knots and $n = 2.07$. From Eq. (11.4), for the negative case we have $V_B = 231.1$ knots and $n = -0.07$. By substituting $V_C = 273.0$ and $U_e = 50$ ft/s into Eq. (11.4), we get $n = 1.91$ and $n = 0.09$. For $V_D = 309.6$ knots and $U_e = 25$ ft/s, $n = 1.52$ and $n = 0.48$. For this case, the gust envelope is contained within the maneuver envelope.

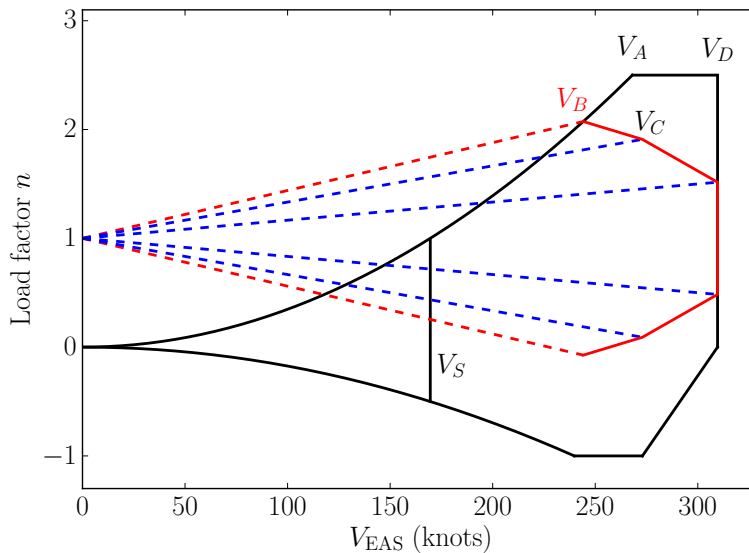


Figure 11.8: V - n diagram including gust lines for max. weight at 20,000 ft.

Diagram for minimum weight at 20,000 ft Now, we consider the diagram with a wing loading equal to $0.52 \times 142.0 \text{ lbs}/\text{ft}^2$. The operating empty weight of this aircraft is approximately 48% of the MTOW, so considering a minimum weight situation where the aircraft is near the end of a delivery or training flight, a wing loading that is 52% the maximum wing loading is used. As shown in Fig. 11.9, the stall curves and gust lines change because they depend on the wing loading. The outermost solid lines give the complete envelope.

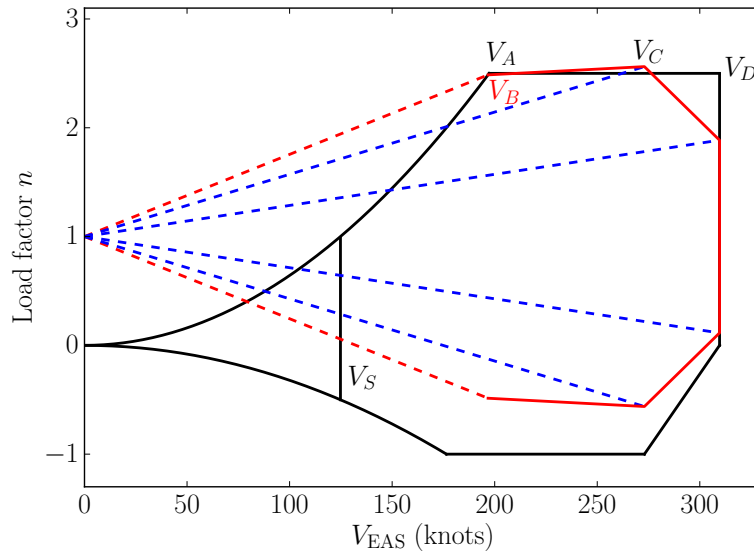
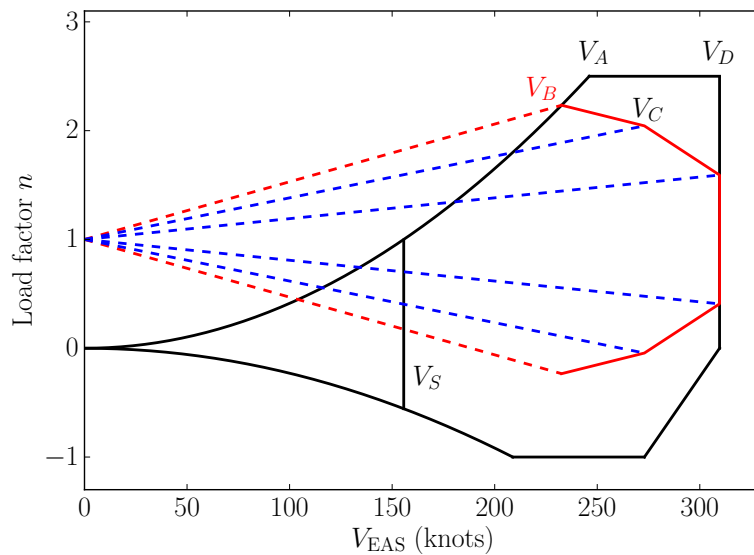
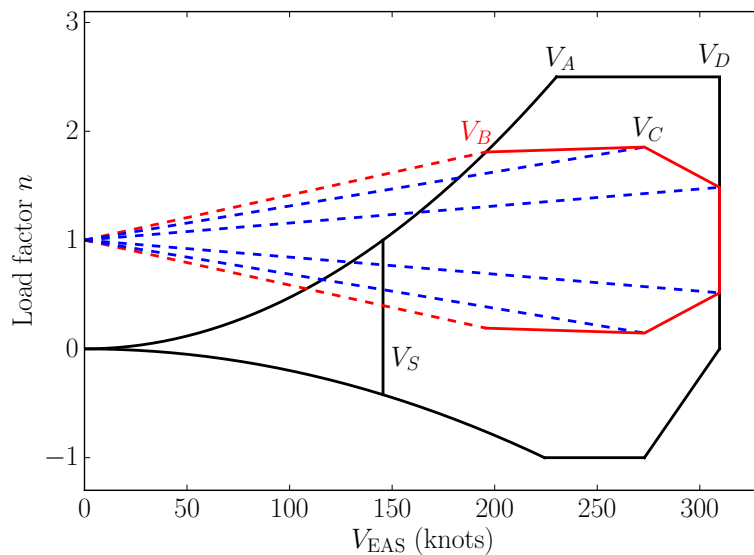


Figure 11.9: V - n diagram including gust lines for min. weight at 20,000 ft.

Diagram for minimum weight at 35,000 ft Similarly, we can obtain the diagram for flight at 35,000 ft. Assuming $C_{L_{\max}} = 0.9$ and $C_{L_{\min}} = -0.5$ (without high-lift devices), we get the curves shown in Fig. 11.10. For 35,000 ft, the gust speeds are $U_{e_D} = 18.75 \text{ ft/s}$, $U_{e_C} = 37.5 \text{ ft/s}$, and $U_{e_B} = 52 \text{ ft/s}$. Notice that the min. weight diagram for 20,000 ft shows higher loads for a greater range of speeds. The max. weight diagram for this altitude is not shown because with the maximum wing loading at cruise altitude, this aircraft cannot perform a 2.5g maneuver at an EAS less than V_D (the wing stalls).

Diagrams for max. and min. weights at sea level Similarly, we can obtain the diagrams for flight near sea level. Assuming $C_{L_{\max}} = 1.9$ and $C_{L_{\min}} = -0.8$ (without high-lift devices), we get the curves shown in Figs. 11.11 and 11.12. For sea level, the gust speeds used in Eq. (11.4) are the same ones used for 20,000 ft.

NOTE: Different $C_{L_{\max}}$ and $C_{L_{\min}}$ values were used for the different altitudes. These are estimated using the Reynolds and Mach numbers corresponding to the true airspeeds around V_A for the different altitudes.

Figure 11.10: V - n diagram envelope including gust critical points at 20,000 ft.Figure 11.11: V - n diagram including gust lines for max. weight at sea level.

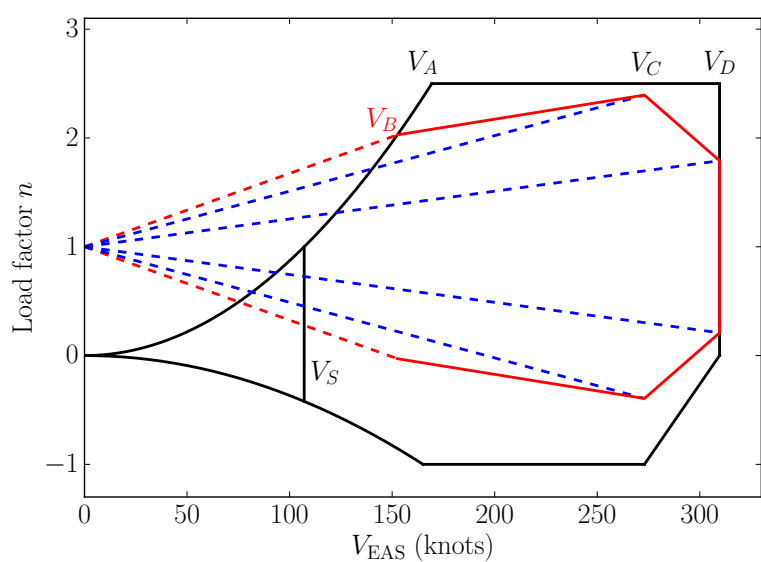


Figure 11.12: V - n diagram including gust lines for min. weight at sea level.

Bibliography

Denis Howe. *Aircraft Loading and Structural Layout*. AIAA, 2004.

Ilan M. Kroo. Aircraft design: Synthesis and analysis. URL <http://adg.stanford.edu/aa241/AircraftDesign.html>.

Ajoy Kumar Kundu. *Aircraft Design*. Cambridge University Press, 2010.

Leland M. Nicolai and Grant E. Carichner. *Fundamentals of Aircraft and Airship Design, Vol I — Aircraft Design*. AIAA, Reston, VA, 2010.

Kermit G. Pratt and Walter G. Walker. A revised gust-load formula and re-evaluation of $v-g$ data taken on civil transport airplane from 1933 to 1950. Technical Report 1206, NACA, 1954.

Daniel P. Raymer. *Aircraft Design: A Conceptual Approach*. AIAA, 5th edition, 2012.

Chapter 12

Sensitivity Studies

12.1 Introduction

Sensitivity studies are extremely useful in aircraft design. The relative magnitudes of the sensitivities provide the designer with an idea of what parameters drive the design. When using numerical optimization, gradient-based algorithms use the sensitivities to guide the optimization algorithm in the multidimensional design space (more on this later). There are numerous other applications for sensitivities.

Sensitivity analysis is a broad term that can have various meanings in mathematics and engineering. In our context, sensitivities quantify the variation in the output of a computation with respect to a parameter used in that computation. This parameter could be a design variable (e.g., the wing area), a modeling parameter (e.g, the constants in a regression used to estimate weight), or any other parameter that can change (e.g. fuel price).

You can think of sensitivities as partial derivatives, the definition of which is:

$$\frac{\partial f}{\partial x} = \lim_{h \rightarrow 0} \frac{f(x + h) - f(x)}{h} \quad (12.1)$$

The partial derivative is a function of x , so this sensitivity provides only *local* information. When x is a vector, then the sensitivities with respect to each component of x form the gradient ∇f . More generally, f itself could also be a vector, in which case ∇f becomes a Jacobian matrix.

The partial derivative defined above has the units of f/x and represents an *absolute variation*. Another way of reporting sensitivities is to report the *relative variation*

$$\frac{\partial f}{\partial x} \frac{x}{f} \quad (12.2)$$

which yields the percentage change in f corresponding to a 1% change in x .

12.2 Methods for Computing Sensitivities

12.2.1 Finite Differences

Finite-difference formulae are very commonly used to estimate sensitivities. Although these approximations are neither particularly accurate or efficient, this method's biggest advantage resides in the fact that it is extremely easy to implement.

All the finite-difference formulae can be derived by truncating a Taylor series expanded about a given point x . Suppose we have a function f of one variable x . A common estimate for the first derivative is the *forward-difference* which can be derived from the expansion of $f(x + h)$,

$$f(x + h) = f(x) + hf'(x) + \frac{h^2}{2!}f''(x) + \frac{h^3}{3!}f'''(x) + \dots, \quad (12.3)$$

Solving for f' we get the finite-difference formula,

$$f'(x) = \frac{f(x + h) - f(x)}{h} + \mathcal{O}(h), \quad (12.4)$$

where h is called the *finite-difference interval*. The truncation error is $\mathcal{O}(h)$, and hence this is a first-order approximation.

For a second-order estimate we can use the expansion of $f(x - h)$,

$$f(x - h) = f(x) - hf'(x) + \frac{h^2}{2!}f''(x) - \frac{h^3}{3!}f'''(x) + \dots, \quad (12.5)$$

and subtract it from the expansion (12.3). The resulting equation can then be solved for the derivative of f to obtain the *central-difference* formula,

$$f'(x) = \frac{f(x + h) - f(x - h)}{2h} + \mathcal{O}(h^2). \quad (12.6)$$

More accurate estimates can also be derived by combining different Taylor series expansions.

Formulas for estimating higher-order derivatives can be obtained by nesting finite-difference formulas. We can use, for example the central difference (12.6) to estimate the second derivative instead of the first,

$$f''(x) = \frac{f'(x + h) - f'(x - h)}{2h} + \mathcal{O}(h^2). \quad (12.7)$$

and use central difference again to estimate both $f'(x + h)$ and $f'(x - h)$ in the above equation to obtain,

$$f''(x) = \frac{f(x + 2h) - 2f(x) + f(x - 2h)}{4h^2} + \mathcal{O}(h). \quad (12.8)$$

When estimating sensitivities using finite-difference formulae we are faced with the *step-size dilemma*, that is the desire to choose a small step size to minimize truncation error while avoiding the use of a step so small that errors due to subtractive cancellation become dominant.

Forward-difference approximation:

$$\frac{df(x)}{dx} = \frac{f(x + h) - f(x)}{h} + \mathcal{O}(h). \quad (12.9)$$

With 16-digit arithmetic,

$f(x + h)$	+1.234567890123431
$f(x)$	+1.234567890123456
Δf	-0.0000000000000025

For functions of several variables, that is when x is a vector, then we have to calculate each component of the gradient $\nabla f(x)$ by perturbing the corresponding variable x_i .

The cost of calculating sensitivities with finite-differences is therefore proportional to the number of design variables and f must be calculated for each perturbation of x_i . This means that if we use forward differences, for example, the cost would be $n + 1$ times the cost of calculating f .

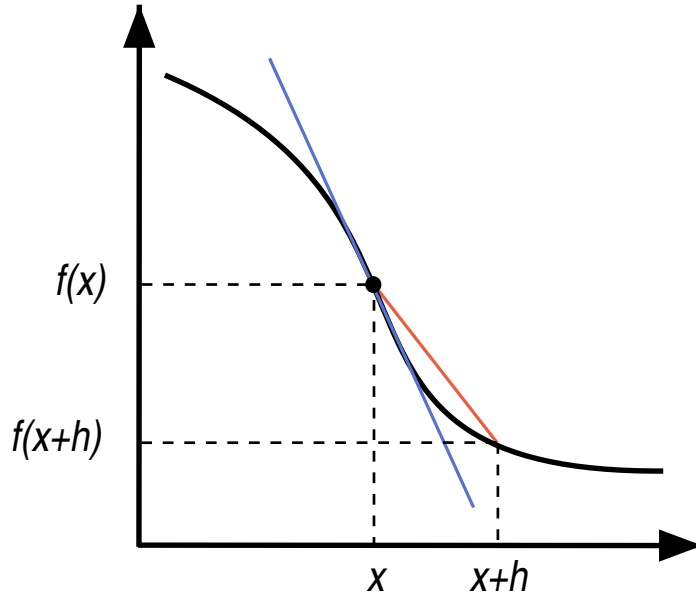


Figure 12.1: Graphical representation of the finite difference approximation

12.2.2 Complex-Step Method

The use of complex variables to develop estimates of derivatives originated with the work of Lyness (1967) and Lyness and Moler (1967). Their work produced several methods that made use of complex variables, including a reliable method for calculating the n^{th} derivative of an analytic function. However, only recently has some of this theory been rediscovered by Squire and Trapp (1998) and used to obtain a very simple expression for estimating the first derivative. This estimate is suitable for use in modern numerical computing and has shown to be very accurate, extremely robust and surprisingly easy to implement, while retaining a reasonable computational cost (Martins et al., 2003).

12.2.3 Basic Theory

We will now see that a very simple formula for the first derivative of real functions can be obtained using complex calculus. The complex-step derivative approximation can also be derived using a Taylor series expansion. Rather than using a real step h , we now use a pure imaginary step, ih . If f is a real function in real variables and it is also analytic, we can expand it in a Taylor series about a real point x as follows,

$$f(x + ih) = f(x) + ihf'(x) - h^2 \frac{f''(x)}{2!} - ih^3 \frac{f'''(x)}{3!} + \dots \quad (12.10)$$

Taking the imaginary parts of both sides of (12.10) and dividing the equation by h yields

$$f'(x) = \frac{\text{Im}[f(x + ih)]}{h} + h^2 \frac{f'''(x)}{3!} + \dots \quad (12.11)$$

Hence the approximations is a $\mathcal{O}(h^2)$ estimate of the derivative of f . We call this the *complex-step derivative approximation*. This estimate is not subject to subtractive cancellation error, since it does

not involve a difference operation. Not having the difference operation constitutes a tremendous advantage over the finite-difference approaches expressed in (12.4, 12.6).

Example 12.1: The Complex-Step Method Applied to a Simple Function

To show the how the complex-step method works, consider the following analytic function:

$$f(x) = \frac{e^x}{\sqrt{\sin^3 x + \cos^3 x}} \quad (12.12)$$

The exact derivative at $x = 1.5$ was computed analytically to 16 digits and then compared to the results given by the complex-step method (12.11) and the forward and central finite-difference approximations.

Relative error in the sensitivity estimates given by finite-difference and the complex- step methods with the analytic result as the reference, i.e.,

$$\varepsilon = \frac{|f' - f'_{ref}|}{|f'_{ref}|}. \quad (12.13)$$

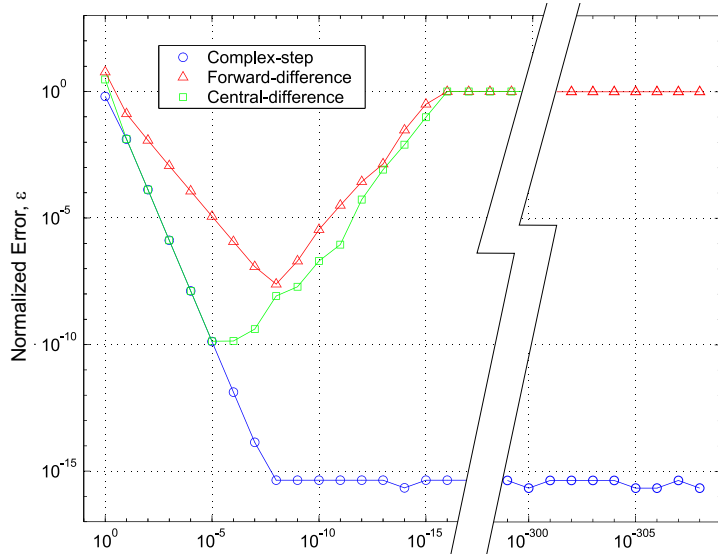


Figure 12.2: Relative error of the sensitivity vs. decreasing step size

The forward-difference estimate initially converges to the exact result at a linear rate since its truncation error is $\mathcal{O}(h)$, while the central-difference converges quadratically, as expected. However, as the step is reduced below a value of about 10^{-8} for the forward-difference and 10^{-5} for the central-difference, subtractive cancellation errors become significant and the estimates are unreliable. When the interval h is so small that no difference exists in the output (for steps smaller than 10^{-16}) the finite-difference estimates eventually yields zero and then $\varepsilon = 1$.

The complex-step estimate converges quadratically with decreasing step size, as predicted by the truncation error estimate. The estimate is practically insensitive to small step sizes and below an h of the order of 10^{-8} it achieves the accuracy of the function evaluation. Comparing the best accuracy of each of these approaches, we can see that by using finite-difference we only achieve a fraction of the accuracy that is obtained by using the complex-step approximation.

The complex-step size can be made extremely small. However, there is a lower limit on the step size when using finite precision arithmetic. The range of real numbers that can be handled in numerical computing is dependent on the particular compiler that is used. In this case, the smallest non-zero number that can be represented is 10^{-308} . If a number falls below this value, underflow occurs and the number drops to zero. Note that the estimate is still accurate down to a step of the order of 10^{-307} . Below this, underflow occurs and the estimate results in NaN.

Comparing the accuracy of complex and real computations, there is an increased error in basic arithmetic operations when using complex numbers, more specifically when dividing and multiplying.

12.2.4 Other Methods

Finite differencing and the complex-step method have been introduced here because they are straightforward to implement. Other more involved methods for computing derivatives exist and are briefly described below. For a more comprehensive review of the various methods, including those that can be used for computing the derivatives of coupled multidisciplinary systems, see [Martins and Hwang \(2012\)](#) (a draft of the journal paper version of this is also available upon request [Martins and Hwang \(2012\)](#)).

Symbolic differentiation can be used to differentiate simple explicit functions and is as accurate as the computation of the function. Unfortunately it is restricted to explicit functions and cannot be used to compute the sensitivities of an iterative computation (unless you do it line by line, which in essence is the idea behind automatic differentiation — see below)

Automatic differentiation tools automatically process the source code of the computation of interest and produce new code that computes the sensitivities of that computation. There are various automatic differentiation tools that can handle all the mainstream programming languages. For more information on automatic differentiation, see [Mader et al. \(2008\)](#)

Semi-analytic methods differentiate the governing equations, which can be given as a linear or nonlinear system of equations, and can be generalized to PDE-governed systems. These methods are very efficient and accurate, but require long development and implementation times. A subclass of these methods, the adjoint method, is able to compute the sensitivities with respect to large numbers of inputs extremely efficiently. Semi-analytic methods can be combined with automatic differentiation for the best of both worlds ([Mader et al., 2008](#)). These methods can be used to compute the coupled sensitivity of multidisciplinary systems ([Kenway and Martins, 2014](#); [Kenway et al., 2014](#))

Bibliography

Gaetan K. W. Kenway and Joaquim R. R. A. Martins. Multipoint high-fidelity aerostructural optimization of a transport aircraft configuration. *Journal of Aircraft*, 51(1):144–160, January 2014. doi:[10.2514/1.C032150](https://doi.org/10.2514/1.C032150).

Gaetan K. W. Kenway, Graeme J. Kennedy, and Joaquim R. R. A. Martins. Scalable parallel approach for high-fidelity steady-state aeroelastic analysis and derivative computations. *AIAA Journal*, 52(5):935–951, May 2014. doi:[10.2514/1.J052255](https://doi.org/10.2514/1.J052255).

J. N. Lyness. Numerical algorithms based on the theory of complex variable. In *Proceedings — ACM National Meeting*, pages 125–133, Washington DC, 1967. Thompson Book Co.

J. N. Lyness and C. B. Moler. Numerical differentiation of analytic functions. *SIAM Journal on Numerical Analysis*, 4(2):202–210, 1967. ISSN 0036-1429 (print), 1095-7170 (electronic).

Charles A. Mader, Joaquim R. R. A. Martins, Juan J. Alonso, and Edwin van der Weide. ADjoint: An approach for the rapid development of discrete adjoint solvers. *AIAA Journal*, 46(4):863–873, April 2008. doi:[10.2514/1.29123](https://doi.org/10.2514/1.29123).

Joaquim R. R. A. Martins and John T. Hwang. Review and unification of methods for computing derivatives of multidisciplinary systems. In *53rd AIAA/ASME/ASCE/AHS/ASC Structures, Structural Dynamics, and Materials Conference*, Honolulu, HI, April 2012. AIAA 2012-1589.

Joaquim R. R. A. Martins, Peter Sturdza, and Juan J. Alonso. The complex-step derivative approximation. *ACM Transactions on Mathematical Software*, 29(3):245–262, September 2003. doi:[10.1145/838250.838251](https://doi.org/10.1145/838250.838251).

William Squire and George Trapp. Using complex variables to estimate derivatives of real functions. *SIAM Review*, 40(1):110–112, 1998. ISSN 0036-1445 (print), 1095-7200 (electronic).